ΕΘΝΙΚΟ ΜΕΤΣΟΒΙΟ ΠΟΛΥΤΕΧΝΕΙΟ

ΣΧΟΛΗ ΗΛΕΚΤΡΟΛΟΓΩΝ ΜΗΧΑΝΙΚΩΝ
ΚΑΙ ΜΗΧΑΝΙΚΩΝ ΥΠΟΛΟΓΙΣΤΩΝ

ΤΟΜΕΑΣ ΕΠΙΚΟΙΝΩΝΙΩΝ, ΗΛΕΚΤΡΟΝΙΚΗΣ
ΚΑΙ ΣΥΣΤΗΜΑΤΩΝ ΠΛΗΡΟΦΟΡΙΚΗΣ

Σχεδίαση και ανάπτυξη βιοαισθητήρα για την ταχεία ανίχνευση του SARS-CoV-2

ΔΙΔΑΚΤΟΡΙΚΗ ΔΙΑΤΡΙΒΗ

Αντώνιος, Α Γεωργάς

Αθήνα, Νοέμβριος 2022

ΕΘΝΙΚΟ ΜΕΤΣΟΒΙΟ ΠΟΛΥΤΕΧΝΕΙΟ

ΣΧΟΛΗ ΗΛΕΚΤΡΟΛΟΓΩΝ ΜΗΧΑΝΙΚΩΝ
ΚΑΙ ΜΗΧΑΝΙΚΩΝ ΥΠΟΛΟΓΙΣΤΩΝ

ΤΟΜΕΑΣ ΕΠΙΚΟΙΝΩΝΙΩΝ, ΗΛΕΚΤΡΟΝΙΚΗΣ
ΚΑΙ ΣΥΣΤΗΜΑΤΩΝ ΠΛΗΡΟΦΟΡΙΚΗΣ

Σχεδίαση και ανάπτυξη βιοαισθητήρα για την ταχεία ανίχνευση του SARS-CoV-2

ΔΙΔΑΚΤΟΡΙΚΗ ΔΙΑΤΡΙΒΗ

Συμβουλευτική Επιτροπή: Evangelos Hristoforou
Alessandro Trifiletti
Γεώργιος Ματσόπουλος

Εγκρίθηκε από την εφταμελή εξεταστική επιτροπή την 28/11/2022.

.....	.....	.....
Ευάγγελος Χριστοφόρου	Alessandro Trifiletti	Δημήτριος Διονύσιος Κουτσούρης
Καθηγητής ΕΜΠ	Professor La Sapienza	Καθηγητής ΕΜΠ

.....	.....	.....	.....
Γεώργιος Ματσόπουλος	Ιωάννης Γκόνος	Παναγιώτης Τσανάκας	Θεόδωρος Ματίκας
Καθηγητής ΕΜΠ	Καθηγητής ΕΜΠ	Καθηγητής ΕΜΠ	Καθηγητής Παν. Ιωαννίνων

Αθήνα, Νοέμβριος 2022

Αντώνιος Γεωργάς

Διπλωματούχος Ηλεκτρολόγος Μηχανικός και Μηχανικός Υπολογιστών Ε.Μ.Π.

Copyright © Αντώνιος Γεωργάς, 2022.

Με επιφύλαξη παντός δικαιώματος. All rights reserved.

Απαγορεύεται η αντιγραφή, αποθήκευση και διανομή της παρούσας εργασίας, εξ' ολοκλήρου ή τμήματος αυτής, για εμπορικό σκοπό. Επιτρέπεται η ανατύπωση, αποθήκευση και διανομή για σκοπό μη κερδοσκοπικό, εκπαιδευτικής ή ερευνητικής φύσης, υπό την προϋπόθεση να αναφέρεται η πηγή προέλευσης και να διατηρείται το παρόν μήνυμα. Ερωτήματα που αφορούν τη χρήση της εργασίας για κερδοσκοπικό σκοπό πρέπει να απευθύνονται προς τον συγγραφέα.

Οι απόψεις και τα συμπεράσματα που περιέχονται σε αυτό το έγγραφο εκφράζουν τον συγγραφέα και δεν πρέπει να ερμηνευθεί ότι αντιπροσωπεύουν τις επίσημες θέσεις του Εθνικού Μετσόβιου Πολυτεχνείου.

NATIONAL TECHNICAL UNIVERSITY OF ATHENS

SCHOOL OF ELECTRICAL AND COMPUTER ENGINEERING

DIVISION OF INFORMATION TRANSMISSION SYSTEMS AND MATERIAL TECHNOLOGY

Design and development of a biosensor for the rapid detection of SARS-CoV-2

DOCTORAL THESIS

Antonios, A Georgas

Athens, November 2022

NATIONAL TECHNICAL UNIVERSITY OF ATHENS

SCHOOL OF ELECTRICAL AND COMPUTER ENGINEERING

DIVISION OF INFORMATION TRANSMISSION SYSTEMS AND MATERIAL TECHNOLOGY

Design and development of a biosensor for the rapid detection of SARS-CoV-2

DOCTORAL THESIS

Advisory Board: Evangelos Hristoforou
Alessandro Trifiletti
George Matsopoulos

Approved by the advisory board on 28/11/2022.

.....	.....	.....
Evangelos Hristoforou	Alessandro Trifiletti	George Matsopoulos
Professor N.T.U.A	Professor La Sapienza	Professor N.T.U.A

.....	.....	.....	.....
Dimitrios Koutsouris	Panayiotis Tsanakas	Ioannis Gonos	Theodore Matikas
Professor N.T.U.A	Professor N.T.U.A	Professor N.T.U.A	Professor Uol

Athens, November 2022

Antonios Georgas

PhD Candidate, Electrical and Computer Engineer

Copyright © All rights reserved.

Περίληψη

Στόχος αυτής της διατριβής είναι η ανάπτυξη ενός ηλεκτροχημικού βιοαισθητήρα για την ανίχνευση του SARS-CoV-2 σε βιολογικά δείγματα.

Στο πρώτο μέρος της διατριβής αναπτύσσεται το αισθητήριο στοιχείο, που βασίζεται στην ακινητοποίηση του φυσικού υποδοχέα του ιού, του ενζύμου ACE2, στην επιφάνεια πυκνωτών ενδοδιαπλεκόμενων ηλεκτροδίων. Τα αποτελέσματα των μετρήσεων του βιοαισθητήρα συσχετίζονται με τα αποτελέσματα της real-time PCR για τα ίδια δείγματα.

Στην συνέχεια, αφού έχει επαληθευτεί η ορθή λειτουργία του αισθητήρα, ο αισθητήρας ενσωματώνεται σε μια φορητή συσκευή που αναπτύχθηκε στο εργαστήριο. Αυτή η συσκευή αποτελείται από ένα πρωτότυπο ηλεκτρονικό κύκλωμα ακριβείας που πραγματοποιεί μετρήσεις της σύνθετης αντίστασης. Ακόμα, χρησιμοποιώντας Bluetooth, η συσκευή μεταδίδει ασύρματα τα αποτελέσματα της μέτρησης σε εφαρμογή για κινητά android που αναπτύχθηκε στα πλαίσια της διατριβής.

Το τελικό στάδιο αφορά το πακετάρισμα του βιοαισθητήρα και της ηλεκτρονικής συσκευής, αλλά και την κατασκευή της διασύνδεσης μεταξύ των δύο. Το πακετάρισμα της συσκευής και η κατασκευή της διασύνδεσης πραγματοποιούνται με χρήση τρισδιάστατης εκτύπωσης. Το πακετάρισμα του βιοαισθητήρα πραγματοποιείται με την χρήση μιας φωτοευαίσθητης ταινίας, της ORDYL SY 300, η επεξεργασία της οποίας γίνεται με την μέθοδο της οπτικής λιθογραφίας.

Λέξεις-κλειδιά: *βιοαισθητήρας, SARS-CoV-2, χωρητικός αισθητήρας, ενδοδιαπλεκόμενα ηλεκτρόδια, ηλεκτρονικό κύκλωμα ανάγνωσης, πακετάρισμα*

Abstract

The aim of this thesis is the development of an electrochemical biosensor for the rapid detection of SARS-CoV-2 in biological samples.

In the first part of the thesis, the sensing element is developed, based on the immobilization of the natural receptor of the virus, the enzyme ACE2, on the surface of interdigitated electrode capacitors. The results of the biosensor measurements are correlated with the real-time PCR results for the same samples.

Then, after the sensor has been verified to function properly, the sensor is integrated into a lab-developed portable device. This device consists of a custom precision electronic circuit that performs impedance measurements. Also, using Bluetooth, the device wirelessly transmits the measurement results to an android mobile application developed in the framework of the thesis.

The final stage concerns the packaging of the biosensor and the electronic device, but also the construction of the connector between the two. The packaging of the device and the manufacturing of the connector are done using 3D printing. The packaging of the biosensor is carried out using a photosensitive film, ORDYL SY 300, which is processed by the method of optical lithography.

Keywords: *biosensor; SARS-CoV-2; capacitive sensor; interdigitated electrodes; readout circuit; packaging*

Εκτενής Περίληψη στα Ελληνικά

Μέρος Α

Η εξάπλωση του SARS-CoV-2 και η αυξανόμενη απειλή του για την ανθρώπινη υγεία σε όλο τον κόσμο έχει καταστήσει επιτακτική την ανάγκη ανάπτυξης νέων τεχνολογικών εργαλείων για την καταπολέμηση του ιού. Ιδιαίτερη έμφαση δίνεται στην ανάπτυξη διαγνωστικών μεθόδων που καταγράφουν την εξάπλωση του ιού γρήγορα και αποτελεσματικά. Αυτή η διδακτορική διατριβή περιγράφει την ανάπτυξη ενός βιοαισθητήρα για την ταχεία ανίχνευση του κορονοϊού, που βασίζεται στην ακινητοποίηση της πρωτεΐνης-υποδοχέα ACE2 στην επιφάνεια χρυσών ενδοδιαπλεκόμενων ηλεκτροδίων. Το ACE2 είναι ο βασικός υποδοχέας για τους ιούς SARS-CoV. Η σύνδεση αυτών των ιών γίνεται με την βοήθεια της γλυκοπρωτεΐνης S την οποία διαθέτουν στο εξωτερικό τους περίβλημα.

Αρχικά, στην επιφάνεια χρυσών ενδοδιαπλεκόμενων ηλεκτροδίων δημιουργείται μια επίστρωση κυστεΐνης (αμινοξύ με συντακτικό τύπο HO2CCH(NH2)CH2SH). Η κυστεΐνη διαθέτει μια πλευρική αλυσίδα η οποία χαρακτηρίζεται από την παρουσία της χαρακτηριστικής ομάδας του σουλφυδρυλίου. Με την σειρά του το σουλφυδρύλιο της κυστεΐνης είναι πολύ δραστικό και συμμετέχει σε πολλές ενζυμικές αντιδράσεις. Η προσθήκη της κυστεΐνης είναι απαραίτητη να προστεθεί στην επιφάνεια του χρυσού για να βοηθήσει στην ακινητοποίηση του ACE2. Για να τοποθετηθεί το ACE2 κατασκευάστηκε ένα διάλυμα το οποίο περιείχε 5 μL ACE2, 5 μL EDC και 10 μL MES. Το EDC και το MES είναι απαραίτητα για να γίνει η χημική αντίδραση και να τοποθετηθεί το ACE2 στην επιφάνεια του χαλκού. Συγκεκριμένα το EDC και το MES ενεργοποιούν το καρβοξυλικό άκρο (-COOH) του ACE2. Με το που ενεργοποιηθεί το καβοξυλικό άκρο του ACE2 γίνεται η αντίδραση με την αμινομάδα (-NH2) της κυστεΐνης σχηματίζοντας έναν ομοιοπολικό πεπτικό δεσμό. Με αυτόν τον τρόπο το ACE2 ακινητοποιείται στην χρυσή επιφάνεια των ηλεκτροδίων.

Στην συνέχεια τοποθετείται βιολογικό δείγμα (ρινοφαρυγγικό ή σάλιο) πάνω στο στρώμα του ACE2. Αν σε αυτό το δείγμα υπάρχουν σωματίδια του ιού, ή και μόνο η πρωτεΐνη S, τα σωματίδια δεσμεύονται από το ACE2 επιφέροντας μια αλλαγή στις διηλεκτρικές ιδιότητες του υλικού ή στο πάχος του διηλεκτρικού στρώματος. Αυτή η αλλαγή καταγράφεται ως αλλαγή στην αντίσταση και την χωρητικότητα μεταξύ των ηλεκτροδίων του πυκνωτή. Η παρακολούθηση της αλλαγής της χωρητικότητας πραγματοποιείται με τον εξής τρόπο: 2 χρυσές βελόνες τοποθετούνται στα άκρα του πυκνωτή, όπου και εφαρμόζεται μια διαφορά δυναμικού. Οι βελόνες είναι συνδεδεμένες με ένα επιτραπέζιο μηχάνημα LCR (Hewlett Packard, μοντέλο 4284A Precision) το οποίο μετράει σε πραγματικό χρόνο την χωρητικότητα και την αντίσταση.

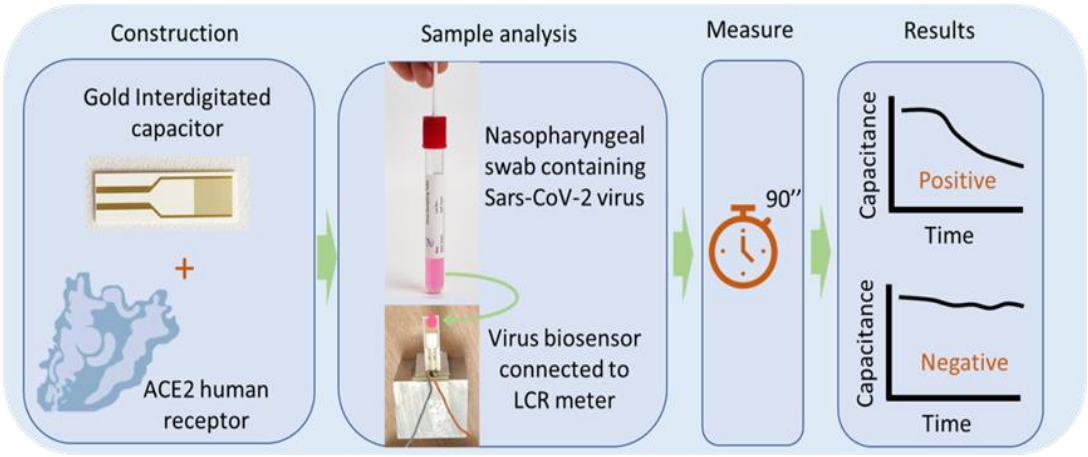

Τα βιολογικά δείγματα αποκτήθηκαν στο Κωνσταντοπούλειο Γενικό Νοσοκομείο Νέας Ιωνίας. Κατά την απόκτηση των δειγμάτων ακολουθήθηκαν όλα τα προβλεπόμενα πρωτόκολλα ασφαλείας, ενώ διατηρήθηκε η ανωνυμία των δοτών για προστασία των προσωπικών τους δεδομένων.

Παράλληλα με την διαδικασία μέτρησης των δειγμάτων με τον βιοαισθητήρα, τα δείγματα μετρήθηκαν και με την μέθοδο της real-time PCR, ώστε να υπάρξει εκ των υστέρων η συσχέτιση των αποτελεσμάτων. Για την εξαγωγή του RNA χρησιμοποιήθηκε το GXT NA Extraction Kit DNA/RNA 200 virus. Στην συνέχεια το RNA μετατράπηκε σε cDNA και πολλαπλασιάστηκε με χρήση του YouSeq® SARS-CoV-2 COVID-19 RT-qPCR kit (YouSeq, Winchester, England).

Το διάστημα μέτρησης με τον βιοαισθητήρα είναι 1 λεπτό. Σε αυτό το διάστημα παρατηρήθηκαν 3 ενδεχόμενα: Για δείγματα που δεν περιείχαν τον ιό η αλλαγή της χωρητικότητας ήταν μικρότερη του 1%. Για δείγματα που περιείχαν μικρό ιικό φορτίο ($<10^3$ virus copy numbers/μL) η αλλαγή στην χωρητικότητα ήταν μεταξύ 1 και 2%. Ενώ για δείγματα με ιικό φορτίο $>10^3$ virus copy numbers/μL η αλλαγή στην χωρητικότητα ήταν μεγαλύτερη του 2%.

Όταν ο αισθητήρας χρησιμοποιήθηκε σε εργαστηριακές συνθήκες για τον έλεγχο δειγμάτων που περιείχαν μόνο την πρωτεΐνη S, επιβεβαιώθηκε η δυνατότητα ανίχνευσης με όριο ανίχνευσης [LOD] τα 750 pg/μL/mm^2. Στην εξέταση ρινοφαρυγγικών δειγμάτων επαληθεύτηκε ότι ο βιοαισθητήρας μπορεί να διακρίνει δείγματα θετικά στον ιό από αυτά που είναι αρνητικά, σε συνολικά 7 θετικά και 16 αρνητικά δείγματα. Ακόμα, δοκιμάστηκε η απόκριση του αισθητήρα σε δείγμα σάλιου, καθώς όταν από τον ίδιο ασθενή αποκτήθηκε και ρινοφαρυγγικό δείγμα και δείγμα σάλιου, παρατηρήθηκε ότι και τα 2 δείγματα μεταβάλλουν την χωρητικότητα, απλά η μεταβολή που επιφέρει το δείγμα σάλιου είναι μικρότερη, πράγμα λογικό αφού στο σάλιο είναι μικρότερο το ιικό φορτίο. Επιπλέον, ο βιοαισθητήρας μπορεί να χρησιμοποιηθεί για ημιποσοτική μέτρηση, αφού οι μετρήσεις του χωρίζονται σε 3 περιοχές, τα αρνητικά δείγματα, τα ελαφρώς θετικά και τα θετικά δείγματα. Η αναπαραγωγιμότητα των πειραμάτων αποδείχθηκε με τουλάχιστον 3 επαναλήψεις ανά δείγμα, ενώ για την δοκιμή της σταθερότητας κάποιοι από τους αισθητήρες διατηρήθηκαν πριν την χρήση τους στο ψυγείο στους 4 ◦C για 7 ημέρες.

Μέρος Β

Το δεύτερο μέρος της διατριβής επικεντρώθηκε στην σχεδίαση και ανάπτυξη μιας φορητής συσκευής, που με βάση τον βιοαισθητήρα που περιγράφεται στο Μέρος Α θα μπορεί να χρησιμοποιηθεί για την ταχεία ανίχνευση του SARS-CoV-2 σε πραγματικές συνθήκες. Οι ηλεκτροχημικοί βιοαισθητήρες είναι ιδανικοί για την χρήση σε τέτοιου τύπου συσκευές, καθώς δεν απαιτούν πολύπλοκα όργανα διέγερσης – ανάγνωσης, είναι ιδιαίτερα ευαίσθητοι, οικονομικά αποδοτικοί και μπορούν να κατασκευαστούν σε πολύ μικρό μέγεθος. Η δυνατότητα ηλεκτρονικής επεξεργασίας των αποτελεσμάτων των τεστ, που προσφέρει μια συσκευή τέτοιου τύπου, σημαίνει ότι μπορεί να ελεγχθεί η εξάπλωση του ιού στο χώρο και στο χρόνο. Με τη χρήση ηλεκτρονικών μεθόδων και του διαδικτύου των πραγμάτων (IoT), μπορεί να γίνει αποτελεσματικός έλεγχος της κατανομής των κρουσμάτων κορονοϊού σε συγκεκριμένες γεωγραφικές περιοχές, καθώς και σε συγκεκριμένα χρονικά διαστήματα. Μάλιστα, με την καταχώρηση των δεδομένων των αποτελεσμάτων των τεστ σε μια πλατφόρμα, μπορεί να γίνει στατιστική επεξεργασία, που μπορεί να δώσει ενδείξεις για τη βελτίωση των ίδιων των διαγνωστικών εργαλείων, αλλά και για τη βελτίωση της στρατηγικής αντιμετώπισης της πανδημίας.

Μετά την ανάπτυξη του βιοαισθητήρα και την επικύρωση της λειτουργίας του στο Α μέρος της διατριβής, στο Β μέρος αναπτύχθηκε ένα πρωτότυπο ηλεκτρονικό κύκλωμα ανάγνωσης για τον αισθητήρα, καθώς και μια εφαρμογή Android που διαβάζει τα αποτελέσματα του βιοαισθητήρα εξ αποστάσεως μέσω Bluetooth. Με αυτόν τον τρόπο, αναπτύχθηκε ένα φορητό ηλεκτρονικό κύκλωμα ανάγνωσης, το οποίο μετράει τις αλλαγές στην σύνθετη αντίσταση του αισθητήρα και αποφασίζει αν ο χρήστης του τεστ είναι θετικός ή αρνητικός στον SARS-CoV-2. Τα αποτελέσματα των τεστ γίνονται διαθέσιμα στο κινητό τηλέφωνο του χρήστη εντός 2 λεπτών, μέσω της εφαρμογής android που είναι εύκολη στην χρήση.

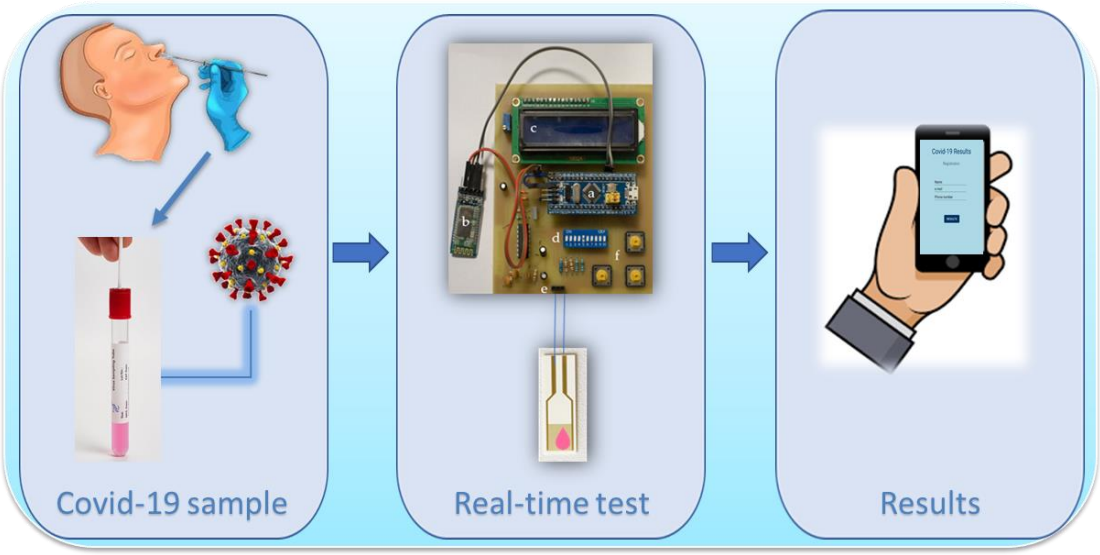

Για την σχεδίαση του κυκλώματος χρησιμοποιείται ένας μικροελεγκτής STM32 (STM32F103C8T6) (MCU), ικανός να παράγει ένα PWM σήμα υψηλής συχνότητας, το οποίο τροφοδοτείται σε ένα βαθυπερατό φίλτρο (LPF). Το LPF σχεδιάστηκε ως φίλτρο Butterworth δεύτερης τάξης με συχνότητα αποκοπής 13 kHz. Η έξοδος του LPF, που είναι ημίτονο 1 kHz ή 10 kHz, οδηγεί έναν διαιρέτη τάσης που αποτελείται από μια γνωστή αντίσταση και την συσκευή υπό δοκιμή (DUT). Μετρώντας τα πλάτη των τάσεων ADC1 και ADC2, καθώς και τη διαφορά φάσης τους, μπορούμε να υπολογίσουμε την σύνθετη αντίσταση του DUT.

Προκειμένου να μειωθεί ο θόρυβος της μέτρησης, τα πλάτη και οι φάσεις της θεμελιώδους συχνότητας υπολογίστηκαν χρησιμοποιώντας τον τύπο του διακριτού μετασχηματισμού Fourier. Το αποτέλεσμα στη συνέχεια υπολογίστηκε ως ο μέσος όρος 512 μετρήσεων και κανονικοποιήθηκε διαιρώντας κάθε μέτρηση με τη μέγιστη μετρούμενη τιμή.

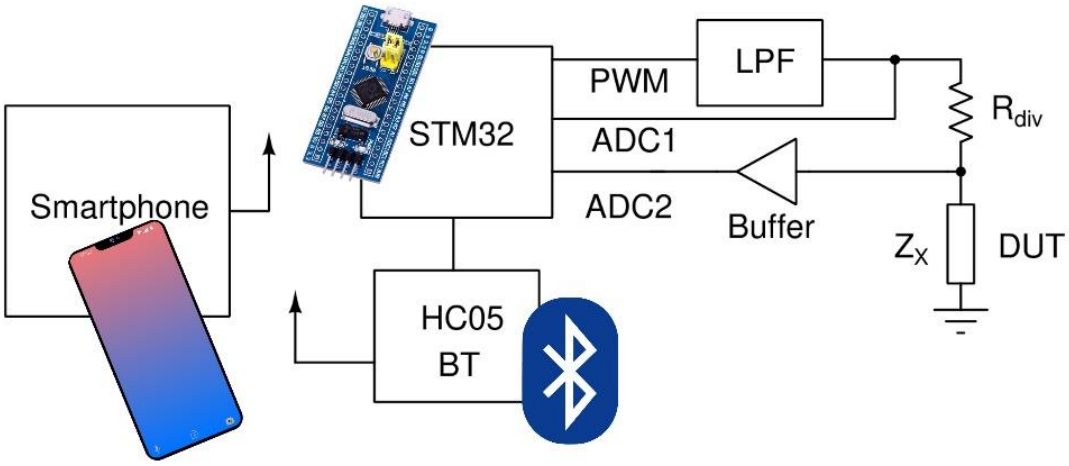

Προκειμένου να τονιστεί το κύριο πλεονέκτημα του αισθητήρα, δηλαδή η γρήγορη απόκτηση του τελικού αποτελέσματος, αναπτύχθηκε μια συνοδευτική εφαρμογή για κινητά android, η οποία είναι σε θέση να παρέχει τα αποτελέσματα των τεστ σε πραγματικό χρόνο και σε μορφή εύκολα αναγνώσιμη από τον χρήστη. Η εφαρμογή που αναπτύχθηκε βασίζεται στην επικοινωνία μεταξύ ενός smartphone android και του κυκλώματος ανάγνωσης του αισθητήρα με χρήση Bluetooth. Η πλακέτα STM32 δεν έχει τη δυνατότητα άμεσης επικοινωνίας μέσω Bluetooth. Ως εκ τούτου, μια μονάδα πομποδέκτη (HC-05), η οποία είναι σε θέση να μεταδίδει δεδομένα στην εφαρμογή χρησιμοποιώντας το τυπικό πρωτόκολλο Bluetooth, προστέθηκε στο κύκλωμα ανάγνωσης.

Η διαδικασία ανάγνωσης είναι η εξής: Το smartphone συνδέεται με τη συσκευή Bluetooth, δηλαδή τη μονάδα HC-05. Στη συνέχεια, η συσκευή μπορεί να επιλεγεί μέσω της εφαρμογής Android, ώστε να δημιουργηθεί μια σύνδεση μεταξύ των δύο τμημάτων. Όταν δημιουργηθεί η σύνδεση, η εφαρμογή λαμβάνει τα κατάλληλα πακέτα δεδομένων σε μορφή JSON, τα οποία αποστέλλονται από το κύκλωμα ανάγνωσης. Όλες οι απαραίτητες πληροφορίες αποθηκεύονται σε αυτά τα πακέτα δεδομένων, όπως το αποτέλεσμα της μέτρησης, η μετρούμενη τιμή και μια χρονική σήμανση. Τέλος, το αποτέλεσμα του τεστ (θετικό ή αρνητικό) εμφανίζεται στην οθόνη.

Μέρος Γ

Το Γ μέρος της διδακτορικής διατριβής αφορά στην διαδικασία βελτιστοποίησης του βιοαισθητήρα, αλλά και στο πακετάρισμα του βιοαισθητήρα και του ηλεκτρονικού κυκλώματος μέτρησής του.

Αν και οι χωρητικοί βιοαισθητήρες παρουσιάζουν ιδιαίτερα καλές ευαισθησίες και είναι πολύ δημοφιλείς ως διαγνωστικά εργαλεία σε βιοϊατρικές εφαρμογές, υπάρχουν και διάφορες προκλήσεις που πρέπει να ξεπεραστούν όσον αφορά την χρήση τους. Μια πολύ σημαντική πρόκληση, αφορά στην αντιμετώπιση του θορύβου, και συνεπώς στην γραμμικότητα και επαναληψιμότητα της ηλεκτρονικής μέτρησης, που εισάγεται από τον βιοαισθητήρα, αλλά και από το κύκλωμα ανάγνωσής του.

Στην περίπτωση του βιοαισθητήρα που έχει αναπατυχθεί και περιγραφεί στα μέρη Α και Β, τόσο η γραμμικότητα, όσο και η επαναληψιμότητα των μετρήσεων μπορεί να επηρεαστεί από την διάχυση του υγρού αναλύτη στην επιφάνεια του βιοαισθητήρα. Συγκεκριμένα, η σταγόνα που εναποτίθεται στην επιφάνεια του βιοαισθητήρα μπορεί να αρχίσει να διαχέεται στην επιφάνεια, μεταβάλλοντας την μετρούμενη χωρητικότητα.

Για αυτό τον λόγο, στο μέρος Γ της διατριβής δημιουργούνται πηγάδια στην επιφάνεια του βιοαισθητήρα, τα οποία εμποδίζουν την ανεξέλεγκτη διάχυση του υγρού και βελτιώνουν τις ηλεκτρικές μετρήσεις. Τα πηγάδια δημιουργούνται με την χρήση μιας φωτοευαίσθητης ταινίας, της ORDYL SY 300, στην οποία πραγματοποιείται φωτολιθογραφία με την έκθεσή της σε υπεριώδη ακτινοβολία. Συγχρόνως, η ταινία λειτουργεί και ως μονωτικό στρώμα που προστατεύει τα μέρη του αισθητήρα που καλύπτει από τυχαίες φθορές, οι οποίες είναι πολύ εύκολο να συμβούν, καθώς το μέγεθος του βιοαισθητήρα είναι πολύ μικρό, κάτι που τον καθιστά αρκετά ευαίσθητο σε φθορές.

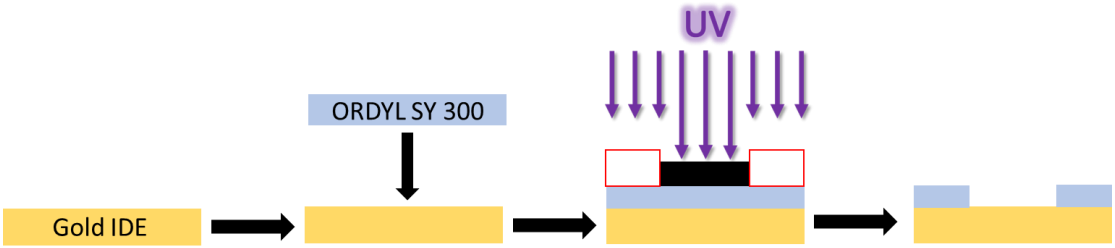

Πέρα από την βελτιστοποίηση του βιοαισθητήρα και το πακετάρισμά του, σε αυτό το Γ μέρος περιγράφεται και η διαδικασία πακεταρίσματος του ηλεκτρονικού κυκλώματος ανάγνωσης, ώστε να μπορεί να χρησιμοποιηθεί σε πραγματικές συνθήκες, χωρίς να υπάρχει ο κίνδυνος για φθορές στα ηλεκτρονικά. Συγκεκριμένα, με την χρήση τρισδιάστατης εκτύπωσης σχεδιάζεται και δημιουργείται αρχικά μια διεπαφή μέσω της οποίας ενώνεται ο βιοαισθητήρας με το κύκλωμα μέτρησης, αλλά και μια προστατευτική θήκη για το κύκλωμα.

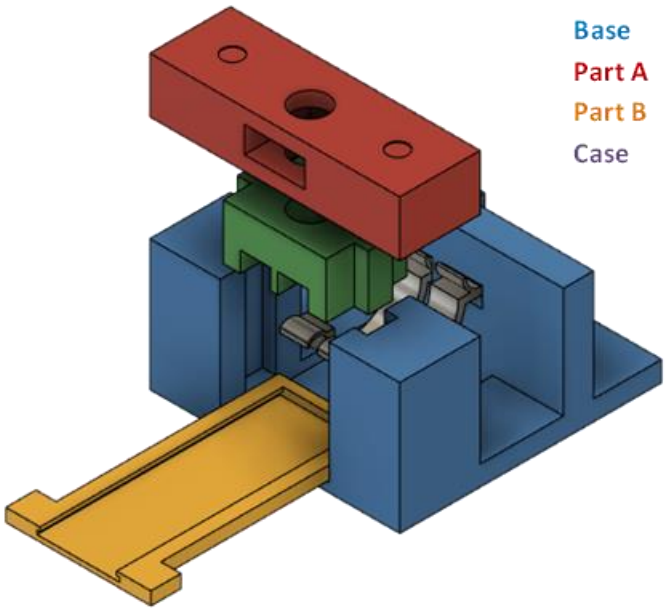

Λόγω του μικρού μεγέθους του βιοαισθητήρα, ήταν σημαντικό να σχεδιαστεί μια διεπαφή μέσω της οποίας θα μπορούν να γίνουν οι μετρήσεις με μη – καταστροφικό τρόπο. Έτσι σχεδιάστηκε μια θήκη στην οποία κουμπώνει ο βιοαισθητήρας και στην συνέχεια, δύο αγώγιμα ελάσματα ακουμπούν στα αγώγιμα άκρα του. Τα ελάσματα πιέζονται με την χρήση μιας βίδας, ώστε να διασφαλιστεί η καλή επαφή.

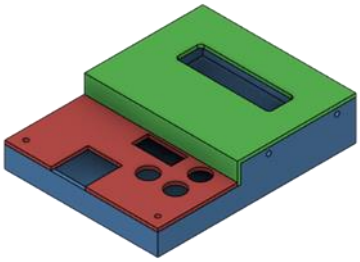

Η διεπαφή στην συνέχεια κουμπώνει πάνω στο ηλεκτρονικό κύκλωμα μέτρησης, δημιουργώντας έτσι μια πλήρη φορητή συσκευή. Από την θήκη του κυκλώματος μέτρησης προεξέχουν οι διάφοροι διακόπτες του κυκλώματος, καθώς και η οθόνη LCD στην οποία εμφανίζονται οι μετρήσεις, ενώ φυσικά υπάρχει και μια εσοχή στην οποία τοποθετείται ο πομπός Bluetooth.

Acknowledgements

For the completion of this PhD thesis, I would like, first of all, to thank the supervising Professor Dr. Evangelos Hristoforou, not only for the opportunity he gave me to deal with this specific topic, but also for the trust he showed me and his valuable guidance.

I would also like to thank Angelo Ferraro for his constant guidance and the precious advice he gave me on a daily basis.

I also thank the members of the advisory and examination committee for their advice and suggestions, which contributed to the improvement of this thesis.

I thank all the members of the team of Laboratory of Electronic Sensors for the excellent collaborative environment and the beautiful moments we had these years.

I also thank the students who trusted me to supervise their undergraduate or graduate thesis. Some of the results of these thesis have been integrated into this PhD thesis. Especially, I thank Konstantinos Agiannis for his contribution to chapter 4 and Lampros Nestoras for his contribution to chapter 5.

I thank my colleagues, research workers and members of Panhellenic Union of Workers in Research and Higher Education (ΣΕΡΕΤΕ) who struggle to improve the daily lives of research workers.

I thank my friends who have put up with me all these years and have stood by me in difficult moments.

Most of all I thank my parents, my brothers and Nefeli for their trust, love, and constant support.

This thesis is dedicated to the memory of Professor Panagiotis Tsarabaris who passed away while a member of this thesis advisory committee.

Πίνακας περιεχομένων

List of Figures

List of Tables

1 Introduction

1.1 SARS-CoV-2

Coronaviruses are a large family of viruses. These are viruses that have an outer shell and carry a single-stranded RNA genome. They were named for their shape, reminiscent of a crown due to their outer perimeter bumps. Coronaviruses usually cause upper respiratory infections in humans, as they can also cause pneumonia.

SARS-CoV-2 was detected for the first time in December 2019 in the Wuhan area of China[1]. It is a disease associated with severe respiratory distress and has been renamed severe acute respiratory syndrome (SARS-CoV-2) by the International Committee for the Classification of Viruses. As the spread of the virus increased rapidly, the health agency classified the SARS-CoV-2 outbreak as a pandemic on March 11, 2020[2]. Research has shown that the baseline number of reproduction (R0) depends on each country and the actions it takes. The value of the reproduction number practically shows the number of people that the virus can be transmitted from one patient. Specifically, R0 in January 2020 was around 3.6 (before being applied in quarantine countries)[3]. When R0 price reported is higher than 1, it means that SARS-CoV-2 is spreading at an increasing rate in all countries.

Coronaviruses cause mild to moderate upper respiratory tract disease in both humans and animals. There have been two major outbreaks in recent decades, Acute Respiratory Syndrome Coronavirus (SARS-CoV) and Middle East Respiratory Syndrome Coronavirus (MERS-CoV). Phylogenetic analysis revealed that the SARS-CoV-2 virus bore greater similarities to SARS-CoV than to MERS-CoV. The viral pathogenesis of SARS-CoV-2 is still unknown, however studies have shown that SARS-CoV-2 uses the enzyme ACE2 as a cell entry receptor. ACE2 is also a well-known host cell receptor for SARS-CoV[4].

The main symptoms of SARS-CoV-2 are fever, dry cough and fatigue. In addition, more common symptoms are sore throat, diarrhea, conjunctivitis, headache and loss

of taste or smell. Finally, the serious symptoms of the virus are difficulty in breathing or shortness of breath, chest pain or pressure, and loss of speech or movement. Symptoms take an average of 5-6 days to appear from the time of infection; however it can take up to 14 days. It is estimated that 81% of the patients infected with SARS-CoV-2 develop mild symptoms (up to mild pneumonia), 14% severe such as shortness of breath and hypoxia while 5% develops critical symptoms such as respiratory failure, shock and dysfunction of many organs[5]. At least one third of patients do not show obvious symptoms, so they do not get tested and transmit the virus[6], [7]. People who are positive for the virus but do not have any of the symptoms of the disease are just as capable of infecting other people as those who have symptoms. In addition, the viral load in asymptomatic patients decreases at a slower rate than in symptomatic ones. Two of the main reasons for the rapid spread of SARS-CoV-2 are the many days until the onset of symptoms as well as the asymptomatic hosts.

Most people with COVID-19 eventually get over the disease. However, many experience symptoms of fatigue for a long time after they recover, for a period that can reach 6 months. This phenomenon is called long covid[8].

1.2 SARS-CoV-2 Structure

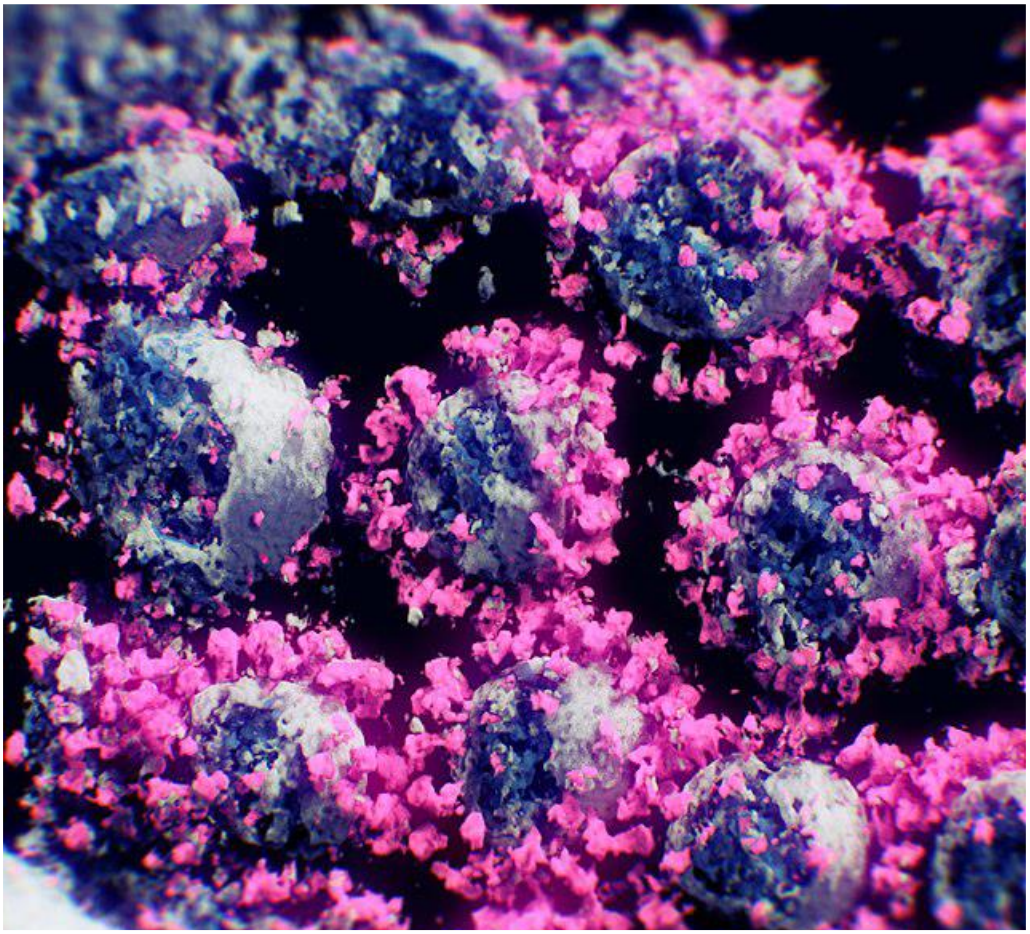

Figure 1. Photograph of SARS-CoV-2 using electronic cryotherapy[9].

SARS-CoV-2 is an enveloped virus that has a single-stranded RNA as its genome. The name of the coronavirus family comes from their characteristic crown-like shape and is due to the glycoprotein S (Spike, spike). Figure 1 shows the spike proteins in purple.

SARS-CoV-2 is a member of the Coronaviridae family and Nidovirales species. It is a member of the Coronavirinae subfamily whose members are divided into (a) a coronaviruses comprising human coronaviruses (HCoV), (b) b coronaviruses including SARS and MERS, (c) c coronaviruses comprising viruses from birds and whales, (d) d coronaviruses from birds and pigs. SARS-CoV-2 belongs to the β-coronaviruses[10]. It has an average diameter of 60 - 140 nm[11]. The virus particles are mainly oval in shape with spikes (S proteins) on their outer shell. Its genetic information is encoded by nearly 29,000 ribonucleotides. SARS-CoV-2 has in its outer shell the glycoproteins

S with which it can adhere to the surface of cells and then be able to enter them. In addition to glycoprotein S, SARS-CoV-2 contains transmembrane proteins M and E, as well as nucleoprotein N, which forms a viral ribonucleoprotein (vRNP) complex with viral RNA.

Many Coronaviruses use the glycoprotein S, which they have in their shell, to bind to cellular receptors. Protein S comprises subunits S1 and S2. The S1 subunit contains the receptor binding domain and is responsible for binding to cellular receptors while the S2 is responsible for fusion. Protein binding activates a number of events that lead to fusion between cell and viral membranes, resulting in the protein entering the cell. Studies have shown that the interaction of SARS-CoV-2 protein S with the ACE2 receptor causes the S1 subunit to cleave with ACE2, leading S2 to a steady state that is necessary to create the fusion membrane[12]. Figure 2 shows a schematic representation of a SARS-CoV-2 particle.

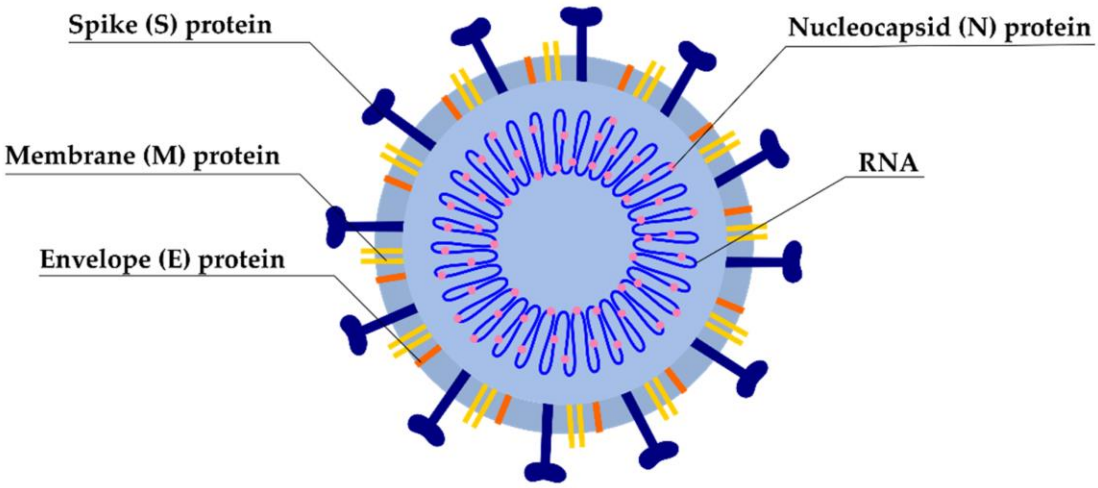

Figure 2. Schematic representation of SARS-CoV-2 particle structure[13].

Understanding the binding of the virus to the ACE2 receptor plays an important role in the vast spread of SARS-CoV-2, as well as in the control of the pandemic. This binding is due to electrostatic forces that develop between the virus S protein and the ACE2 receptor, as will be studied below.

1.3 SARS-CoV-2 Receptor

1.3.1 Virus receptors

SARS-CoV-2, like any virus, initiates its infection by attaching to a specific receptor on the surface of a sensitive host cell. The receptor prepares how the virus enters the cell. Therefore, the expression of the receptor in specific cells and tissues of the host is an important and determining factor in the entry of the virus into this cell[14].

In cell biology, a receptor is a structure in the cell membrane or inside the cell that binds to an infectious agent (e.g., a virus) to alter a function of the cell. Receptors are chemical structures, which are made up of proteins and their main function is to receive and transmit signals that can be integrated into biological systems. There are three main categories of receptors that can be distinguished by their action: signal retransmission, amplification or integration.

The main receptor for SARS-CoV-2 is the enzyme ACE2, which is found to a very large extent in the human body and especially in the lungs. This is why the spread of the virus is so great and a patient with this virus has mainly respiratory symptoms.

1.3.2 Peptides

Peptides are molecules that consist of two or more amino acids and are linked by peptide bonds[14]. Amino acids have a general structure R - CH (NH2) COOH. Amino acids are a monomer, which forms a polymer peptide chain with other amino acids. This binding occurs when the carboxyl group of one amino acid (-COOH) reacts with the amino group (NH2) of another amino acid, thus forming a covalent bond.

Peptides can function biologically on their own or they can act as a subunit for larger molecules. Peptides are in many cases the subunits of proteins as they are also important building blocks of enzymes, cells, hormones and body tissues.

Peptides are of medical interest, as they function as structural components of cells, tissues, antibiotics, etc. Also all proteins are made up of peptides, which makes peptides very important in organisms. Proteins are large peptides that contain up to 50 or more amino acids.

Peptides can be divided into several categories depending on their function as follows:

1. antibiotic peptides
2. Bacterial peptides
3. brain peptides
4. Cancer and anti-cancer peptides
5. Cardiovascular peptides
6. endocrine peptides
7. Fungal peptides
8. Gastrointestinal peptides
9. invertebrate peptides
10. opiate peptides
11. plant peptides
12. renal peptides
13. Respiratory peptides
14. vaccine peptides
15. Venom peptides

Finally, the name of the peptides depends on the number of amino acids they have, as well as their function.

1.3.3 Enzymes

Enzymes are substances that act as catalysts for a biological reaction. Their function does not affect the equilibrium constant of the reaction and does not bring about any chemical change, which would otherwise be unfavorable. Enzymes are usually proteins and act only to reduce the activation energy of a reaction, thus making the reaction much faster. Glucosidase enzymes, which hydrolyze

polysaccharides, increase the reaction with a factor of 10^{17}, thus achieving the reaction from millions of years in just a few fractions of a second[14].

Enzymes are classified into 6 categories depending on the type of reaction they catalyze:

1. Oxidoreductases catalyze oxidations,
2. Transferases catalyze the transfer of a group from one substrate to another,
3. Hydrolases catalyze hydrolysis reactions of esters, amides and related substrates,
4. Lyases catalyze the removal or addition of a small molecule such as water (H2O) from or to a substrate,
5. Isomerases catalyze isomerization,
6. Ligases catalyze the binding of two molecules.

The systematic name of an enzyme has two parts, ending in -ase. The first part identifies the enzyme substrate and the second part determines its class.

1.3.4 Angiotensin – converting enzyme 2

Angiotensin – converting enzyme 2 (ACE2) is an enzyme that is found on the surface of many cells and is responsible for making small proteins. Specifically, ACE 2 is attached to the cell membranes of cells located in the lungs, arteries, heart, kidneys and intestines. ACE 2 is abundant in the lungs and is found in type 2 pneumocytes. Type 2 pneumocytes are an important type of cell in the lung chambers that absorb oxygen and release carbon dioxide[15].

ACE2 is a vital element that is critical to regulating various processes in an organism, such as blood pressure, wound healing, and inflammation. ACE2 also helps regulate many activities of a protein called angiotensin 2, increasing blood pressure and inflammation. It also increases the damage to the lining of the blood vessels and the various tissue injuries. ACE2 practically converts angiotensin 2 to other molecules in order to compensate for the effects of this protein.

ACE 2 is present in all humans but the amount varies between individuals and in different cell tissues. Studies have shown that ACE2 concentration is higher in patients with hypertension, diabetes and coronary heart disease. ACE2 deficiency is associated with severe tissue damage to the heart, lungs and other types of tissue. As ACE2 is the major receptor for the virus, the main symptoms caused in a host by SARS-CoV-2 are in the organs that contain ACE2 in abundance, which are the lungs and the heart. Figure 3 shows the schematic representation of a cell which has the ACE2 enzymes externally and perimetrically[16].

Figure 3. Schematic representation of the ACE2 receptor[16].

1.4 SARS-CoV-2 entering to humans

1.4.1 Amino acid reactions

To understand how SARS-CoV-2 and ACE2 react, one must first refer to the protein-to-protein reaction. To study the reaction between proteins, the reactions between the amino acids should be considered. Amino acids can react in many ways. These reactions play a very important role in the structure of proteins[17].

The amino acids can be linked by a condensation reaction, in which a hydroxide (OH) is lost from the carboxylic group of one amino acid together with a hydrogen from the amino group of the second, as shown in Figure 4. In this way a water molecule is formed and thus the two amino acids are joined together by an amide, creating a peptide bond. When individual amino acids combine to form proteins, their carboxyl groups and amino groups do not act as acids or bases, as they have reacted to form the peptide bond. Thus a protein behaves as a base or as an acid, depending on the overall ionization characteristics of the individual R groups of the amino acids[18].

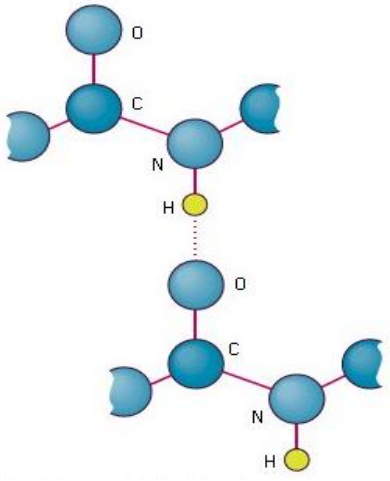

Figure 4. Schematic representation of an amino acid reaction[18].

Amino acids that bind after a series of peptide bonds form a peptide. Upon incorporation into a peptide, the individual amino acids are referred to as amino acid residues. A protein molecule is a polypeptide chain, which consists of many amino acid residues, with each residue attached to the next by a peptide bond. Lengths for

different proteins range from a few tens to thousands of amino acids, and each protein contains different relative proportions of the 20 typical amino acids. Thus proteins react with other proteins depending on the reactions that will result from the amino acids that make them up.

1.4.2 SARS-CoV-2 and ACE 2 binding

Studies have shown that ACE2 is the major receptor for SARS-COV viruses. Specifically, SARS-COV-2 can enter cells that have ACE2 and not cells that do not have this enzyme. The binding of these viruses is done with the assistance of glycoprotein S which they have in their outer shell. Studies reported below have shown that the binding of SARS-COV-2 to ACE2 is approximately 10 to 20 times greater than its binding to SARS-COV. Some transmembrane proteinases, such as TMPRSS2 and ADAM17, are also involved in this process as shown in Figure 5[19]. SARS-CoV-2 particles can use TMPRSS2 to initiate proteins in cell lines. Infected cells and inflammatory cells stimulated by viral antigens can produce pro-inflammatory cytokines and chemokines to activate immune responses and inflammatory responses to fight viruses. The combination of the virus membrane and the infected cell is activated after binding, as the virus RNA is released into the cytoplasm, thus creating infection.

ACE2 is expressed in almost all human organs. In the respiratory system, ACE2 is expressed primarily in type II cellular epithelial cells, but is poorly expressed on the surface of epithelial cells in the oral and nasal mucosa and nasopharynx, indicating that the lungs are the primary target of SARS-CoV-2.

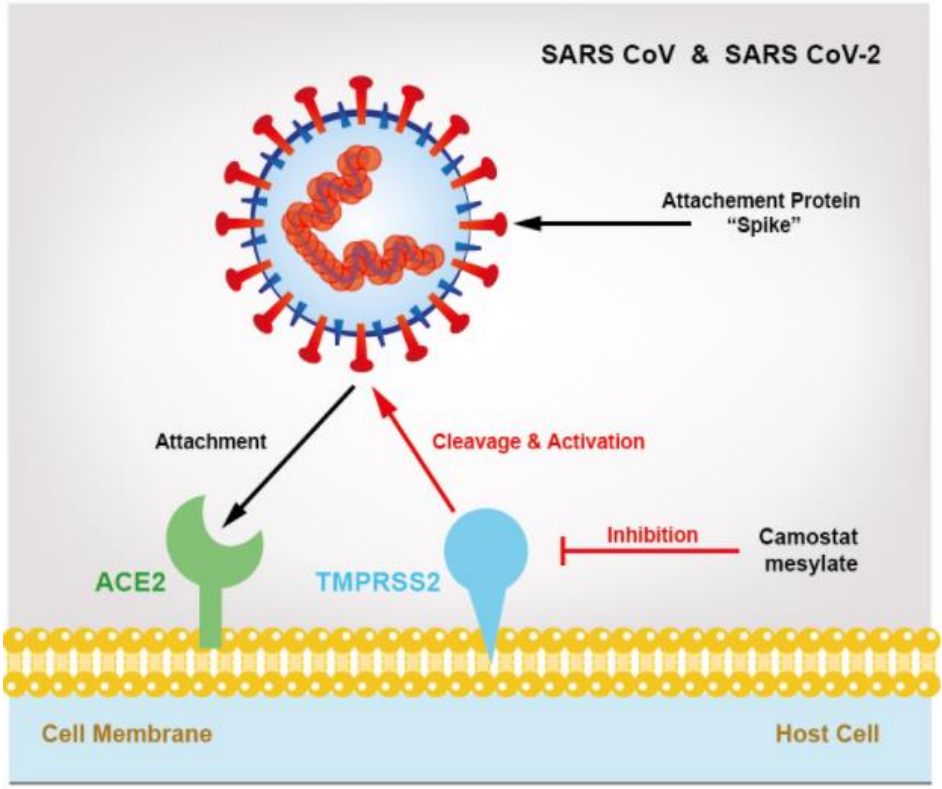

Figure 5. Schematic representation of virus and ACE2, TMPRSS2 and ADAM17 receptors[20].

1.5 Differences between SARS-CoV-2 and SARS-COV binding to ACE2

Although SARS-COV and SARS-COV-2 protein S have a very similar structure, the binding of SARS-COV-2 protein S to the ACE2 receptor is much greater than that of SARS-COV. This is probably the main reason why SARS-COV-2 is spreading faster than SARS-COV. In this case, explaining the differences between SARS-COV and SARS-COV-2 will help to understand how fast the virus spreads and how it affects human health.

In the study Spike Proteins of SARS-CoV and SARS-CoV-2 Utilize Different Mechanisms to Bind With Human ACE2[21] the electrostatic characteristics of the S protein binding of SARS-CoV and SARS-CoV-2 to the ACE2 receptor using the DelPhi program. The calculation was performed as this program solved the Poisson - Boltzmann equation.

$$\nabla \times [\varepsilon(\mathrm{r})\nabla\varphi(\mathrm{r})] = -4\pi\rho(\mathrm{r}) + \varepsilon(\mathrm{r})k^2(\mathrm{r})\sinh(\frac{\varphi(\mathrm{r})}{k_B T}) \quad (1.1)$$

Where ϕ(r) is the electric field,

ε(r) the dielectric function,

ρ(r) the charge density which depends on the atomic structure,

k is the Debye-Huckel parameter,

k_B the Boltzmann constant,

T is the temperature.

In the process of solving the Poisson Boltzmann equation the dielectric constants were set to 2.0 for proteins and 80.0 for water respectively. The protein filling rate was set at 70.0. The detector radius to create a molecular surface was 1.4 Å. The salt concentration was set to 0.15 M. The limit condition for the Poisson Boltzmann equation was set as a bipolar limit condition. Finally, according to DelPhi calculations, the resolution was set to 1 grid per Å.

Through the above equation, calculations were made for the electric fields generated by SARS-CoV and SARS-CoV-2 as well as the electrostatic forces that develop between the viruses and the ACE2 receptor, proving that the electrostatic forces between SARS-CoV-2 and ACE2 receptor are stronger[21].

1.5.1 S protein mutations between SARS-CoV and SARS-CoV-2

Figure 6 shows the main differences between SARS-CoV and SARS-CoV-2 in their binding to ACE2. The positions of these mutations have been mapped in Figure 6 using 4 colors, in a single chain of protein S. Red represents residues that mutate to be more negative, blue represents residues that mutate to be more positive, yellow represents residues that mutate from polar to hydrophobic and cyan represents residues that mutate from hydrophobic to polar. It is observed that most mutations are distributed on the surface of the S protein. It was also observed that the mutation of the RBD (receptor-binding domain) receptor binding site is located close to the interface with the ACE2 receptor. This observation reveals that the mechanism by which SARS-CoV binds to the ACE2 receptor may be slightly different from that of binding SARS-CoV-2 to ACE2.

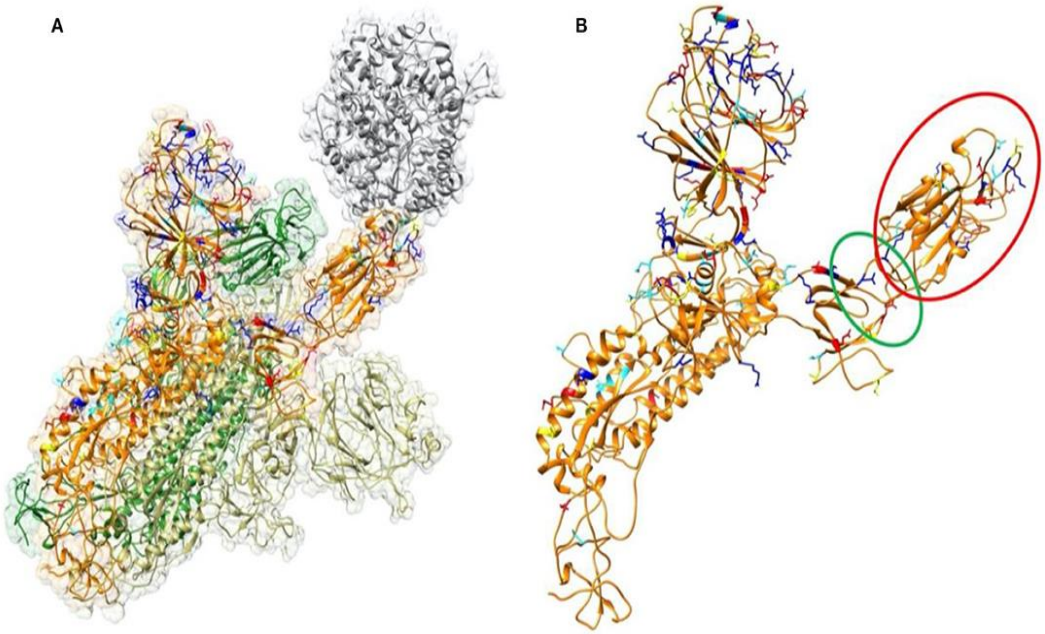

Figure 6. Structure of the S protein of SARS-CoV-2 and the ACE2 receptor. (A) The structure of S protein binding to ACE2. ACE2 is shown in gray. The three monomers of protein S are shown in yellow, orange and green respectively. Mutations of SARS-CoV and SARS-CoV-2 are presented in 4 colors. Red represents residues that mutate to be more negative, blue

represents residues that mutate to be more positive, yellow represents residues that mutate from polar to hydrophobic, and blue represents residues that mutate from polar to hydrophobic. (B) Structure of a single S. monomer protein. RBD appears in the red circle when it binds to ACE2. The green circular region indicates the compound between RBD and the rest of protein S[21].

1.5.2 Electrostatic binding forces between viruses and receptor

As already mentioned, the binding of SARS-CoV-2 and SARS-CoV to the ACE2 receptor is different. This is mainly due to the electrostatic forces that develop between the viral S proteins and the ACE2 receptor[21]. As shown in Figure 7, the surface of SARS-CoV-2 protein S is more positively charged than the surface of SARS-CoV protein S. Also the surface of the ACE2 receptor is for the most part negatively charged resulting in it being attracted more easily by the S protein of SARS-CoV-2. This is the main reason why SARS-CoV-2 is more contagious than SARS-CoV because there is a greater electrostatic interaction with the ACE2 receptor.

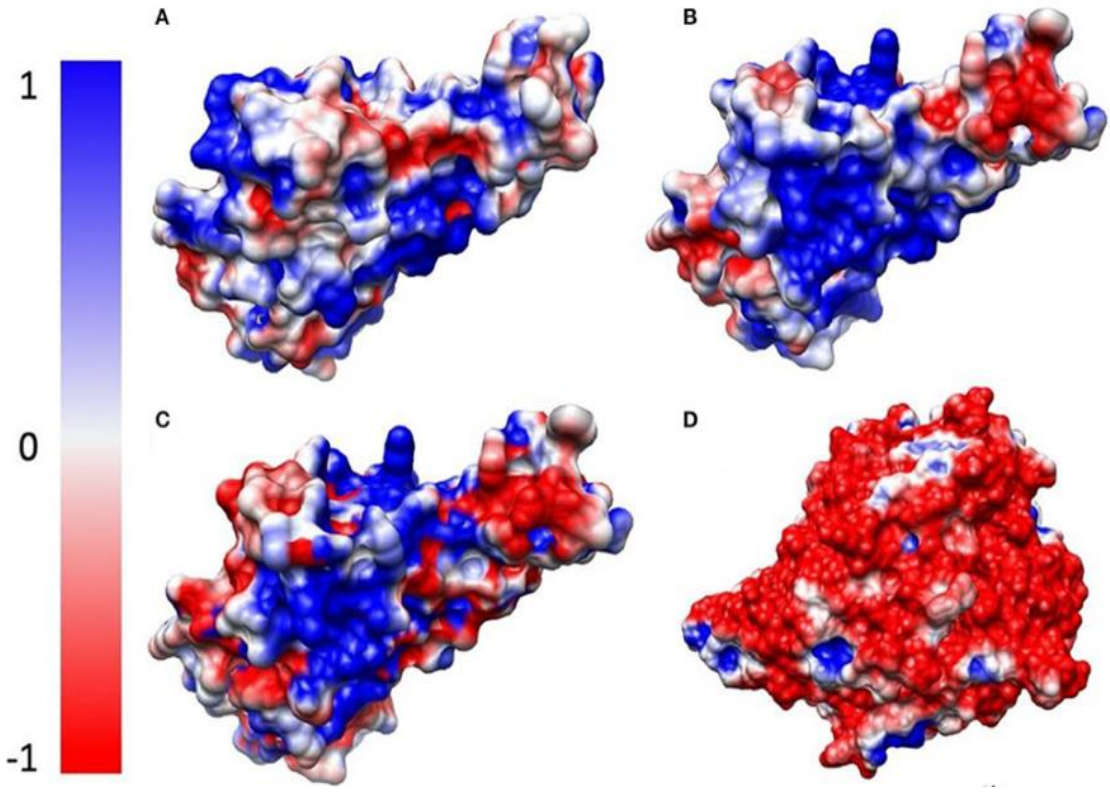

Figure 7. (A) Electrostatic surface of protein S, RBD of SARS-CoV, (B) Electrostatic surface of protein S, RBD of SARS-CoV-2, (C) electrostatic difference between proteins S, RBD of SARS-CoV and SARS- CoV-2, (D) electrostatic surface of human ACE2 receptor[21].

1.6 Main methods of SARS-CoV-2 detection

For COVID-19 disease caused by SARS-CoV-2, there is still not enough effective treatment. Vaccines developed a year after the outbreak of the pandemic have significantly reduced its spread, but not enough. New mutations in SARS-CoV-2 such as the Omicron mutation greatly reduce their effectiveness as it includes mutations in the S protein that they target[22]. In addition, vaccines have little efficacy in immunosuppressed individuals. That is why treatment ισ necessary.

Medications given to people with severe symptoms are mainly anti-inflammatory drugs such as dexamethasone, baricitinib and tocilizumab. Heparin, an anticoagulant, is given prophylactically to prevent blood clots. In addition, remedisivir is given as an antiviral drug that inhibits viral RNA polymerases. In case of bacterial pneumonia, antibiotics are also given[23].

As treatments and vaccines are not enough, an important weapon in dealing with the pandemic is the cheap and accurate detection of people with COVID-19, even if they have no symptoms. The 2 main methods used are nucleic acid amplification assays by polymerase chain reaction (PCR) and antigen-based assays.

1.6.1 PCR

PCR polymerase chain reaction is a laboratory technique for amplifying a DNA sequence using enzymes and without the use of a living microorganism such as the bacterium E.coli.

The reaction is divided into 3 stages[24]:

1. **Denaturation**: At this stage the mixture is heated to 94-98 ° C for 30-45 sec. This results in the cleavage of DNA molecules into 2 clones breaking the hydrogen bonds between the nitrogenous bases.
2. **Annealing**: The mixture is cooled to 50-65 ° C for 30-60 sec so that the primers hybridize to their complementary regions in the two chains.
3. **Elongation/extension**: The mixture is heated at 72 ° C for 30-120 sec during which DNA polymerase is ligated into the primers and then sequentially free nucleotides are added to form the complementary DNA

strand. Taq polymerase is usually used as a polymerase which is a temperature resistant polymerase derived from the bacterium Thermus aquaticus (Taq) which lives in very warm environments.

This process is repeated for many cycles and in each cycle the number of copies is doubled. Special machines called thermal cyclers are used to change the temperature in each phase of the reaction.

1.6.2 Real – time PCR

Real-time PCR is a laboratory technique based on PCR through which it is possible to quantify the initial amount of target RNA. Generally in PCR in each cycle the target genetic material is doubled. But this happens up to a point where there is saturation. To estimate the initial amount of DNA it is necessary to make the measurement in the area where the increase in the target genetic material is exponential. To achieve this, a fluorescent substance is used, which is usually the fluorophore, and using a camera, the number of amplified target DNA is counted in each cycle.

1.6.3 Real – time PCR test

Reverse transcriptance polymerase chain reaction (real – time PCR) is a method of detecting small amounts of RNA. When the COVID-19 pandemic broke out, the first virus detection tests developed were real – time PCR. These tests became the main way of detecting the virus[25]. Using the reverse transcriptase enzyme, the RNA we want to detect is reverse transcribed into a cDNA strand. Then, using real - time PCR, this DNA is amplified into millions or billions of copies and the initial amount of target RNA is estimated. The whole process last a few hours[26].

Real – time PCR can also detect viruses in an individual carrier. By taking a sample from the individual, the genetic material of the virus is detected directly, making the method highly specific. The sample for the real - time PCR test is taken from the nasopharynx or from bronchial secretions. It can also be taken by the oropharynx[27].

1.6.4 Antigen – based assays

A cheaper and faster test for the presence of a virus is the antigen test. An antigen is any substance that can elicit an immune response against it[28]. Antigens can be toxins, bacteria, viruses, or various other chemicals. Through the immune response, the body tries to produce antibodies that are specific for this antigen only. Rapid antigen tests are tests that look for an antigen from the surface of the virus. For SARS-CoV-2, the target antigens are usually proteins S and N, with a preference for protein S because there is less chance of false recognition of a virus related to SARS-CoV-2[29].

Acquiring a sample from the individual, it is placed in paper strips containing artificial antibodies to the target protein. The antibodies bind to the virus antigen and give a visual effect.

Although antigen tests are less sensitive than PCR tests because they do not multiply the target substance and demonstrate worse specificity, they are a very important tool for the course of a pandemic. As antigen tests are cheap and fast, they can be done en masse by identifying asymptomatic carriers and carriers with a high viral load leading to isolation.

1.6.5 Antibody test

A person who has been infected by a virus, after a period of about a week begins to produce antibodies. With antibody tests it is possible to assess whether a person has a history of SARS-CoV-2 or has enough antibodies to prevent future serious illness. The main types of antibodies produced are IgM and IgG. IgMs appear initially during the disease while IgGs later. Studies have shown that IgG antibodies decrease significantly after 2-3 months[30].

2 Theoretical Framework

2.1 Biosensors

2.1.1 Sensors

A sensor is a device that converts a macroscopic quantity, such as light, temperature, etc., into an electrically measurable quantity and then converts this electrical signal into a standard signal with certain characteristics[31]. The part that converts the macroscopic quantity into an electrically measurable signal is called the Converter, while the part that converts the converter's electrical signal into a standard form is called the Driving Circuit[32]. The inverter and the drive circuit are the sensor.

The inverter is the most basic part of a sensor, as it determines its characteristics. The inverter is constructed in such a way that changes in macroscopic size can cause a change in an electrically measurable quantity. The inverter alone is not a very reliable solution as a sensor, as usually the electrical signals it gives are of very low intensity. For this reason a sensor usually also consists of a mutant, so that there is a more stable signal. The stabilization subcircuit is part of the sensor driving circuit.

The last feature of a sensor is the shell in which it will be assembled (package). The packaging of a sensor is determined by the requirements of the environment in which it will be placed. Most often it is not only the sensor carrier but also the means of protection from the environment (high temperature, corrosive atmosphere, electromagnetic interference). Consequently, the characteristics of a sensor packaging can have a significant impact on the performance of the sensor itself, especially its response time.

Sensors are classified into different categories based on their function (for example, a temperature sensor, etc.) or the physical principle on which their operation is based (for example, magnetic resistance, etc.). The basic categories of

sensors are classified, based on the main form of energy carried by their signal, into the following types[33]:

- Mechanical sensors
- Electrical sensors
- Magnetic sensors
- Thermal sensors
- Radiation sensors
- Chemical sensors

The sensor that we will deal with in the present thesis is a biochemical sensor.

2.1.2 Biosensor classification

A biosensor is a device that measures the amount of chemicals of biological interest. The chemical we want to detect is called an analyte. Biosensors are used to monitor diseases, discover drugs, detect pollutants, pathogens and markers that are signs of a disease in the body[34], [35].

A biosensor consists of:

- The bioreceptor that is a molecule that interacts with the analyte. The bioreceptor is often an enzyme, antibody, cell or aptamer.
- The converter, which converts a biological or biochemical identification into a measurable signal. The output of the converter is usually an electrical or optical signal.
- The electronic driving circuit that reads the electrical or optical signal of the converter and performs the final measurement of the sensor.

2.1.2.1 Optical biosensors

Optical detection and measurement techniques have the ability to accurately obtain all the clinical properties of individual microparticles rapidly. Optical biosensors offer significant benefits over conventional analytical techniques as they allow the immediate, real-time detection of many biological and chemical substances. Their advantages are high specialization and sensitivity, fast detection. However, each of their numerous applications has its own requirements concerning the concentration, the production accuracy, the reuse time or the system cleaning.

Optical detection is performed based on the interaction of the visual field with a bio-recognition element. Optical sensors are based on the change in phase, polarization or frequency of the incoming light and this change is related to the detection or measurement process. An optical biosensor, in other words, is a compact analytical device that contains a bio-recognition element integrated in an optical transducer system. The main purpose of the sensor is to generate a signal

proportional to the concentration of a measured substance called an analyte. Various biological materials such as enzymes, antibodies, antigens, receptors, nucleic acids and tissues can be used as bio-recognition elements (Figure 8)[36], [37]. Optical techniques can be divided into two categories: label-free and label-based. In the former, the detected signal is generated directly by the interaction of the analyzed material with the inverter. Instead, the second category involves the use of a label and the optical signal is then generated by a colorimetric, fluorescent or luminous method[38].

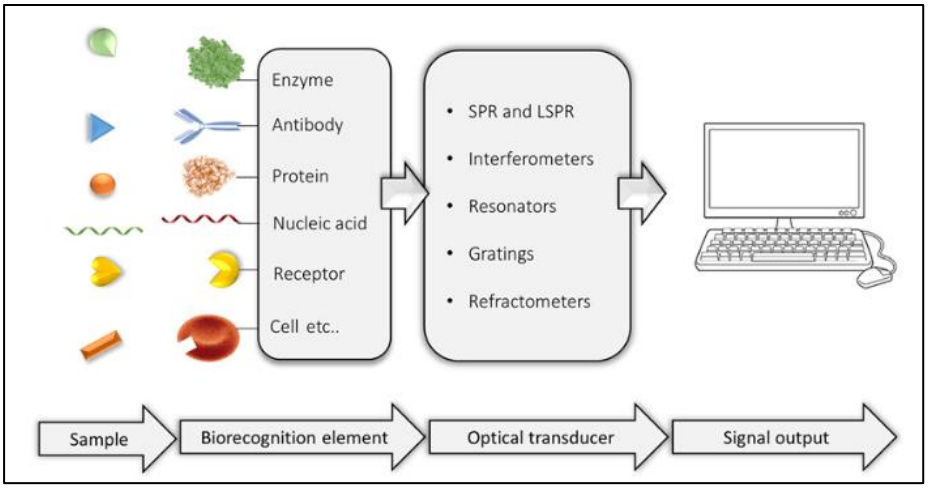

Figure 8. Schematic diagram of an optical biosensor[39].

2.1.2.2 Magnetic biosensors

Recently, magnetic techniques for detecting, measuring and identifying substances have emerged as a promising new technology platform for various sensors. These methods are generally based on observing the magnetic field of a magnetically labeled biomolecule that interacts with a complementary biomolecule attached to a sensor. Magnetic biosensors have several advantages. They are distinguished for their stability over time which is extremely important for labeling tests on tissues and organs while at the same time they do not present noise effects[40].

Magnetic nanobeads-MNBs or magnetic nanoparticles-MNPs are commonly used in magnetic biosensors. The magnetic core gives super-paramagnetic properties to MNBs, which cause them to move along dynamic lines under the

influence of an external magnetic field and disperse after its removal. The polymer shell imparts to MNBs various functions that allow them to be further modified with various desired biochemical materials for specific binding to biological targets. Magnetic nanospheres are characterized by excellent paramagnetic properties, highly specialized surface area, rapid reactions, good biological compatibility and these advantages are the reason why they have often been reported for biological labeling, signal amplification, or both in various biosensors[41].

2.1.2.3 Chemical-biochemical sensors

Chemical or biochemical sensors are devices that convert a chemical or biological quantity into an electrical signal. The structure of such a sensor consists of a position of selective recognition of an atomic, molecular or ionic substance associated with a type of inverter. This sensor aims to identify and analyze a substance, which is in gaseous or liquid form, as it may be in combination with many other substances. The transducer in the chemical sensors translates the presence of the selected analyte into a detectable physical signal, which can then be collected and interpreted. Their structure usually involves the direct interaction of part of the analyte with some real component of the inverter itself[33], [42], [43].

2.1.2.4 Amperometric Biosensors

Amperometry is the detection of the presence of ions in a solution based on the change in electric current. Such applications usually require a working electrode (microelectrode), a reference electrode, an auxiliary electrode, a voltage source and a device for measuring current and voltage. The amperometric method is based on the measurements of the changes in current passing through the electrode system over time, relative to the potential applied to the operating electrode. More specifically, amperometric biosensors operate by generating current when a potential is applied between two electrodes. The analyte is involved in a redox reaction followed by the measurement of current in an electrochemical cell. It has been shown that almost all biochemicals can now be detected amperometrically by their enzyme-catalyzed electro-oxidation or electro-reduction or their involvement

in a bio-affinity reaction that allows electro-oxidation or electro-reduction. The analyte being measured or the biomolecule involved is changing the oxidation state at the electrode and the electron transfer signal being measured is proportional to the amount of redox active substances at the electrode. In amperometry, changes in current are directly monitored as a function of time[44].

2.1.2.5 Capacitive Biosensors

Capacitance appears in the capacitor, an electrical element consisting of two separate plates, between which there is a dielectric material. In general, this concept describes how two conductive objects with a gap between them respond to a voltage difference applied to them. Capacitive sensors operation is based on changes in dielectric properties, charge distribution, dimension or shape, when the target (e.g. antigen / antibody complex) appears on the surface of an electrode[45]. Actually, in capacitive sensors, when a target molecule attaches to the receptor, the displacement of counter ions around the electrode leads to a change in capacitance. The greater the number of targets attached to the receptor, the greater the change in capacitance[46], [47].

A key advantage of capacitive sensors over other detection approaches is their ability to detect different types of materials in a simple 1-step way. They are also highly sensitive and have been used successfully in the field of substance detection as biosensors for the detection of proteins, nucleotides, saccharides or small organic molecules. However, they are affected by environmental conditions and require electronic signal reading and processing circuits suitable for any application. Their special disadvantage compared to other types of direct biosensors is that the immobilization of the bio-recognition layer is more critical. If it is not sufficiently insulated, ions can move through the mattress causing the system to short circuit, leading to a reduction or absence of the signal[45].

2.1.3 Affinity Biosensors

The sensor to be studied in the present thesis is a biochemical - capacitive sensor. Specifically, the sensor belongs to the category of affinity biosensors. These are sensors that consist of low molecular weight biospecific ligands, such as proteins, enzymes, nucleic acids and antibodies[48]. Cell membrane components, cellular organelles as well as whole cells can also be used in these sensors. Unlike biosensors that rely on the ability of inhibitors to bind to the receptor component and slow the conversion of the substrate to determine the inhibitor, affinity biosensors combine the principle of affinity with enzymatic amplification reactions. In this case, the binding is evaluated and not the analyst's chemical reaction. These are low-cost sensors and the use of low molecular weight ligands avoids the use of any radioactive material that would be needed in other sensors[46], [49].

2.1.4 Biosensor Characteristics

There is a wide range of characteristics that are of great importance for the evaluation of a biosensor. The most important are:[50]–[52]

1. Selectivity:

   Selectivity refers to the ability of the biosensor to detect a particular substance by making any other impurities. It is one of the most important features of the sensor as low selectivity leads to completely wrong results. A classic example of selectivity is the relationship between an antigen and an antibody in which an antibody is capable of binding to only one type of antigen.

2. Repeatability:

   Repeatability refers to the ability of a sensor to produce the same results in different uses under the same conditions.

3. Stability:

   A sensor has great stability when its result does not depend much on external conditions. Examples of external factors that may affect the measurement are temperature, humidity, radiation and dust. An additional influencing factor of the measurement is the reduction of the efficiency of the bioreceptor over time.

4. Sensitivity:

   The sensitivity of a biosensor is determined by the minimum amount of target chemical it can detect. In many applications, a sensor must be able to detect concentrations of even ng / mL. An example is the prostate-specific antigen (PSA) test where concentrations of 4ng / mL are associated with prostate cancer[34].

5. Linearity:

   Linearity is the characteristic of a sensor that shows whether it produces results that approach a straight line, ie it is of the form y = ax + b. Linearity is

a very important property when the processing of the signal produced is done with an analog circuit because it greatly simplifies its implementation. However, when processing digitally, it is easy to process even non-linear sensors using LUT (look up tables). A basic condition, however, is that the sensor output is monotonous.

2.2 Interdigitated electrodes

2.2.1 Interdigitated capacitor

Capacitors with interdigitated electrode structure have been studied in depth since the 1970s[53]–[56]. These are rectangular capacitors which consist, in addition to the two parallel plates, of a plurality of overlapping combs of electrodes with length L and width W at a distance G from each other, as shown in Figure 9. They are widely used in applications that include microwave integrated circuits[57], [58], acoustic wave devices[59] and dielectric thin film studies[60]. Also in recent years they are widely used in chemical sensors[61]–[64]. Dimensions of such capacitors are usually reported on a micro or nano scale[65].

When a voltage is applied between static and moving combs, attractive forces are developed which cause them to pull together. The combs are arranged so that they never touch each other, as then there would be no potential difference. The force developed is proportional to the change in capacitance between the two combs and increases with increasing number of combs, the gap between the teeth as well as with increasing tension.

The structure of these capacitors is usually preferred in chemical sensors due to the flat configuration of the electrodes and the electrodes do not block the diffusion of the analytes. For that reason the device has a small response time. The sensors that use these capacitors are usually made of an inert substrate, on which the two comb-shaped electrodes are formed. The electrodes are then covered on top with a sensitive layer, which is usually polymer[56], [62].

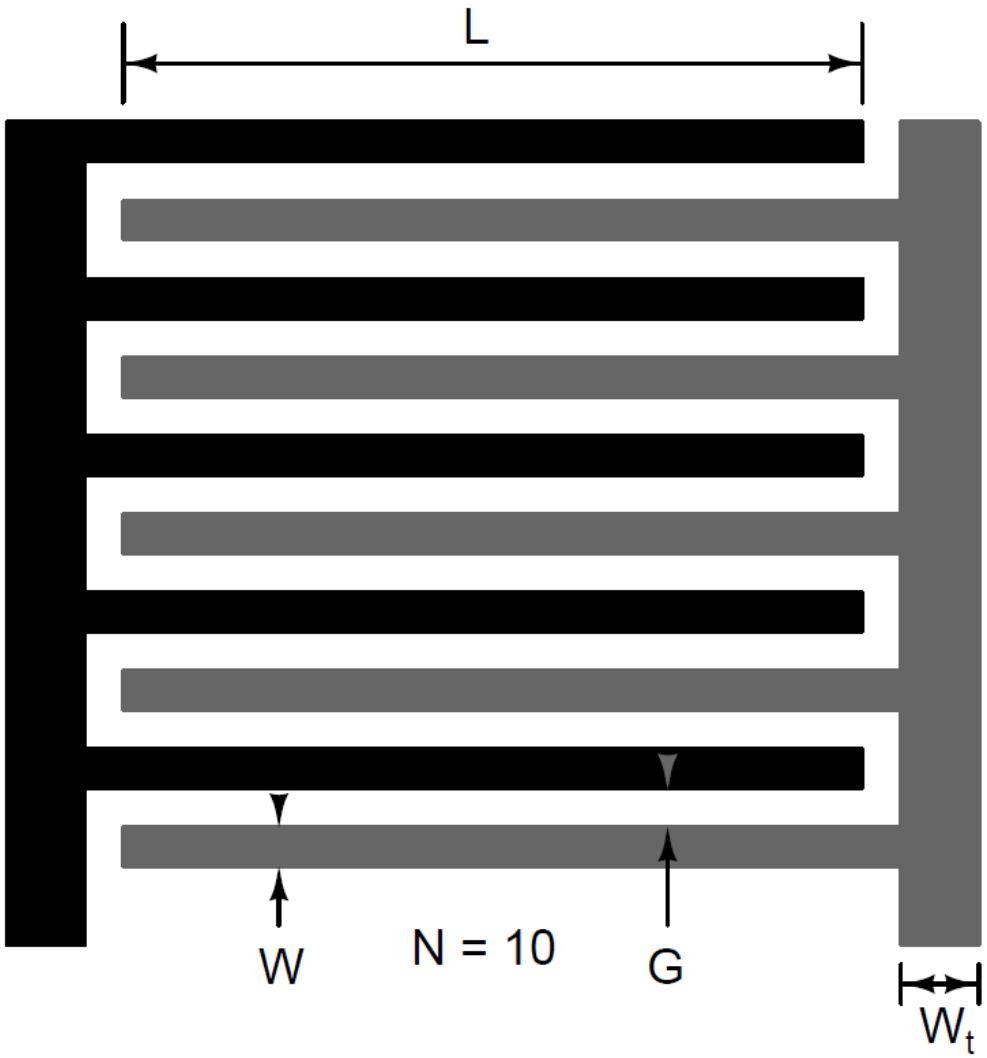

Figure 9. Interdigitated electrode capacitor.

2.2.2 Interdigitated electrode capacitance calculation

Important for the development of a sensor that utilizes such a capacitor, is the theoretic calculation of the capacitor characteristics. The capacitance of this capacitor is a complex quantity and is the sum of two capacitances, the capacitance created between the C electrodes (Normal Capacitance Between Beams) and the capacitance created by the end of each electrode with the Cf wall (Fringe Capacitance) Figure 10 shows the contribution of each capacitance in the system.

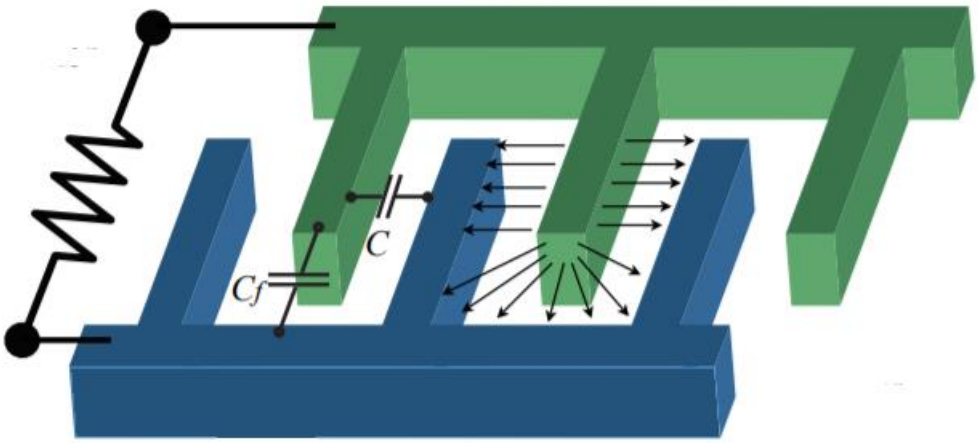

Figure 10. Representation of an interdigitated electrode capacitor when voltage is applied[57].

Therefore the capacitance of such a capacitor is given by the equation:

$$C_{tot} = C + C_f \tag{3.1}$$

Where the capacitance C will be given by the basic capacitance ratio of a capacitor:

$$C = \frac{\varepsilon S}{G} = \varepsilon_r \varepsilon_0 L_0 t \,/\, G \tag{3.2}$$

The contribution of C_f capacitance is significant and cannot be ignored. However, this capacitance is non-linear and changes with different initial and limit conditions. For example it depends on the length of each electrode as well as the length of the overlapping region L_0, as shown in Figure 11. As the distance between the electrodes from the edge increases, the capacitance C_f decreases, because the capacitance of a

capacitor is inversely proportional to the distance between the two plates. Various methods have been developed to calculate the relative capacitance. One way to calculate it is the Palmer equation:

$$C_f=\varepsilon \frac{WL}{g}(1+\frac{G}{\pi W}(1+\ln(\frac{2\pi W}{G})))x(1+\frac{G}{\pi L}(1+\ln(\frac{2\pi L}{W}))) \quad (3.3)$$

Where ε is the dielectric constant of the dielectric material($A^2 \bullet s^4 \bullet kg^{-1} \bullet m^{-3}$),

ε_0 is the dielectric constant of air,

ε_r the relative dielectric constant of the material between the electrodes,

L the length of the electrodes,

W the width of the electrodes

G the gap between the electrodes

G the gravity acceleration (m / s^2)

t the thickness of the electrodes,

x_0 the distance between 2 electrodes,

L_0 the depth of the overlapping teeth,

S the electrode surface (m^2).

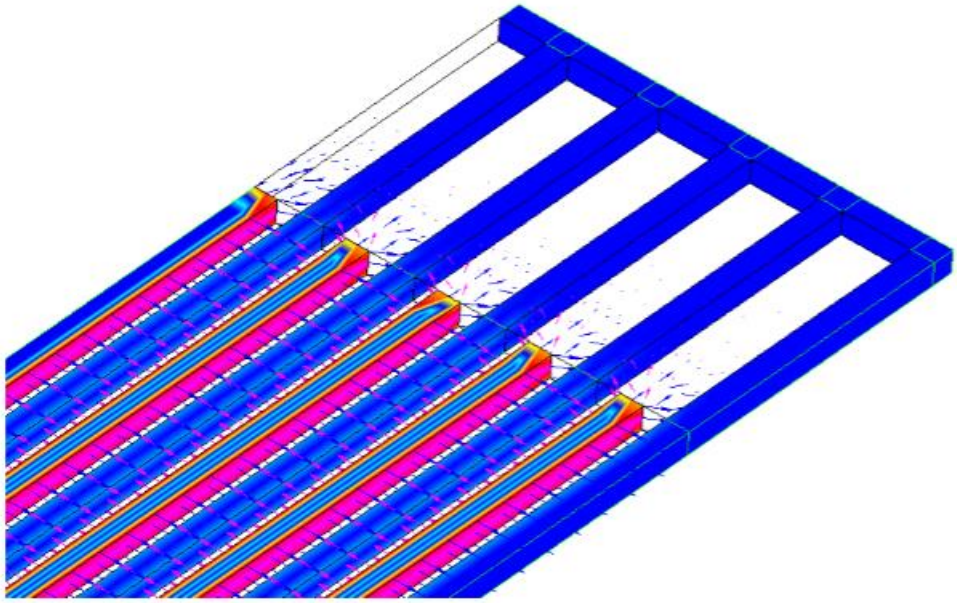

Figure 11. Electric field representation created inside an interdigitated electrode capacitor[57].

2.2.3 Resistive sensors with interdigitated electrodes

The resistance sensor bases its operation on measuring the change in the electrical resistance of a polymer detector (present on the sensor) in relation to changes in the environment. When the sensor is exposed to certain chemicals, there is a direct interaction between the polymer and the chemicals, resulting in a change in the properties of the polymer detection, such as an increase in the volume of the material or a decrease in its conductivity. The mechanism of interaction between substances and the polymer also determines the change of properties. During the exposure of the sensor to the gases two main phenomena take place: the polymer absorbs the vapors and swells, as well as the dielectric constant changes due to the presence of the gas inside the polymer matrix[64], [66]–[68].

Interdigitated electrodes are used a lot in these types of sensors[69]–[72]. Figure 12 illustrates the configuration of such a sensor. The electrode pair is placed on a tablet (usually silicon) based on a pattern and then the polymer is deposited. The placement of the polymer can be done by spin coating, or spray coating, or dip coating, or drop casting. This configuration maximizes the contact surface between the electrodes, the polymers and the chemicals. The two electrodes are usually connected to an external data processing unit to analyze the electrical and chemical changes of the sensor.

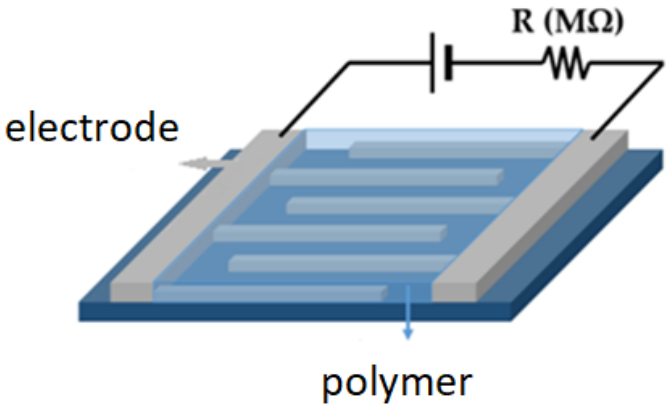

Figure 12. Schematic illustration of a chemiresistive sensor[69].

These sensors demonstrate several advantages, such as high sensitivity and short response time. In addition, sensor arrays can be fabricated using different conductive polymers to improve their selectivity. A very promising feature is their ability to operate at room temperature.

In addition, they are portable structures that can be easily moved and consume small amounts of energy. However, they are considered to have a short lifespan. In addition, depending on the detection material selected, the sensitivity of these sensors may be affected by the saturation effect of certain volatile organic compounds and humidity.

2.3 Impedance measurement circuits

2.3.1 Impedance

When operating linear circuits with sinusoidal excitations of the same frequency we make the following important observation. After an initial transition period, the voltages at all nodes of the circuit and the currents in all branches have a sinusoidal shape with the same frequency as the sources. That is, every voltage V and every current I can be written in the form $A\sin(2\pi ft + \theta)$. This is due to the fact that when solving the linear circuit, a system of linear differential equations with constant coefficients results. The system solution is a linear combination of a homogeneous solution that includes the term e^{-t} and a special solution that has the same form as the stimulation. As the homogeneous solution for a large t tends to 0, after a short time after the circuit is turned on the voltages and currents will take the form $A\sin(2\pi ft + \theta)$. The only unknown variables in this form are amplitude A and phase θ. When in the circuit the homogeneous solution becomes negligible, we say that it is in the sinusoidal steady state.

For the representation of variables of this form, most of the time, we resort to the use of complex numbers. So every variable of form $A\sin(2\pi ft + \theta)$ we assign it to a complex number of the form $Ae^{j\theta}$ a that is called a phasor, as illustrated in Figure 13. This complex number can be thought of as a vector of length A that forms an angle θ with the x-axis[73], [74]. With this mapping we can solve a linear circuit that is in the sinusoidal steady state, as if it were operating continuously, simply by doing operations with complex numbers.

But in order to solve the linear circuit, we must find a representation of the passive elements of the circuit, namely the resistors, capacitors and coils. We represent them with a size called impedance. It is denoted by Z and it holds that:

$$Z = \frac{V}{I} \tag{4.1}$$

That is, it has the same form as Ohm's law. V and I are voltage and current phasors respectively corresponding to the element. Each impedance Z element can be written as:

$$Z = R + jX \tag{4.2}$$

where R is the ohmic resistance and X is the reactive resistance of the element. For capacitors the reactive resistance jX is equal to:

$$Z = \frac{1}{j\omega C} \tag{4.3}$$

Whereas in coils it is equal to:

$$Z = \mathrm{j}\omega\mathrm{L} \tag{4.4}$$

Where:

$$\omega = 2\pi f \tag{4.5}$$

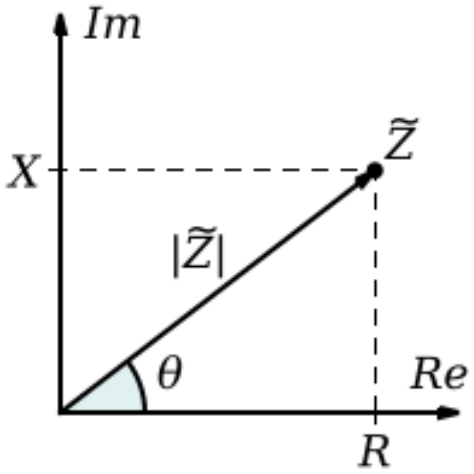

Figure 13. Phasor representation with vector

2.3.2 Lumped electronic circuits

vMost of the time, when studying electrical circuits we assume that all their elements are lumped. A system is considered lumped when the dependent variables we are interested in depend only on time. Instead the system is considered distributed when the dependent variables also depend on spatial coordinates[75], [76]. We make this distinction because lumped systems can be solved with ordinary differential equations while distributed systems require the use of partial differentials[77].In order for an electrical circuit to be considered as concentrated, we must accept the following assumptions[78]:

1. The change in magnetic flux φ_B over time outside a conductor is 0. That is,

$$\frac{\partial \phi_B}{\partial t} = 0 \tag{4.6}$$

2. The change in charge q over time within an element is 0. That is,

$$\frac{\partial q}{\partial t} = 0 \tag{4.7}$$

3. For the frequencies we are interested in, the transmission time of the electromagnetic waves in the circuit is much shorter than the wave period.

   Making these 3 assumptions we can derive Kirchhoff's 2 rules. For Kirchhoff's voltage law, from the Maxwell-Faraday equation we have that in a closed loop the voltage is:

$$V = \oint_{\partial \Sigma} \mathrm{E} \cdot \mathrm{d}\ell = -\frac{d}{dt} \iint_{\Sigma} \mathrm{B} \cdot \mathrm{dS} = -\frac{d}{dt} \varphi_B = 0 \tag{4.8}$$

   Kirchhoff's current law, on the other hand, is a direct result of the second assumption, since at a node it holds:

$$\sum I = \frac{\partial q}{\partial t} = 0 \tag{4.9}$$

With the third assumption, we make sure that the electromagnetic waves propagate momentarily, which is true when the maximum dimension of the circuit is much less than the wavelength of the EM waves at the operating frequency.

2.3.3 Real electrical components

Electrical components are never ideal. For example, all electrical conductors have parasitic resistance, capacitance and inductance. So, to model the real components we can use a combination of ideal components. Thus, the simplest electrical element, a conductor, can be modeled as a resistor with an inductor in series with it, as illustrated in Figure 14.

Figure 14. Simple equivalent conductor circuit.

On the other hand, a capacitor can be modeled as illustrated in Figure 15.

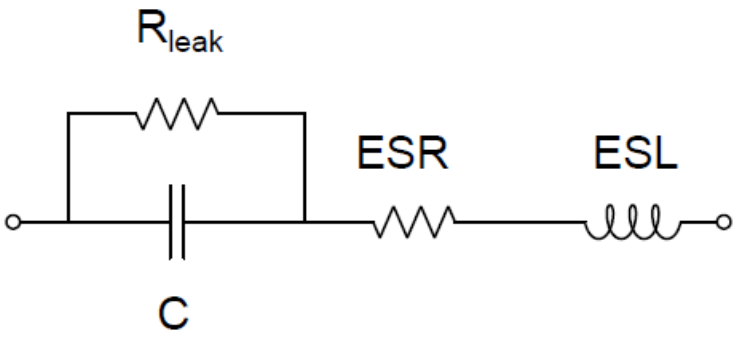

Figure 15. Equivalent real capacitor circuit.

In Figure 15, R_{leak} is the leakage current of the dielectric, ESR (Effective Series Resistance) its equivalent in-series resistance and ESL its equivalent in-line inductance.

But in reality a capacitor is a distributed element, which in order to study exactly we need to resort to the solution of Maxwell's equations or make use of a huge number of equivalent elements. But a model like the one above, in addition to being quite good in practice, greatly simplifies the calculations. This is why the solution of Maxwell equations is avoided whenever possible.

2.3.4 Parameter dependence on frequency

From the above equivalent circuit of the capacitor we can deduce that its impedance can be calculated as follows:

$$Z_c = ESR + jwL - R_{leak} // \frac{1}{jwC} \tag{4.10}$$

We observe therefore that the impedance of the coil for large w is greater than that of the capacitor, because as the frequency increases, the impedance of the capacitor decreases, while that of the coil increases. For the next operations we will assume that the R_{leak} is too large to simplify the operations. That is:

$$R_{leak} // \frac{1}{jwC} = \frac{1}{jwC} \tag{4.11}$$

Based on this assumption the capacitor has a capacitive character, i.e. the imaginary part of the impedance is negative when for f>0:

$$wL - \frac{1}{wC} < 0 \leftrightarrow w^2 < \frac{1}{LC} \leftrightarrow f < \frac{1}{2\pi\sqrt{LC}} \tag{4.12}$$

From the above equation we observe that each capacitor with the above equivalent model has a maximum operating frequency which decreases as its capacitance increases.

This frequency $\frac{1}{2\pi\sqrt{LC}}$ at which the capacitor ceases to have capacitive character is called Self Resonant Frequency (SRF)[79].

In addition the capacitance of Cx can be calculated from the formula:

$$-\frac{1}{wC_x} = wL - \frac{1}{wC} \leftrightarrow C_x = \frac{1}{\frac{1}{C} - Lw^2} \tag{4.13}$$

Therefore, we conclude that to measure the capacitance of a capacitor, we are interested in the operating frequency of the circuit, as its capacitance depends on it.

2.3.5 Quality factor

In a capacitor we want to have as little ESR effect as possible. For this reason we define a parameter, the quality factor Q[80], [81], which is defined as [82]:

$$Q = \frac{X_c}{ESR} = \frac{1}{2\pi f C R} \tag{4.14}$$

Where Xc is Im(Zc). The higher the value of Q, the closer the capacitor is to an ideal. The inverse value of the quality factor is the Dissipation Factor (DF) that equals to Q^{-1}.

2.4 Packaging - 3D Printing

2.4.1 Introduction to 3D Printing

3D printing is a method of processing, by which 3D objects can be developed by depositing successive layers of material. The materials used are usually polymer plastics, but in recent years ceramic as well as metal printers have appeared. As a process, although it is still in an evolving stage, we can say that it consists of three main parts[83], which will be analyzed in this section:

1. Design of the model in a specialized CAD software (Computer Aided Design)

2. Slicing of the model and production of G-code

3. Print the item and finish

The concept of 3D printing dates back to the middle of 1945, when it appeared in literary texts[84][85] but it was not until 1986, when Chuck Hull[86] was given the patent for the technology called Stereolithography (SLA - Stereolithography). He then founded the company 3D Systems®, through which the first 3D printer became commercially available (Figure 16) and which is still active in the field of 3D printing.

Figure 16. The first 3d printer[86].

The technological leaps from 1984 to the present, where 3D printers have become accessible, even at the amateur level, have been enormous. One of these was when in 1989 S. Scott and Lisa Crump founded the company Stratasys and filed a

patent[87] for a form of rapid prototyping, which they named Fused Deposition Modeling (FDM).

Until 2005, when Stratasys FDM patent expired, 3D printers were not available to the general public, but only to companies. At that time, two new initiatives were launched, the RepRap Project[88] and the Fab@Home[89], to develop and share this technology in order to make it accessible to a wider range of people.

The RepRap project was initiated in England by Dr. Adrian Bowyer at the University of Bath for developing a low-cost printer capable of producing its own components. All designs were free to the public, allowing users to make changes and alterations to the original design. This led to the rapid development of the first RepRap printer which evolved into many versions, as shown in Figure 17. The Prusa Mendel 3 was to become the basis for a huge range of printers called the i3.

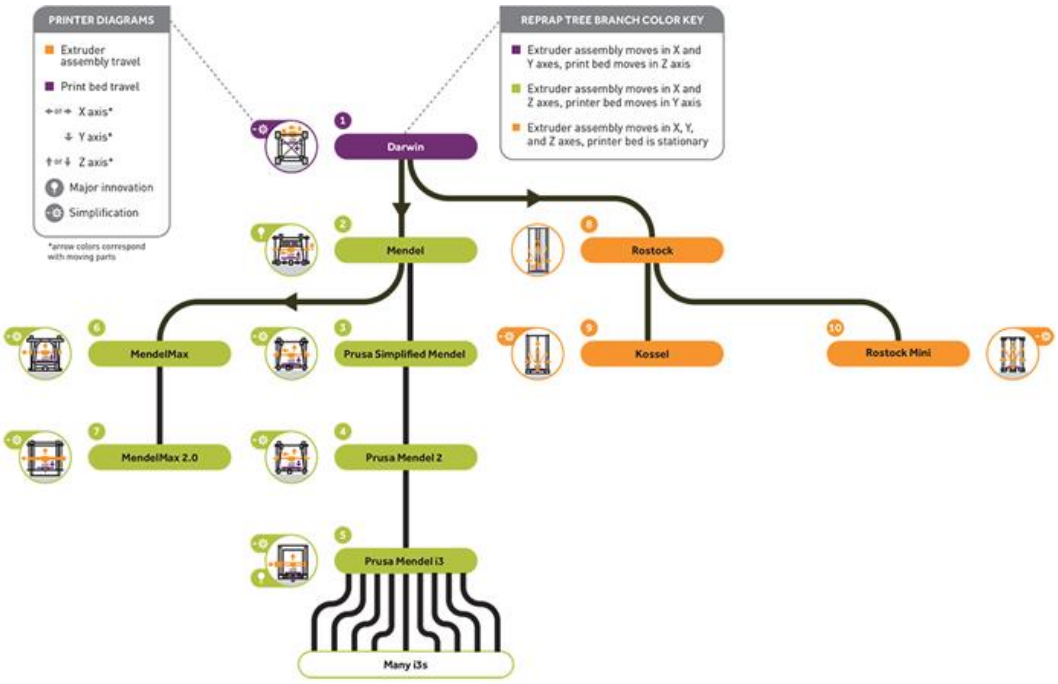

Figure 17. Evolution of RepRap printers[88].

The Fab@Home initiative had the same goal as the RepRap Project initiative, which was to create a customizable low-cost 3D printer accessible to the public. This project was developed by members of Cornell University and the first official version of the Fab@Home Model 1 3D printer (Figure 18) was released in 2006. Then, with the help of University students, the Fab @ Home Model 2 was released (Figure 18)

with major upgrades the easy assembly, the absence of electrical welds and the existence of fewer pieces[90]. In 2012 the project stopped, having achieved its goal, as 3D printers had already become accessible to every consumer.

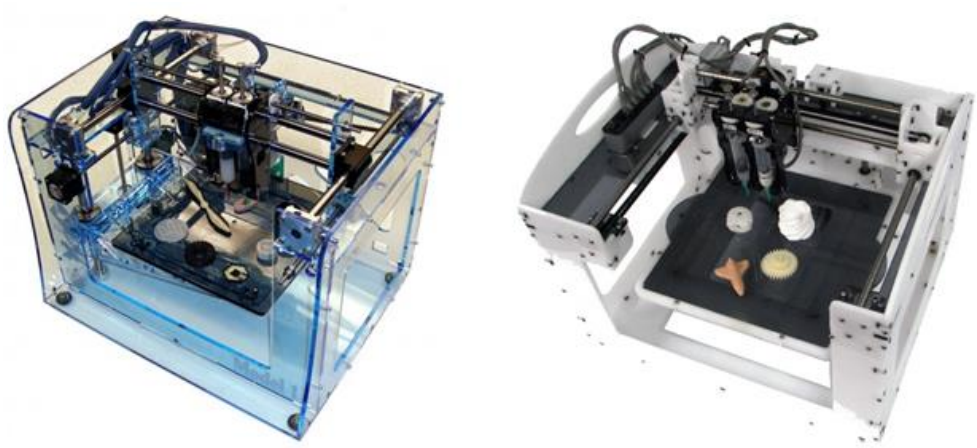

Figure 18. 3D printers Fab@Home Model 1 και Model 2[89].

2.4.2 Main types of 3D Printing

2.4.2.1 Fused Deposition Modelling (FDM)

This technology is the most popular and most affordable of all, as it is used in most commercial and non-commercial 3D printers. Thermoplastic polymers are used for printing. The resolution that can be achieved through this technique can be from 0.3mm up to 0.1mm, which depends mainly on the size of the printhead.

The process consists of 3 steps[91] as shown in Figure 19. In the first step, the thread, either through a PTFE pipe (Bowden) or directly enters the component called hotend. At the end of the hotend there is the nozzle, which is heated via an NTC thermistor to a suitable temperature, which depends on the material. The molten material is deposited on an also heated surface, the printing surface (hotbed). These two temperatures play a dominant role in the success of the treatment, as they contribute to the bonding of the layers with each other, but also between the first layer and the surface, so as not to create warping effects.

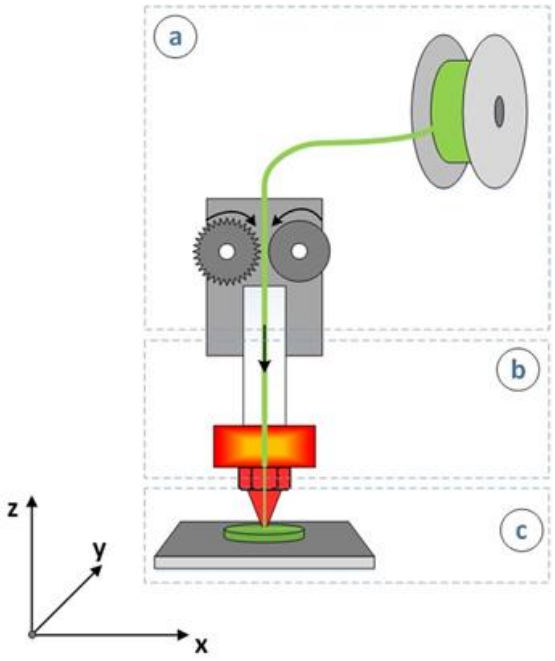

Figure 19. Steps of FDM 3d printing[92].

2.4.2.2 Stereolithography (SLA)

Stereolithography, invented by Charles Hull in 1984, is based on the controlled photopolymerization of fluid resins by means of a laser beam to create three-dimensional object[93]. The main difference of Stereolithography, compared to other 3D printing techniques is the high print resolution, which depends on the laser beam to be used. This method uses a photopolymer material inside a tank, which can be solidified upon exposure to a light source such as x-rays, or the predominant UV radiation, which aids in direct absorption by the resin and leads to faster photopolymerization[94].

The printing surface is immersed in this tank to a depth equal to the desired thickness and a laser head scans the appropriate areas of the surface as defined by the CAD drawing. It is then sunk to the thickness of the next section and this process continues until the object is completed. Finally, the printed object is placed in a washing and curing chamber.

2.4.2.3 Digital Light Processing (DLP)

The principle of operation of this technique is similar to Stereolithography, where the printing surface enters a tank of photopolymer material, but with the difference that a simpler form of light is used instead of a laser[95]. A digital projector flashes the cross-sectional image of the drawing to be printed, so curing is achieved simultaneously for all points.

2.4.2.4 Jetting Methods

The main materials for making objects through the method of binder jettingare polymers, metals and ceramics in powder form, while solutions of organic substances are used as bonding materials. The construction material, in powder form, is spread evenly over the printing platform and a printing head, which can and does move in the x-y plane, successively deposits the bonding material which is in liquid form, forming a layer[96]. Then the printing surface changes height and the above process is repeated.

Material jetting method is a 3D printing technology that works in a similar way to inkjet printers. The construction material is dispensed in the form of powder from a print head, near which there is a source of ultraviolet radiation[97]. The construction materials are thermosetting photopolymers in liquid form, which are solidified by the emitted ultraviolet radiation. The droplets that are sprayed are of the order of 100μm and because the curing takes place immediately, there are no oozing effects, resulting in the production of objects of high precision and smooth surface.

2.4.3 3D Printing procedure

This section discusses the procedures that must be done, so that from the CAD design we can arrive at the successful construction of a three-dimensional object, through the method of material deposition. The first step involves capturing the idea of the object to be designed and designing it into appropriate CAD software. Because there is a plethora of software, and therefore files, the 3D drawing is then converted to another file format, so that it can be sliced. In the present thesis, the conversion was done in .STL[98] (Standard Tessellation Language) format files, which converts

the drawing surfaces into a set of triangular seats. After converting the design to STL format, it is inserted into suitable slicer software to make the necessary adjustments, such as the thickness of each layer, the addition of supports, if necessary, and the print speed. The next step is to print and evaluate the print. At this stage, if the results are not satisfactory, we return to the slicing software to make the necessary changes. Finally, after the object is printed, it is finally processed, ie removal of unnecessary material, sanding and in some cases, painting.

2.4.3.1 Slicing

Before printing the objects, it is necessary to convert them to a suitable code, called GCODE[99]. It is a programming language that is also used in CAM (Computer Aided Manufacturing) processes for the numerical control of machines. Appropriate software is used to cut the 3D models. In the present work, the Simplify3D® software[100] (Figure 20) was used, as it is a shredding program used by many professionals and amateurs around the world.

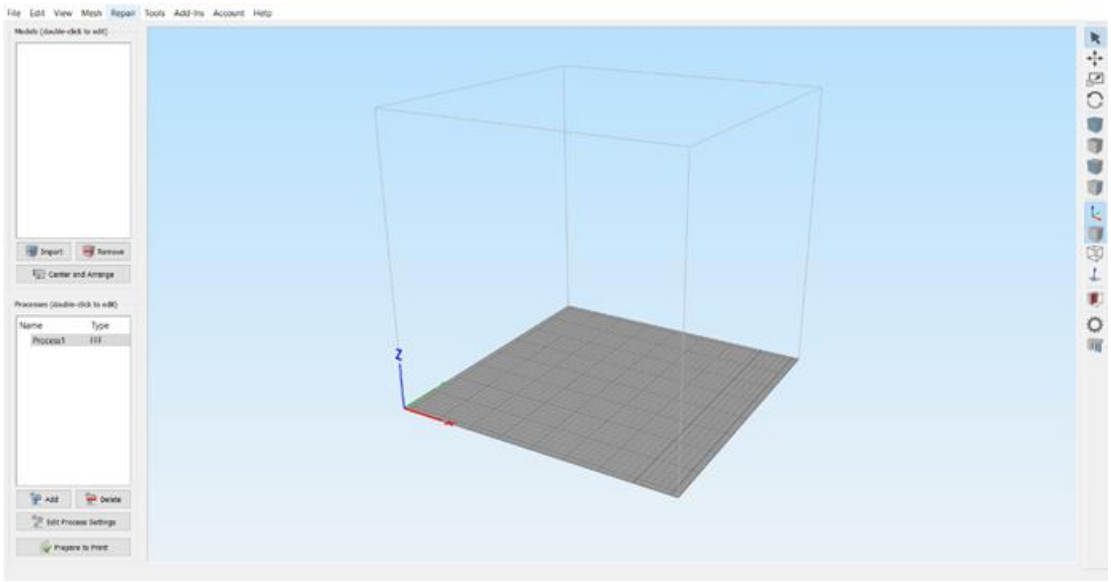

Figure 20. The Simplify3D® software.

2.4.4 3D Printing advantages

3D printing offers many advantages over conventional packaging techniques. Almost all geometric shapes can be made using 3D printing technologies, reducing

costs, as it is independent of the geometry of the object, unlike traditional techniques such as molding or welding techniques[101].

There is also a wide range of construction materials, as mentioned. These materials can differ in thermal and mechanical properties, depending on the needs of the device, but can also differ in texture, using threads with admixtures of wood fibers or carbon fiber.

Each design idea can be constructed directly and evaluated simultaneously, as different objects can be constructed simultaneously using either multiple printers or multiple heads.

Finally, the cost of buying a 3D printer is such that it allows the construction to be done internally, thus reducing the delivery time.

3 SARS-CoV-2 Biosensor

3.1 Introduction

Human susceptibility to certain viruses has been well-documented, and the effect of viruses on the human population varies from the relatively benign to deadly pandemics that may cause illness and loss of life. The 2020 pandemic caused by the spread of the SARS-CoV-2 has, to date, led to millions of reported deaths, and a major disruption of global commerce and economy, education and societal behavior in general. Transmission of the virus mainly occurs via airborne respiratory droplets or from contact with surfaces containing undamaged virus particles, also named virions. While viable tests for determining the presence of the virus in a human host have been developed, most of the methods used require either a significant amount of time to be completed or are implemented through complex and expensive methods.

The standard method that is used world-wide to detect SARS-CoV-2 is quantitative real-time PCR. This method is highly specific because it detects a portion of virus' genome. To perform this analysis multiple steps are required along with several reagents, enzymes and machines able to amplify the cDNA and at the same time measure fluorescent light. From the time samples reach the analysis center, at least 5-6 hours are required to obtain results. Despite the high accuracy and specificity, real-time PCR is an expensive and time-consuming method. The development of a quick and accurate detection assay is considered vital aiming to control the possible sources of infection in order to design effective measures to prevent further transmission.

For this reason, the need to develop easy-to-use devices for cheap, fast and efficient detection has been emphasized[102], and electrochemical biosensors are proposed to fulfill this purpose[103]. Even though research aimed to find solutions for a rapid and reliable detection method has been boosted by the unprecedent effects of SARS-CoV-2 on global economy, up to this point few devices have been developed for the detection of the of native virus particles[104]–[108], including

biosensors like lateral flow devices (LFID) and enzyme linked immunosorbent assays (ELISA). However, what seems to be more exciting is the detection of certain biomarkers associated with SARS-CoV-2[109].

It is well known that ACE2 protein is the membrane surface receptor used by SARS-CoV-2 to bind and infect human cells[12], [110]. The binding happens through the virus' structural spike(S) protein, which has very high and specific affinity for ACE2 protein, as the virus is positively charged, whereas ACE2 is negatively charged[111]. In particular, the extracellular domain of ACE2 interacts with its N-terminal region with the receptor binding domain (RBD) of S protein[12]. Therefore, the use of ACE2 as binding element for native SARS-CoV-2 particles represents a marvel opportunity to set up a biosensor for rapid and efficient virus detection.

Interdigitated electrodes (IDEs) are simple and very sensitive which makes them one of the most favored transducers in the field of biological and chemical sensors[112]. They are used as capacitance or impedance biosensors for various applications[113]–[115], including virus detection[116]–[120]. IDEs have been also used for SARS-CoV-2 antibodies[108] and nucleocapsid protein[121] detection. Graphene IDE biosensors have also been developed, targeting S protein, based on its interaction with SARS-CoV-2 antibodies[122].

Interdigitated electrodes serve as the transducer, when used as capacitive biosensors. A receptor is immobilized on the electrode surface and the interaction of an analyte with it brings about a change in the material's dielectric properties or in the thickness of the dielectric layer[45]. The basic equation according to which the IDE capacitance changes is given by Equation (6.1) [62]:

$$C = \frac{\varepsilon_0 \varepsilon_r A}{d} \tag{3.1}$$

where ε_0 is the vacuum permittivity, ε_r is the relative permittivity of the medium between the plates, A is the electrodes' surface area and d is the distance between the electrodes. According to equation 6.1, when the distance between the electrodes increases, the total capacitance decreases.

In this thesis a label-free affinity-based capacitive IDE sensor is developed for detecting both recombinant SARS-CoV-2 S protein and the native virions themself with high sensitivity and selectivity in a total time of less than 2 minutes. ACE2 enzyme is immobilized on IDE surface and used as the bioreceptor for virus' S protein. ACE2 immobilized gold IDEs' surface serves as the transducer. When a SARS-CoV-2 particle or S protein molecule binds to ACE2 receptor a displacement of the counter ions around the capacitive electrode results in a decrease in its effective capacitance[123]. The higher the amount of virus molecules bound to ACE2 is, the greater is the decrease in the transducer's capacitance (and therefore the change of the total impedance), detected as an electric signal. At first, preparative experiments were conducted using SARS-CoV-2 S protein. In the second phase, analytical experiments were conducted using real virion containing samples obtained from hospitalized patients. The results of the biosensor testing of the samples were compared to the results of real-time PCR on the same samples.

3.2 Materials and methods

3.2.1 Materials

The sensor includes 2 separate components connected via electrical wires. The first component is the biological part which is able to physically interact with virions particles; the second is the electronic part that detects the interaction between the biological component and virion particles via changes of capacitance and impedance.

For the biological part, the following components have been used: the human extracellular domain of ACE2 protein with tags; the amino acid L-Cysteine in powder form; and reagents named MES, EDC and PBS.

ACE2 protein (InvivoGen, San Diego, USA) was dissolved in distilled water at a concentration of 50 ng/µl. SARS-Cov-2 Spike RBD (RBD) (InvivoGen, San Diego, USA) was dissolved in distilled water at a concentration of 25 ng/µl. L-cysteine (Sigma-Aldrich, St. Louis, USA) was dissolved in distilled water at a concentration of 25 mM. EDC (N-(3-Dimethylaminopropyl)-N'-ethylcarbodiimide) (Sigma-Aldrich, St. Louis, USA) at a concentration of 0.877 g/ml was dissolved in water at a concentration of 0.1 M. MES (2-(N-Morpholino) ethanesulfonic acid and 4-Morpholineethanesulfonic acid) was purchased from Sigma-Aldrich (St. Louis, USA). Cell culture grade PBS (Phosphate Buffered saline) was purchased from Gibco (Carlsbad, USA). Bovine Serum Albumin (BSA) (Sigma-Aldrich, St. Louis, USA) was dissolved in distilled water at a concentration of 50 ng/µl. Gold interdigitated electrodes were purchased from DropSens (Asturias, Spain), cat. N.: PW-IDEAU50. Each IDE has a finger width and spacing of 50 µm, with a total number of 70 fingers, a total electrode length of 7 mm, and electrode surface area of 8.45mm^2.

3.2.2 Grafting ACE2 protein on interdigitated gold surface

To clean the electrodes' surface, interdigitated capacitors were immersed in a solution of 100% isopropanol for 5 minutes and then rinsed in Milli-Q water. 30 µL (25mM) of L-Cysteine were placed on the electrode surface and let to form bonds between gold and the aminoacid's thiol groups. The reaction was stopped when all L-cysteine solution dried out and three washes were performed using PBS to remove

unbound material. Subsequently, a solution containing 5μL (50 ng/ml) of ACE2, 5μL (0.877 g/ml) of EDC and 10μL (0.1 M) of MES was placed on top of the L-Cysteine layer. Specifically, EDC and MES activate the carboxylic terminus (-COOH) of ACE2. Once active the carboxylic terminus of ACE2 reacts with the amine group (-NH2) of L-Cysteine forming a covalent peptide bond. Due to the cross reactivity between C- and N- termini of both ACE2 and L-Cysteine, unwanted covalent bonds were formed also among the C-terminal of L-Cysteine and the N-terminal of ACE2. After each step, the biosensor was rinsed 3 times in Milli-Q water, in order to remove unbound molecules from its surface. The IDE with immobilized ACE2 or L-Cysteine alone was covered with 20 μl of PBS and kept wet until its use (Figure 21). Some of the biosensors were kept standby for 7 days at 4 °C in order to be used for the biosensor stability calibration.

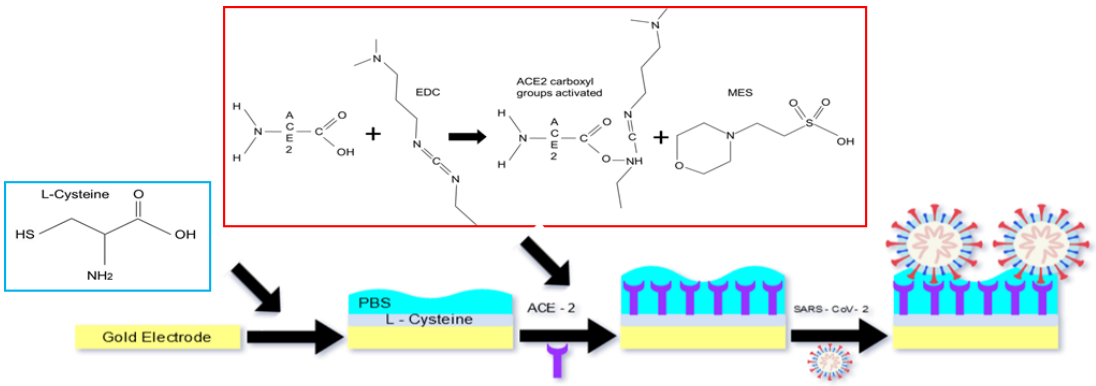

Figure 21. Schematic IDE ACE2-based Sars-CoV-2 biosensor.

3.2.3 SARS-CoV-2 biological fluid and clinical samples collection

For specimen's collection it was used the Citoswab transport medium VTM 3ml product code 2118-0019 and Citoswab collection swab product code 2122-0009 (WellKang, Dover UK). A total of 23 clinical specimens were collected from 22 subjects from Konstantopoulio General Hospital, a CV-19 Reference Hospital in Greece. All specimens had the suspected COVID-19 case definition set by the World Health Organization (World Health Organization, 2020). Sampling was accomplished to our premises with all the required precautions. Nasopharyngeal swabs were collected following the standard procedure to harvest nasopharyngeal fluids using sterile swab and transport solutions and they were subsequently placed in 2 ml of

transport medium. Specimen processing was performed in a class II biological safety cabinet using biosafety level three (BSL3) work practices. All samples were collected according to the safety standards by specialized personnel at the Konstantopoulio General Hospital (Athens, Greece).

3.2.4 Protocol used to measure Spike protein solutions and clinical samples

From each swab sample or solution containing S protein (various concentrations in the range 100pg/μL – 10ng/μL), 20 μl of sample were deposited in the interdigitated capacitor surface and the effective capacitance was monitored in real-time. The measurements were performed at room temperature and were extended for 1-2 minutes. The tests were performed in a blind-blind mode: the swab samples were tested first with the biosensor and then undergone real-time PCR tests. In order to examine the reproducibility of the experiments, each sample was demonstrated with 3 replicates. The capacitance values illustrated in the results section correspond to the average value measured, whereas the error bars correspond to the standard deviation. Capacitance measurements were performed using an HP LCR Meter (Hewlett Packard, model 4284A Precision). Two golden needles were connected with the LCR machine and they were placed at the pads of the capacitor. As the relative dielectric permittivity of the interdigitated capacitor is dependent on the testing frequency[112], a standard 1kHz frequency was selected with the amplitude of 50mV. For better display of results capacitance was normalized. That is, the capacitance values presented in the results section are divided by the maximum capacitance value of each experiment. For example, if the maximum capacitance value measured in an experiment was 700nF, then a 350nF capacitance would be equal to 0.5 or 50%.

3.2.5 Biosensor selectivity

In order to verify the biosensor's selectivity, a second IDE biosensor was covered with 20 μl of BSA solution and effective capacitance was measured. Subsequently, on top of a third sensor 20 μl of a solution (1:1) containing both BSA and S protein was added, and effective capacitance was measured. Solutions containing BSA, S protein

and both were let on the sensor surface for 20 minutes in order to ensure a proper reaction with ACE2. After this time period, PBS was used to wash the three biosensors and 20 µl of PBS were left on in order to avoid measurement errors due to water evaporation.

3.2.6 RNA extraction and real-time PCR

Nucleic acids were isolated from clinical specimens using an automatic extractor (GXT NA Extraction Kit DNA / RNA 200 virus). The RNA was converted to cDNA and subsequently amplified using the YouSeq® SARS-CoV-2 COVID-19 RT-qPCR kit (YouSeq, Winchester, England). The oligonucleotide primers and probes for specific detection of SARS-CoV-2 are designed to detect regions of RNA-dependent RNA (RdRP) labelled with ROX andenvelope protein (E) genes labelled with FAM of the SARS-CoV-2 genome. The kit also contains primers and probe (labelled with VIC/HEX) for detection of human RNA as an endogenous internal control for confirming specimen integrity, nucleic acid isolation, possible inhibitions reverse transcription, amplification and detection.

3.2.7 Standard Curve and Limit of Detection (LOD)

The real-time PCR with standard curve was generated by serial 10-fold dilutions of synthetic positive controls with known copy numbers (106 to 10 copies/µL) (YouSeq, Winchester, England). These dilutions were tested using 10 replicates and they were used as quantification standards to construct the standard curve by plotting the copy number against the corresponding threshold cycle values (Ct). For the biosensor standard curve determination, the biosensor response for 5 PBS solutions of 20µL was tested, each containing different concentrations of S protein (ng/mL).

3.2.8 Biomedical Ethics issues

The collection of clinical data was correlated with the laboratory research results and was conducted in such a way as to fully guarantee the patients' anonymity and personal data confidentiality.

3.3 Results and discussion

3.3.1 Interdigitated capacitance measurements and changes with Spike RBD protein

When interdigitated capacitor was measured with only air on its surface, its capacitance ranges on the scale of few pF. When measurements were performed on IDE containing PBS and L-Cysteine on top of the gold surface, a capacitance increase of about 350nF was observed. After ACE2 was immobilized on top of L–Cysteine monolayer, an additional capacitance increase of about 300nF was detected, bringing the total capacitance up to 650nF (figure 22). This increase in capacitance is justified by the fact that as a solution of proteins (ACE2) in PBS is added on the electrode surface, the dielectric constant of the material increases since chemical bonds are formed, resulting in a total capacitance increase[113], [114], [124]. Apart from that, the ACE2 protein and the bound S protein result in an additional resistivity, parallel to the pure capacitance, thus allowing for the monitoring of an effective capacitance or impedance of the sensing element. However, the measurements in the employed experimental apparatus were realized in terms of capacitance measurements and corresponding monitoring.

Initially, experiments were conducted targeting the SARS-CoV-2 S protein to verify the selectivity and the sensitivity of the biosensor. The addition of S protein (10ng/μL) and its binding to molecules present in the medium bind ACE2 molecules, results in an effective capacitance decrease since S proteins displace ions interaction with ACE2 molecules. L-Cysteine and ACE2 form stable chemical bonds (e.g. covalent bond) among them and with gold electrodes, whereas S and PBS interact with ACE2 with weak transient interactions (e.g. ionic or electric bonds).

As illustrated in Figure 22a, the sensor seems to be selective to S protein since, when electrical measurement was performed after 20 minutes, its effective capacitance was reduced by at least 10 % when a solution containing S protein was added on top of the sensor, compared to the absence of capacitance change when a solution containing BSA was added. Furthermore, the reaction seems to take place even when BSA is present in the S protein solution, confirming the selectivity of ACE2

protein for S protein. The calibration curve of the capacitance change due to different dilutions of S protein is illustrated in Figure 22b. Strong linear correlations (r2 ≥0.9778) were obtained between the S protein concentration and the biosensor capacitance change. The analytical decrease of the capacitance over time is illustrated in Figure 22c. The biosensor sensitivity to S protein is calculated at 750pg/μL/mm^2, since standard deviation of the blank solution is 0, 01 and the slope of the calibration curve is 0,0047μL/ng. The sensors that were kept standby for 7 days at 4 °C showed a similar response to the sensors used directly. The type A and type B uncertainty of the measurements of S protein was calculated. The formula of standard deviation was used:

$$\sigma = \sqrt{\frac{1}{n-1}\sum_{1}^{n}(x_i - \overline{x})^2} \tag{3.2}$$

Variance equals σ^2 and Margin of error equals:

$$\sigma_\chi = \sigma/\sqrt{n} \tag{3.3}$$

Where N corresponds to the number of measurements and x_i corresponds to each measurement. Degrees of freedom v, correspond to the number of independent measurements minus 1;

$$v = n - 1 \tag{3.4}$$

For type B uncertainty calculation, the same statistical procedure was repeated after ignoring the most extreme measurement.

Type A uncertainty:

σ = 0.065194
σ^2 = 0.004250302
σ_χ = 0.016833106
v = 14

Type B uncertainty (93,3%):

$\sigma = 0.060985$
$\sigma^2 = 0.003719184$
$\sigma_\chi = 0.016298956$
$v = 13$

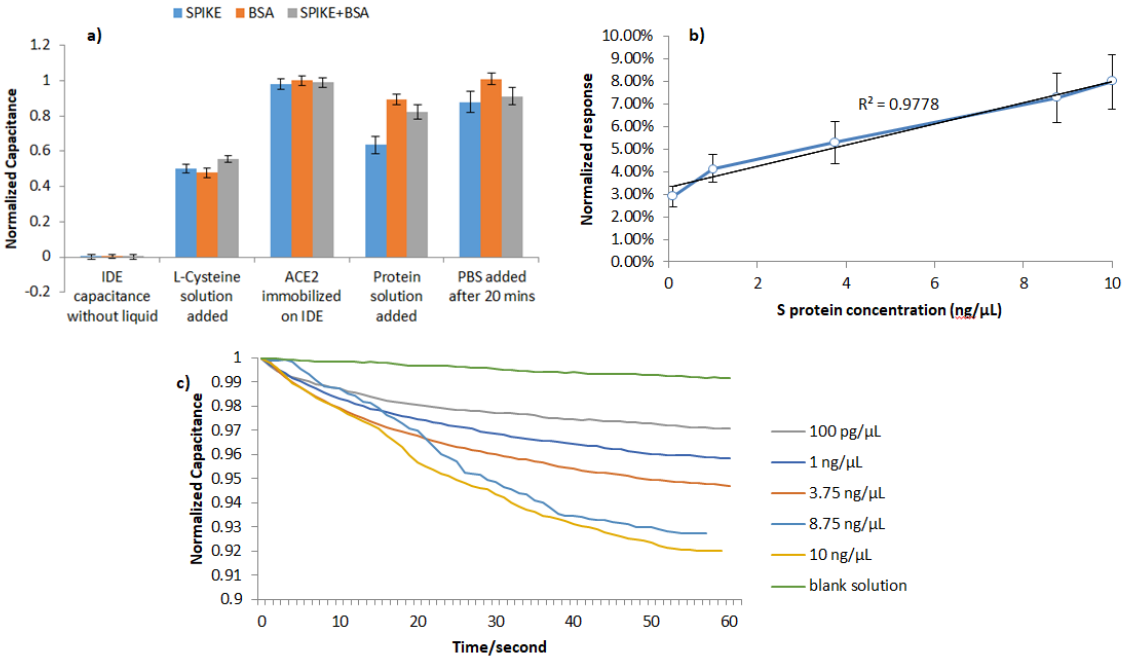

Figure 22. Capacitance changes with S protein. a) Selective response of the sensor towards BSA and S protein; b) Normalized response of the sensor for S protein; c) Real time detection of S protein.

3.3.2 SARS-Cov-2 virions detection

According to the real-time PCR method, 16 samples were negative and 7 of them were positive to SARS-CoV-2. It was observed that for negative swabs the effective capacitance was either increasing or slightly decreasing. In cases where the effective capacitance was decreasing, the range of such changes was very low, in the order of <1% respect to the initial value. The capacitance response over time of the positive to the virus samples and two negative samples with typical behavior is illustrated in Figure 23a, where the positive swab samples are divided into 2 groups according to the viral load. For the positive samples that had a viral load of at least 10^3 virus copy numbers/µL, it was observed that the effective capacitance was constantly and

quickly decreasing. However, for the positive swab samples with a lower viral load, the effective capacitance was slowly decreasing, and the total decrease was sometimes comparable to blank solution. Concerning negative samples, N1 response shows typical negative response, whereas N2 refers to a positive swab sample that was placed on a capacitor missing the ACE2 layer; therefore, it was observed that its behavior was similar to the ones of the negative samples. Figure 23b illustrates the total capacitance change caused by the positive swab samples, depending on the viral copy numbers/µL in each sample, according to the real-time PCR measurements.

To verify if the sensor response can be affected by the typology of sample collected from a positive patient, both a swab and a saliva sample were used, collected from the same positive subject. These samples were tested both with the real-time PCR method and the biosensor. Figure 23c illustrates the biosensor response for the 2 samples. Both samples were found by the real-time PCR to have a high viral load, leading to a reduction in capacitance, which was more evident in the swab samples with respect to the saliva one.

Type A uncertainty:

$\sigma = 0.040120475$
$\sigma^2 = 0.001609653$
$\sigma_\chi = 0.009456487$
$v = 17$

Type B uncertainty (94,4%):

$\sigma = 0.037882087$
$\sigma^2 = 0.001435053$
$\sigma_\chi = 0.009187756$
$v = 16$

Capacitance reduction can be explained in two ways: the first is related to the displacement of the counter ions because of S protein binding on ACE2, as reported in the literature[123]; the second is related to the decrease of ACE2 oscillation due to the applied electric voltage to interdigitated electrodes, caused by S protein or virus assembly on the ACE 2 layer.

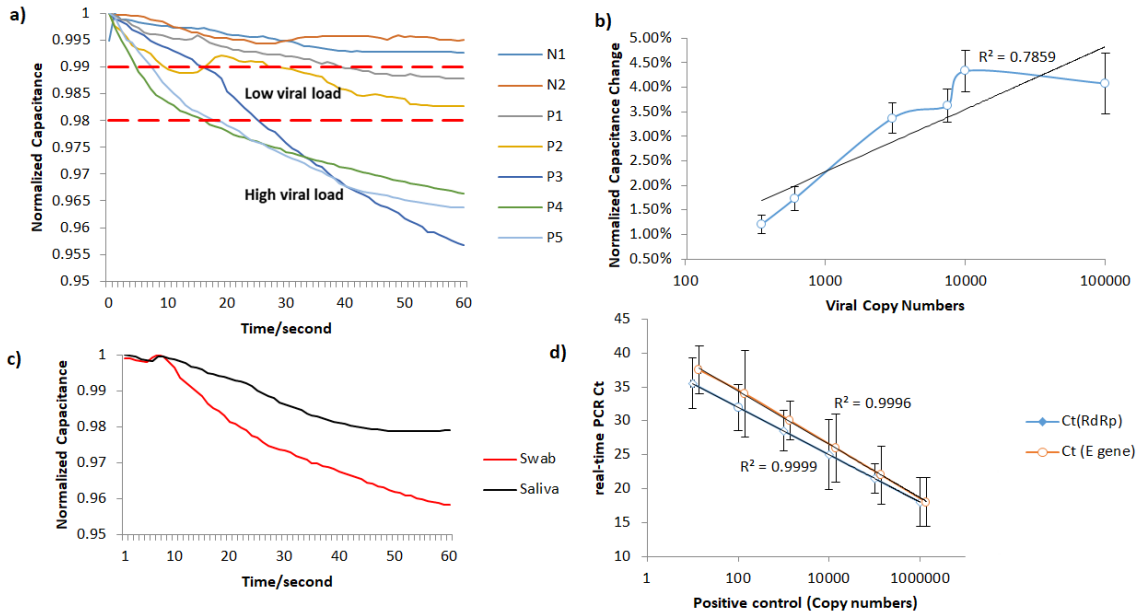

Figure 23. Sensor response towards SARS-CoV-2. a) Samples are distinguished in 3 regions; Negative to SARS-CoV-2, Positive with low viral load and positive with high viral load; b) Normalized response of the sensor for SARS-CoV-2; c) Capacitance change over time for swab and saliva sample of the same person; d) Calibration curve of Ct vs Virus Copy Numbers.

3.3.3 Results for real-time PCR

Table 1. Results for real-time PCR.

Sample	Ct(InternalControl)	Ct (R_dR_p)	Ct (E gene)
P1	29±0.2	31±0.2	32±0.1
P2	30±0.2	30±0.1	31±0.2
P3	26±0.1	25±0.2	26±0.1
P4	23±0.2	28±0.3	28±0.1
P5	26±0.1	27±0.1	27±0.2
Swab	27±0.2	18±0.2	18±0.3
Saliva	27±0.2	25±0.1	24±0.2

The linearity and efficiency of the real-time PCR were determined by generating a standard curve in which serial 10-fold dilutions of positive control were tested, as is illustrated in Figure 23d. The standard curve was generated by plotting the real-time PCR threshold cycle numbers (Ct) of each dilution against the known copy numbers of positive control. The resulting slope showed a linear relationship over 5 orders of magnitude, ranging from 106 to 10 copies/μL with a correlation coefficient R2>0.99. The detection rate was 100 % for up to 10 copies/μL having 10/10 replicates positive for E and RdRp genes.

Strong linear correlations (r2 ≥0.99) were obtained between CT values and transcript quantity. Assay reproducibility and repeatability was tested by using replicate 10-fold serial dilutions of the RNA transcripts evaluated for each dilution point in triplicate on three different days. At the lower copy detection limit for SARS-CoV-2 and assay reproducibility exceeded 95%.

As illustrated in Table 1, all positive RNA samples tested, were positive for the human gene which was included as internal control to evaluate the quality of clinical specimens (nasopharyngeal swabs and saliva) and nucleic acid extraction. The Ct Value of positive specimens ranged from 18 to 34 that corresponded to 106- 102 copy numbers. A 75% of the specimens tested comprised 106- 103 copy numbers of E and RdRp amplicons.

The developed biosensor benefits from using the natural receptor instead of antibodies[107], [122], as in this way it can be used to detect all strains of the virus. When compared to other SARS-CoV-2 biosensors based on interdigitated electrodes[108], [125], the novelty of this biosensor is related to its ability to detect directly the superficial viral S protein and not viral DNA or the antibodies produced against viral proteins.

When compared to classical biochemical tests used on rapid antigen tests which are only qualitative (visual observation), this biosensor benefits from its significantly faster response, as well as from the possibility to provide an electronic measurement which can be used to make quantitative estimation and can be shared and integrated with health-related databases.

However, when compared to antibody-based sensors for the rapid detection of SARS-CoV-2, this biosensor exhibits a slightly reduced sensitivity for the case of samples with viral load of less than 10^3 virus copy numbers/μL.

3.4 Conclusion

The objective of this study was to develop an antibody-free capacitive biosensor for the rapid detection of SARS-CoV-2 native virions. Even though at the time this study was concluded, several biosensors based on antibodies against S protein have been developed, they may fail in the detection of SARS-CoV-2 variants. Indeed, the majority of genetic changes are detected on distinct S protein domains and pose serious concerns also for the vaccine efficacy[126], which ultimately stimulates the production of Spike-targeting antibodies. Therefore, the biosensor was realized by immobilizing ACE2 protein on top of interdigitated electrodes, which binds with high specificity SARS-CoV-2 and with minor, but still consistent, other coronavirus like SARS-CoV-1[127], [128]. ACE2 may be the receptor used by other pathogens to infect the human body, but it was never intended the use of such sensor as solely tool to detect a SARS-CoV-2 infection. Indeed, the standard method to certify the presence of SARS-CoV-2 remains the real-time PCR. Therefore, this biosensor could be used for rapid screening in order to clearly differentiate negative subjects from potential SARS-CoV-2 positive subjects. It is worth noting to mention that the widely used rapid antigenic SARS-CoV-2 detection tests may also recognize other coronavirus species because most systems recognize the N protein (highly conserved among the beta-Coronavirus genus to which SARS-CoV-2 belongs) leading to false positive results[129], [130].

Using the real-time PCR method as a diagnostic standard, the results demonstrated that the biosensor was able to detect clearly the SARS-CoV-2 virion in about one minute, in swab samples with a viral load as low as 10^3 virus copy numbers/μL, or saliva samples with a viral load as low as 10^4 virus copy numbers/μL. Furthermore, the biosensor demonstrated good selectivity towards SARS-CoV-2 S protein, as it was not affected by the presence in the reaction of BSA protein.

4 Biosensor driving circuit with smartphone readout

4.1 Introduction

The standard method for virus detection is real-time PCR. Despite its high efficiency, real-time PCR is a time-consuming and costly method, which requires trained personnel and is not available in remote settings. Therefore, it is important to develop reliable devices for point of care (PoC) virus detection[102].

The most common devices used for PoC virus screening are rapid antigen tests, which, however, show much worse performance than real-time PCR[131]–[133]. An explanation for this worse performance can be given by the fact that the rapid antigen tests are based on visual observation of the results, meaning they only provide qualitative results that cannot be automatically processed[134]. Another explanation could be given by the constant mutations of the virus, which cause changes in its structure, such as in the winding domain of the S protein. These changes reduce the effectiveness of rapid tests based on antibody binding, as well as reduce the effectiveness of vaccines[126].

The problem of the visual-only observation and qualitative results could be solved by developing biosensors that can provide an electrical measurement, meaning a faster response time, improved sensitivity and the possibility of electronic processing of the results[103], [135]. The low sensitivity of antigen tests is primarily caused by the visual readout, because of the intensity of the colored mark that might be difficult to be observed. Additionally, the chemical reaction between the antigen and the ligand plays a role, especially when virus variants arise, changing the affinity between the targeted protein and the ligand[130]. The issue of virus variants affects less the real-time PCR test[136]. Generally, the real-time PCR test takes advantage of genomic regions that are less prone to mutations. Therefore, the real-time PCR test is able to perform properly, even in presence of mutations affecting, e.g. the S protein. Furthermore, since the basic principle of real-time PCR is the amplification of a few copies of virus' RNA, the sensitivity of such a test is superior to the antigen

test which relays only on the amount of antigen collected from the patient. The above-mentioned examples put the electronic biosensors in a better position since they can utilize all the information contained in the analyte and give quantitative results[137].

Electrochemical biosensors, especially, require simple instrumentation and are highly sensitive, cost-effective and can be miniaturized. These specifications make them an ideal choice for PoC screening tests[138], [139]. The possibility of electronic processing of screening tests results means that the spread of the virus in space and time can be controlled. With the use of electronic methods and internet of things (IoT), an effective control of the distribution of positive test cases in specific geographical areas, as well as in specific time intervals can be done[140], [141]. In fact, by storing the screening results data on a platform, statistical processing can be done, that may give indications for the improvement of the diagnostic tools themselves, but also for the improvement of the strategy for dealing with the pandemic[142].

Even though the development of various biosensors has been reported[104], [105], [107]–[109], only a few of them have been used as complete SARS-CoV-2 screening devices, especially as complete standalone platforms that perform the diagnosis and electronic processing of the result. Some examples of standalone platforms are the Lucira (San Francisco, USA)[143], [144] and Cue (San Diego, USA)[145], [146] devices which can perform an amplification of RNA virus. These two devices can deliver results in about 30 minutes, which is the minimum time required to perform a PCR test. While the operation of many biosensors can be proven in the laboratory, and achieve quite high levels of sensitivity and efficiency, the biosensors cannot be used in the struggle against the virus until they are tested in the field. There are quite a few challenges to overcome when attempting to convert an electrochemical biosensor to a PoC device, mainly concerning its stability and reproducibility, and its sensitivity to unprocessed real samples[147].

In the previous chapter, a label-free SARS-CoV-2 electrochemical biosensor based on the binding of the virus structural spike (S) protein to ACE2 protein was developed. ACE2 was immobilized in an interdigitated electrode (IDE) transducer,

and the binding of the S protein (or the virus through S protein) to ACE2 resulted in a change in the IDE electrical properties, hence its effective capacitance. Up to this point, there are cases of similar biosensors reported, that use ACE2 receptor to bind S protein[148]–[150]. However, while various very interesting biosensors are being developed with excellent results, there are not many reports on their conversion to PoC devices.

This is exactly what is demonstrated in this chapter. After developing the biosensor and validating its operation, a prototype electronic readout circuit for the sensor was developed, as well as an Android application that reads the biosensor results remotely through Bluetooth. In this way, a portable microcontroller-based electronic readout circuit was developed, which performs effective capacitance measurements. The screening test results are available at user's mobile phone within 2 min, in a friendly-to-use way.

4.2 Materials and methods

4.2.1 Biosensor Preparation

The biosensor preparation procedure was described at chapter 6. Gold interdigitated electrodes with an electrode length of 7 mm and an electrode surface area of 8.45 mm^2 were purchased from DropSens (Asturias, Spain). On top of the electrodes, ACE2 protein was immobilized. To verify the functionality of the device, S protein was placed on top of the biosensor, resulting in its binding to ACE2 and therefore a change in the electrical characteristics. Moreover, real virus samples acquired form hospitalized patients were used and the biosensor results for these samples were correlated with real-time PCR results for the same samples. ACE2 and S protein were purchased from InvivoGen (San Diego, CA, USA). All the chemicals used were purchased from Sigma-Aldrich (St. Louis, MO, USA).

4.2.2 Readout Circuit

In order to integrate the biosensor to a PoC device, the benchtop LCR meter (Hewlett Packard, model 4284A Precision) that was used in the laboratory should be replaced by a precision electronic circuit that is able to measure the capacitance, as well as the resistance of the biosensor. Such a prototype LCR meter was designed and developed. The circuit was able to measure capacitance, ranging from 1 pF up to 3 μF. The main parts of the design are shown in Figure 24.

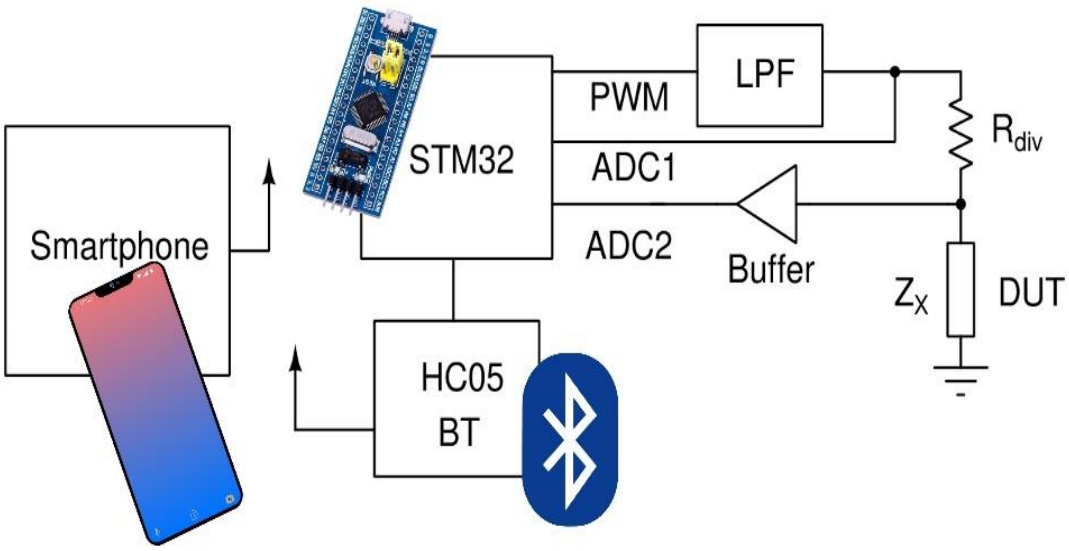

Figure 24. Working principle of the circuit.

The design utilizes an STM32 (STM32F103C8T6) microcontroller unit (MCU), able to generate a high-frequency Pulsed Width Modulated (PWM) signal, which is fed to a low pass filter (LPF). The LPF was designed as a second-order Butterworth filter[151] with a cutoff frequency of 13 kHz. The output of the LPF, which was either 1 kHz or 10 kHz sinewave, drove a voltage divider consisting of a known resistor and the device under test (DUT). By measuring the amplitudes of the ADC1 and ADC2 voltages, as well as their phase difference, we could compute the impedance of the DUT based on the following formulas:

$$Re(Z_x) = \frac{R_{div}|V_2|(V_1 cos(\varphi) - |V_2|)}{{V_1}^2 - 2V_1|V_2| cos(\varphi) + |V_2|^2} \quad (4.1)$$

$$Im(Z_x) = \frac{V_1 R_{div}|V_2| sin(\varphi)}{{V_1}^2 - 2V_1|V_2| cos(\varphi) + |V_2|^2} \quad (4.2)$$

where V1 is the voltage measured by ADC1, V2 is the voltage measured by ADC2, ϕ is the phase of V2 and the phase of V1 is 0.

In order to reduce the noise of the measurement, the amplitudes and phases of the fundamental frequency were computed using the formula of Fourier transform. The result was then calculated by averaging the readings over 512 measurements and normalized by dividing every measurement with the maximum measured value.

The measuring circuit was calibrated by measuring commercially available capacitors and resistors and comparing the results with those of specialized instruments. For capacitance measurement calibration, an Extech LCR Meter (Extech, model 380193) was used. For resistance measurements, a Keithley multimeter (Keithley 2000 Series) was selected.

4.2.3 Mobile Application

In order to emphasize the main advantage of the developed sensor, i.e. the fast acquirement of the final result, an accompanying mobile application was developed, which is able to provide the test results in real-time. The developed application is based on the Bluetooth communication between an Android smartphone and the sensor's board. The STM32 board lacks the ability of direct communication via Bluetooth. Hence, a transceiver module (HC-05), which was able to transmit data to the mobile ap-plication using the standard Bluetooth protocol, was added to the readout circuit. As a result, the Android application was able to display the detection of S protein in the tested sample in real time. A mockup of the developed application is illustrated in Figure 25.

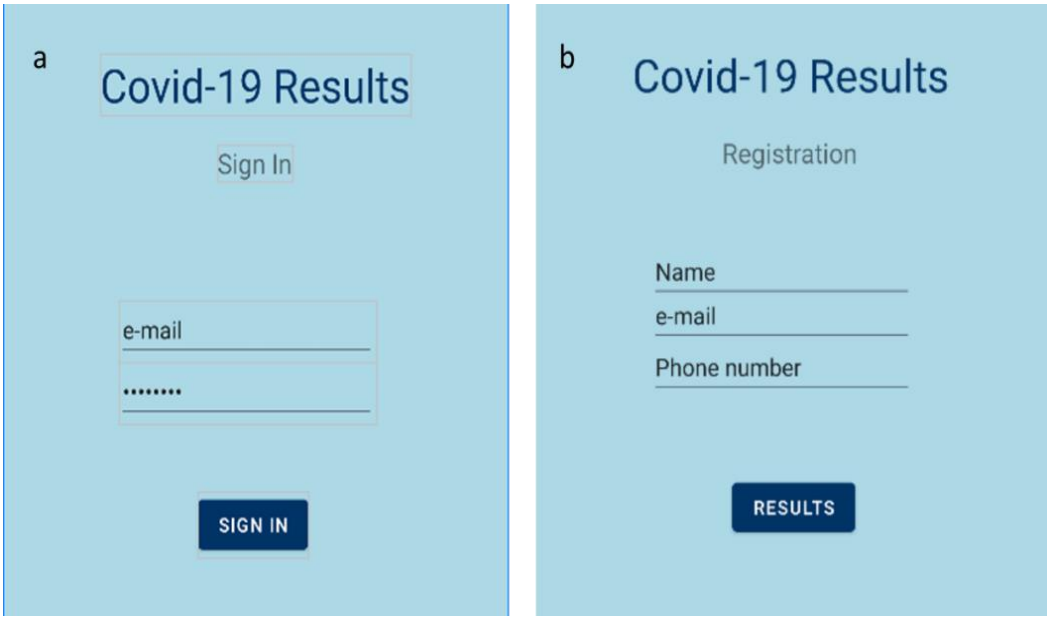

Figure 25. Mobile application's homepage; (a) sign in page; (b) registration page.

Java was selected as the programming language of the mobile application. The development was done using Google Android Studio[152]. The readout procedure is

the following: The smartphone pairs with the Bluetooth device, i.e. the HC-05 module. Then, the device can be selected through the Android application, in order to establish a connection between the two parts. When the connection is established, the application receives the appropriate data packets in JSON format, sent from the readout circuit. All the necessary information is stored in those data packets, such as the outcome of the measurement, the measured value and a timestamp. Finally, the test result (positive or negative) is displayed on the screen, after the user signs in to its personal account.

4.2.4 Swab sample collection and biomedical ethics issues

All nasopharyngeal swab samples were collected from hospitalized patients by specialized personnel at the Konstantopoulio General Hospital (Athens, Greece), according to hospital safety standards. The medium used for the sample collection was the Citoswab transport medium VTM 3ml (product code 2118-0019). Regarding the collection, the Citoswab collection swab (product code 2122-0009, WellKang, Dover UK) was used. The processing of the samples was performed in a class II biological safety cabinet using biosafety level three (BSL3) work practices. This research was conducted in such a way as to fully guarantee the patients' anonymity and personal data confidentiality.

4.3 Results and discussion

4.3.1 Readout Circuit Calibration

The developed prototype board is illustrated in Figure 26. The front side of the board is illustrated in Figure 26A. In the center of the PCB, the Blue Pill STM32 development board was placed, along with the HC-05 BT module on the left, the LCD screen on top and the DIP switches for selecting the suitable range below it. The device under test was connected on the left and right female pins of the three-pin connector at the bottom. Lastly, on the bottom right, there are three buttons responsible for specifying frequency and current range and for performing open-circuit calibration. The back side of the board is illustrated in Figure 26B. The total cost of the readout circuit was less than 20$ (MCU (7.5$) + Bluetooth module (6.5$) + PCB, electronic components, case (~5$)), which makes it extremely competitive in price.

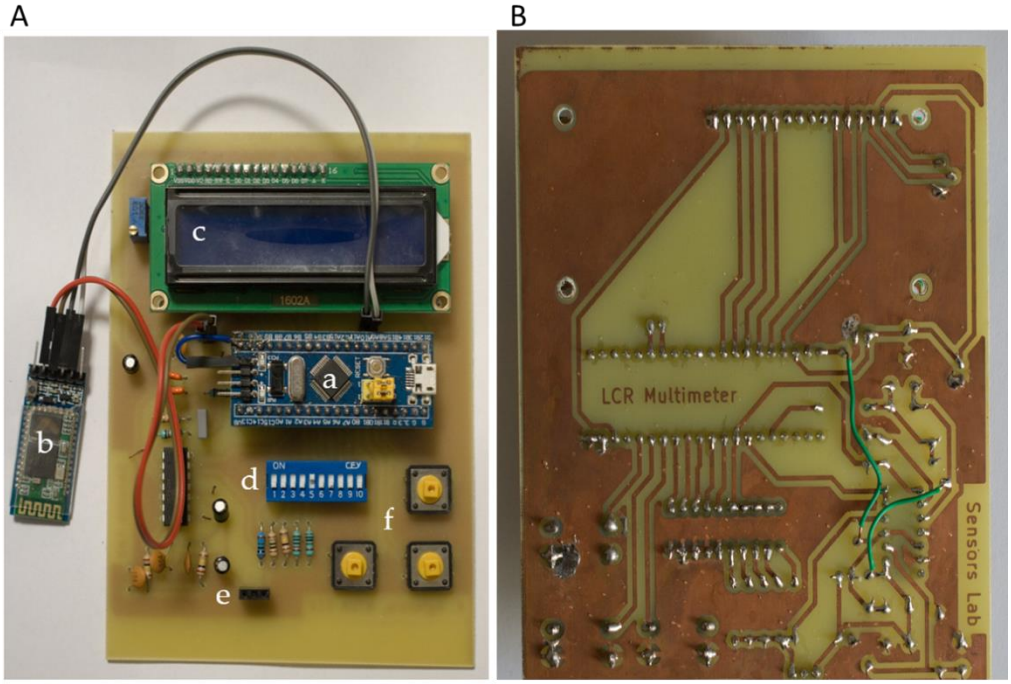

Figure 26. The prototype PCB; A) Front side of the board: (a) Blue Pill STM32 development board; (b) HC-05 BT module; (c) LCD screen; (d) DIP switches; (e) input pins; (f) settings buttons; B) Back side of the board.

Capacitance measurement results are shown in Figure 27, and resistance measurement results are shown in Figure 28. More specifically, Figure 27a shows the

percentage error that the measuring circuit and the Extech LCR meter exhibited during the capacitance measurements of 9 different capacitors, having nominal capacitance values of 10 pF, 100 pF, 1 nF, 2.2 nF, 10 nF, 100 nF, 1 μF, 2.2 μF and 3.3 μF. Figure 27b focuses on the relative difference between the measurements of the reference device and the measuring circuit, regarding the same 9 capacitors.

Similarly, Figure 28a illustrates the percentage error that the measuring circuit and the Keithley multimeter exhibited while measuring the resistance of 9 resistors, having nominal values of 100 Ω, 1 kΩ, 4.7 kΩ, 10 kΩ, 43 kΩ, 100 kΩ, 1 MΩ, 6.8 MΩ and 10 MΩ. Figure 28b shows the relative difference between the measurements of the multimeter and the measuring circuit.

It is shown that the developed circuit can measure capacitance and resistance with high accuracy, across the desired range. The values measured by the developed circuit are very close to the values measured by the two reference instruments. The largest deviation between the measurements of the reference instrument and the developed circuit occurs for the 10 pF capacitor. However, it is possible that the error was due to the LCR meter, as the circuit's measurement was closer to the nominal value. For every capacitor or resistor nominal value, 10 independent measurements were performed. The measurements shown in Figures 27, 28 correspond to the average value of these 10 measurements, whereas the error bars correspond to the standard deviation.

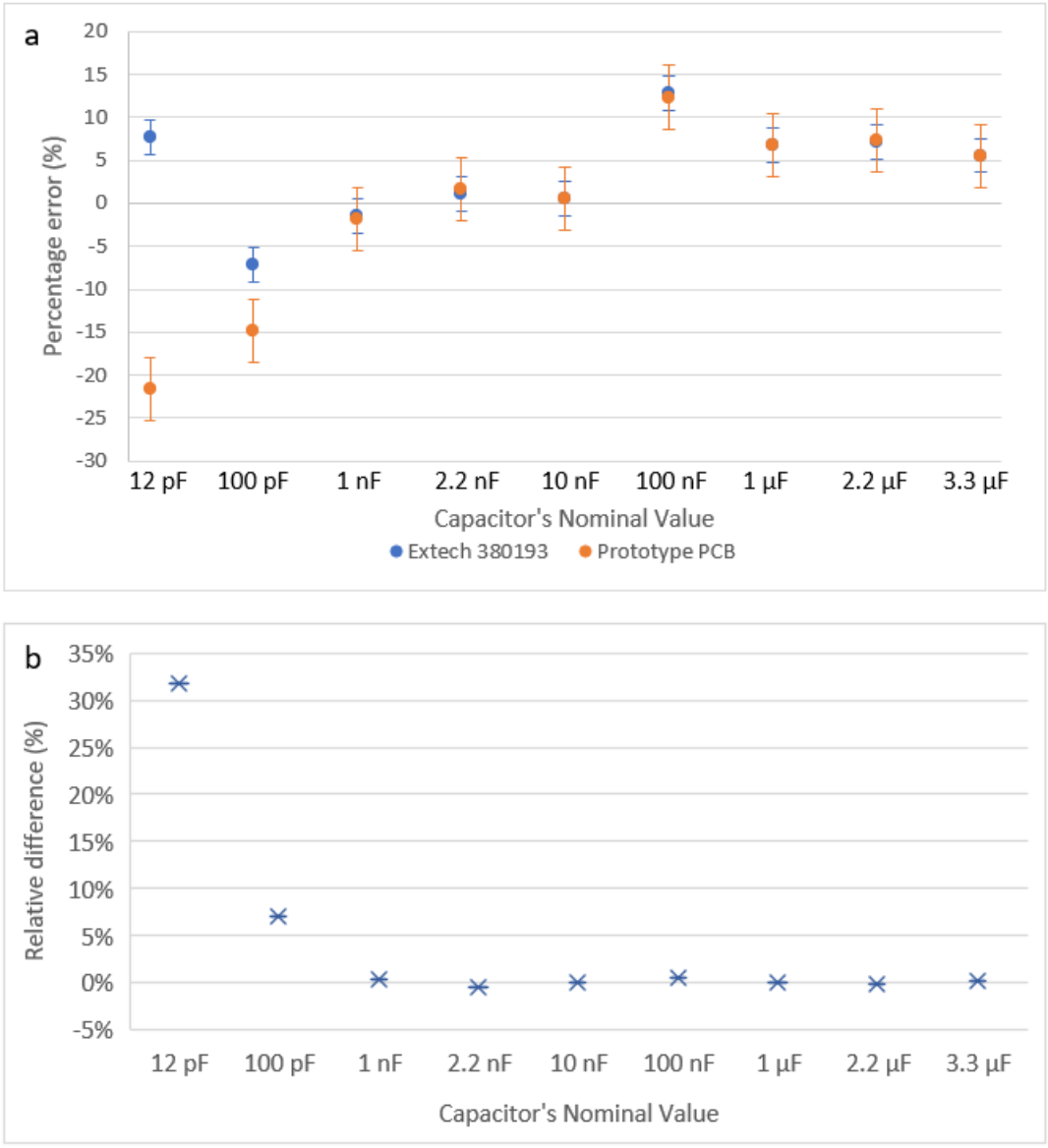

Figure 27. Capacitance measurements of 9 capacitors; (a) The absolute percentage difference between the nominal capacitance value, an LCR meter and the developed circuit; (b) The relative difference between the developed circuit and the reference LCR meter.

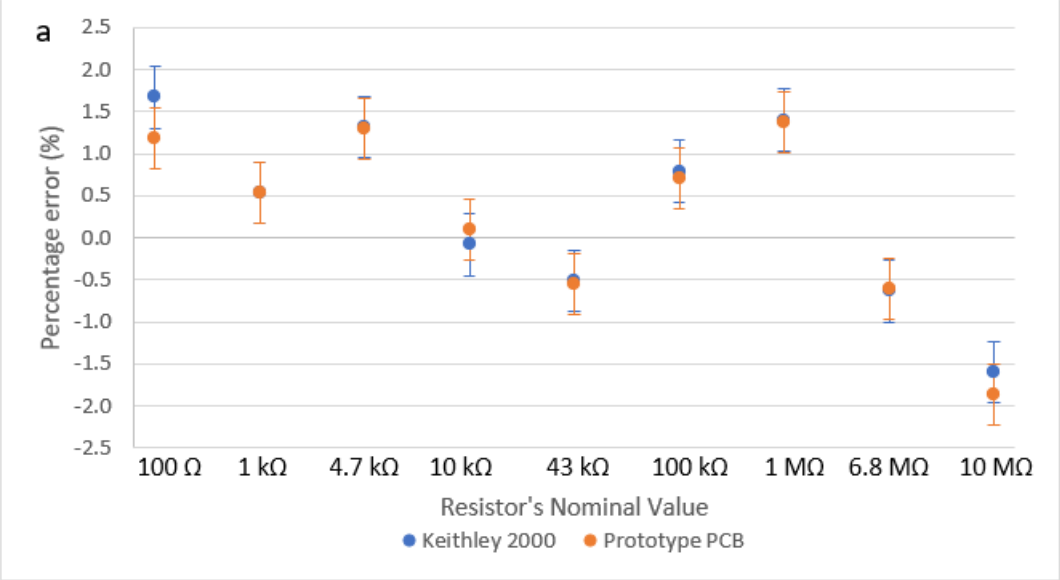

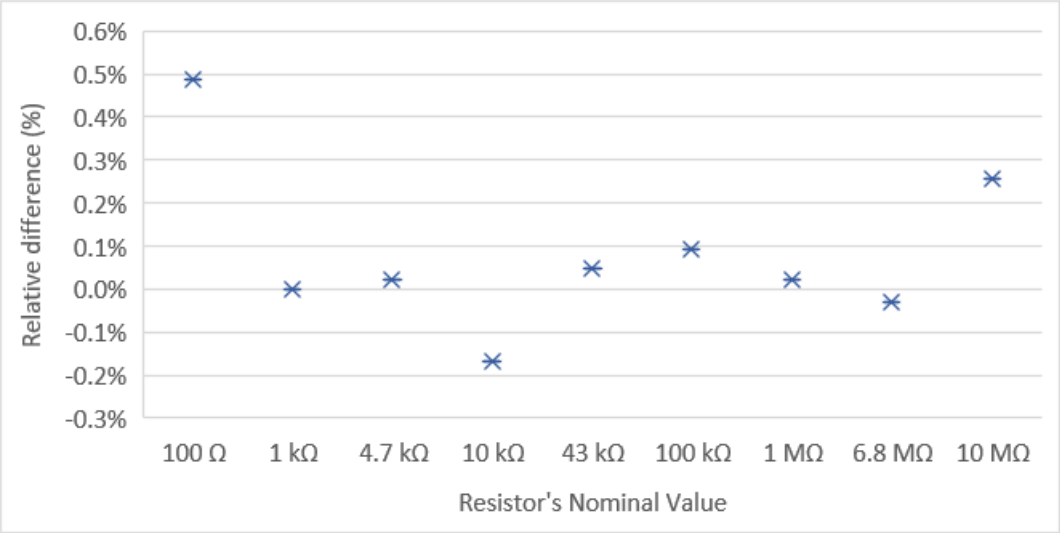

Figure 28. Resistance measurements of 9 resistors; (a) The absolute percentage difference between the nominal resistance value, a benchtop multimeter and the developed circuit; (b) The relative difference be-tween the developed circuit and the reference multimeter.

As has been pointed out in the introduction, integrating a biosensor into an electronic circuit for PoC treatment is a process that involves several challenges[147]. The main challenges faced in this study were the stability and repeatability of the measurements. As is well known, a major challenge in the development of capacitive biosensors and especially in the design of their readout circuits is the treatment of noise interference[153][154][155]. In this case, the first idea was to measure the maximum, the minimum and the time difference between two maxima. This was the first method implemented. The disadvantage of the

method, however, was that the signals had enough noise (ripple noise due to the fact that they are produced by using the Sinusoidal Pulse Width Modulation (SPWM) technique, as well as electrical noise). As a result, the measurements had exhibited a large dispersion. To address these issues, the amplitudes and phases of the fundamental frequency were computed using the formula of discrete Fourier transform. The result was then calculated by averaging the readings over 512 measurements and normalized by dividing every measurement with the maximum measured value.

4.3.2 Device Operation with biological fluids

Experiments were conducted, both with solutions containing S protein and swab samples from hospitalized patients. Initially, 4 biosensors were prepared and kept at a room temperature. At the surface of the first 2, a blank solution containing only Phosphate-Buffered Saline (PBS) was placed, in order to calculate the blank solution response, using an Eppendorf Research® plus pipette. A 20 μL solution containing S protein (6.25 ng/μL) in Phosphate-Buffered Saline (PBS) was placed on top of the third sensor and a 20 μL solution containing S protein (10 ng/μL) in PBS was placed on top of the fourth sensor. The effective capacitance change over time was monitored, as illustrated in Figure 29. Subsequently, experiments were conducted, targeting at detection of real virus molecules, acquired from swab samples of hospitalized patients. Four additional biosensors were prepared. At the surface of the first 2 sensors (N1, N2), only citoswab transport medium was placed, in order to calculate the blank solution response. At the surface of the other 2 (P1, P2), a 20μL solution of citoswab transport medium containing swab samples acquired from patients that were diagnosed positive to the virus was placed. The effective capacitance change over time was monitored, as illustrated in Figure 30.

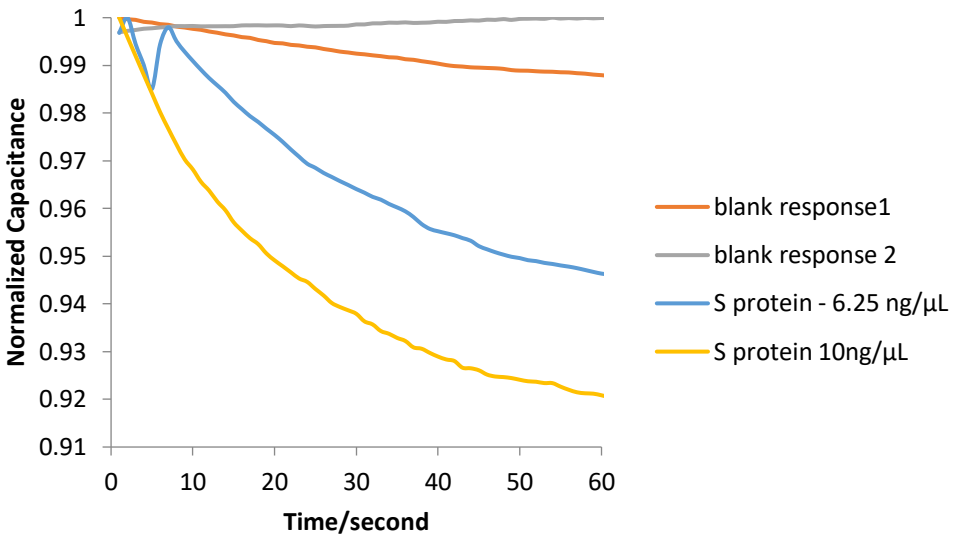

Figure 29. Normalized capacitance change over time for S protein.

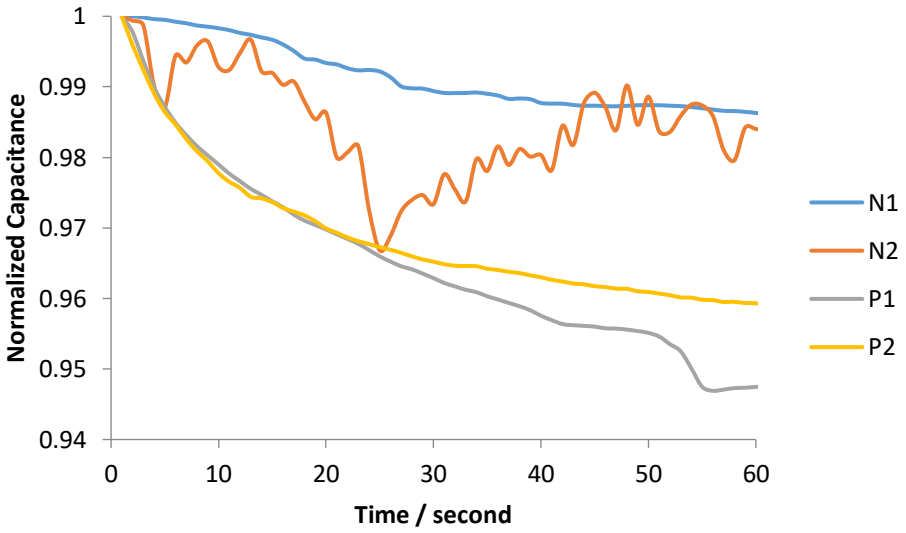

Figure 30. Normalized capacitance change over time for 4 swab samples, 2 negative to the virus (N1, N2) and 2 positive to the virus (P1, P2).

The purpose of S protein measurements was to demonstrate that the prototype electronic circuit could satisfactorily measure protein S in biological samples and to separate samples containing protein S from those without it. As shown in Figure 29, for samples that do not contain protein S only a small change in capacitance is observed, whether it is a small increase or a small decrease. The 2 negative samples shown were selected as they relate to standard responses for samples that do not contain the protein. In contrast, in the case of samples containing protein S, a

significant reduction in capacitance is observed, which in fact is proportional to the concentration of protein in the sample. Capacitance reduction is related to the displacement of the counter ions because of S protein binding on ACE2. Before placing the liquid sample in the biosensor, an ACE2 receptor layer has been coated in the gold electrode surface. Therefore, when a SARS-CoV-2 particle or S protein molecule binds to the ACE2 layer, a displacement of the counter ions around the capacitive electrode results in a decrease in its effective capacitance. The higher the amount of virus molecules bound to ACE2 is, the greater is the decrease in the transducer's capacitance (and therefore the change of the total impedance), detected as an electric signal.

As for the measurements with real virus samples shown in Figure 30, it was selected again to illustrate the response for 2 samples that were negative to the virus (N1, N2) and 2 samples that were positive to the virus (P1, P2). The positive samples were found positive to the virus after being tested with real – time PCR method, with CT (cycle threshold) equal to 22±0.2 (P1) and 26±0.1 (P2). Out of the negative samples, N1 was selected to be illustrated as its response is the one closer to the typical response of the negative samples. N2 refers to a single measurement and it was selected to be shown as an extreme case, with intense noise interference. Such a signal response was noticed only in 1 out of the 16 negative samples that were tested. Malfunctions like this one that could be related either with a mistake during the biosensor development or, most probably, with bad connection of the biosensor to the readout device, are a priority to address in future work. In any case, the purpose of Figure 30 is to prove that positive samples can be distinguished by negative samples, by the fact that their measured response is a decreasing curve and their maximum capacitance change is more than 2%. Reproducibility of the experiments, both with S protein and real virus samples, was demonstrated with 3 replicates. The capacitance values shown in Figures 29 and 30 refer to the average value of the 3 experiments with the same sample, except for the measurement of N2 sample, which refers to a single measurement. All experiments were performed at room temperature.

4.3.3 Measurement procedure and wireless transmission to mobile application

The measurement procedure is the following: The user has to open the Android application and register by entering some personal information (Figure 25b) or sign in, if the user has already been registered, as shown in Figure 25a. Then, the testing procedure begins. After 60 s of measuring with a rate of 1 measurement per second, the resulting value is transmitted to the Android application via Bluetooth. If a) the capacitance response was decreasing and b) the total capacitance change exceeds 2%, the test is listed as positive for the SARS-CoV-2 S protein and the user receives the appropriate response (Figure 31a). Otherwise, if capacitance was not decreasing or the total capacitance change was below 2%, the test is listed as negative, and the user is informed as well (Figure 31b).

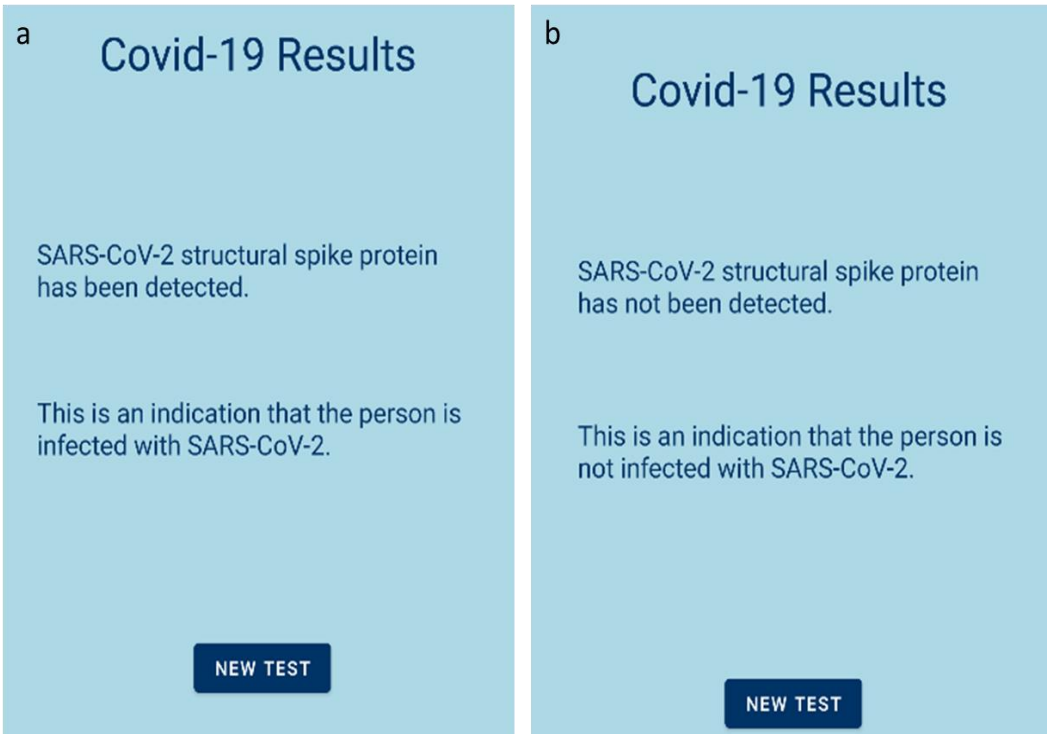

Figure 31. Mobile application results; (a) test positive to S protein; (b) test negative to S protein.

As stated in the introduction section, part of the purpose of a PoC device is to be friendly to use. The development of the mobile application fulfills that purpose, as it is much easier for the user to connect to its mobile phone and read if s/he is positive

or negative to the virus than having to conclude that after reading continuous capacitance measurements.

However, it is not only the friendly-to-use concept that is achieved. The main advantages of this device are the simplicity in the construction and use, the portability and the possibility that offers regarding the collection and processing of the test results. The latter advantage is particularly important, as a good knowledge of the distribution of cases geographically and temporally is a prerequisite for a successful pan-demic policy. The wireless transmission to the mobile application is actually a single example of the possibilities that could be achieved when integrating the biosensor-based screening tests into the Internet of Things.

Regarding the screening tests, when used as diagnosing tools for a small number of patients, they may not have the efficiency and sensitivity of other methods, like real-time PCR, which we do not attempt to replace in this research. Real–time PCR remains the “golden standard” for SARS-CoV-2 testing; however, it is not a screening device, focused on PoC treatment like the one we demonstrate in this work. Screening tests are usually more effective when used in large sections of the population or population groups. Therefore, it is important for screening tests to be designed in a way to be easily acceptable by people and it is important for the test results to be easily assembled and processed, something that is made possible by the IoT and the biosensor platform presented.

Regarding the calibration of the device, it has been taken into account that it is a device intended for medical screening, in which the non-existence of false positives of results is considered a priority[156]. That is why, even though the maximum capacitance decrease caused by the negative samples was lower than 2%, it was selected to list all the results with a capacitance decrease of 2% or less as negative, in order to avoid having false positive results.

4.4 Conclusion

In this chapter, a SARS-CoV-2 S protein detecting device was demonstrated, which uses the ACE2-based capacitance sensor for rapid native SARS-CoV-2 detection that was described at chapter 6. The device consists of a microcontroller-based electronic circuit that, as shown, can measure capacitance and resistance change with high accuracy, and an Android application, where the test results are transmitted via Bluetooth. In this chapter, new experiments were conducted targeting directly SARS-CoV-2 particles in swab samples of hospitalized patients. The device proved to be able to accurately measure the change in capacitance, both for protein S and for swab samples containing virus particles. Regarding the calibration of the device, it was observed that the noise introduced by the citoswab transport medium can be significant and therefore the conditions for a sample to be considered as positive for the virus were modified to: a) “the capacitance response is constantly decreasing” and b) “the total capacitance change exceeds 2%”.

5 Biosensor and readout circuit packaging

5.1 Introduction

As biosensor systems are used in more and more areas of public health, food and environmental technology, and the global economy in general, the need to optimize them so that they can be used in real life is ever-increasing. Capacitive biosensors are one of the most popular types, as they are considered highly sensitive and they can provide results at short time[123]. The basic principle of operation followed in most capacitive biosensors is the following; a capacitive transducer is selected and on its surface is coated a layer that contains some bioreceptor able to bind the targeted information. Then, the analyte containing the targeted information is placed on the biosensor surface and the binding performed results to a change in the measured capacitance[46].

However, there are certain challenges that need to be overcome regarding capacitive biosensors[147]. A major challenge in the development of capacitive biosensors and especially in the design of their readout circuits is the treatment of noise interference[153], [155] and therefore the issues that arise in relation to the stability and repeatability of the measurements. Stability is related to the non-dependence of the sensor effects on external factors, while repeatability is related to the ability of the sensor to provide the same results in the same operating conditions.

Both stability and repeatability may be affected by the analyte diffusion at the biosensor surface. When placing a drop at the biosensor surface for example, the liquid may start spreading to a larger part of the surface, leading to an increase in the dielectric constant and consequently to an increase in the measured capacitance. Therefore, it is important to achieve a control on the diffusion of the liquid analyte, so as to remain confined to the part of the surface that has been selected[157].

One more thing about using biosensors in real conditions is the need to protect their sensitive parts. As biosensors and also electronics is preferred to be used in

micro or nano scale[65], it is very easy for them to be damaged. It is a common solution to use photosensitive polymers to form a bonding and sealing layer at the biosensor surface, as it is a simple, robust and low-cost solution[158].

Biosensors are usually accompanied by an electronic readout circuit, which is mainly used to amplify the measured signal and for noise compensation. The development of Integrated Circuits (ICs) and microelectronic systems (MEMS) has made great strides in every aspect of technology and especially in industry. In order to be able to use them, it is necessary that these circuits are properly packaged and their packaging usually provides a variety of functions[159]. The packaging should provide protection from environmental factors, as any chemical changes may reduce the efficiency of the circuit, as well as mechanical strength and heat management both to increase the reliability and service life of the circuit and to prevent material damage. The circuit also needs to be interconnected with the packaging to enable the interaction with a larger system, such as a user, or the communication of each circuit with another.

Modern packaging techniques must be defined at the beginning of the product or circuit design to match the entire package during the assembly process, but without compromising the performance of the device. Also, it is usually required to order a large number of originals from many different materials, thus increasing the cost of construction. 3D Printing technology simplifies this process. Spraying techniques have already been used to create 3D ICs[160] as well as to encapsulate MEMS devices[161], [162].

In chapter 6, the development of a capacitive biosensor for SARS-CoV-2 detection in real time has been demonstrated. In chapter 7, the biosensor has been integrated into a Point of Care (PoC) diagnosing device, after the development of a precise biosensor readout circuit. In this chapter an acrylic-based dry film, ORDYL SY 300[158], [163], [164], is used in order to address both the issues of biosensor bonding and sealing and controlling analyte diffusion. A protective layer is formed at the biosensor surface, in order to avoid over time damage and at the same time, with the use of UV lithography, wells are patterned on the biosensor sensitive area where the analyte will be placed and will remain confined, in order to avoid the

noise introduced by analyte diffusion. Additionally, 3D Printing technology is used in order to develop a connector between the biosensor and the electronic readout circuit, as well as for the packaging of the readout circuit.

5.2 Materials and Methods

5.2.1 Sensor coating with ORDYL SY 300

Gold interdigitated electrodes (IDEs) were purchased from DropSens (Asturias, Spain), cat. N.: PW-IDEAU50. Each IDE has a finger width and spacing of 50 μm, with a total number of 70 fingers, a total electrode length of 7 mm, and electrode surface area of 8.45mm2. Initially, the IDEs were immersed in an acetone solution, then in 100% isopropanol and then they were washed with distilled water. The chemicals were purchased from Sigma-Aldrich (St. Louis, USA). The experimental procedure is shown in Figure 32; The IDEs were placed in a hot plate at 110℃. An ORDYL SY 300 piece, slightly larger than the IDE sensitive area, was cut, ORDYL protective liner was removed from the one side and the tape was coated at the IDE surface. A photolithography mask was designed and printed. The sample was exposed at UV for 0.8 minutes. The white areas of the mask protected the photosensitive layer from UV, whereas the dark areas were exposed. The ORDYL protective liner was removed from the other side, revealing its photosensitive surface. Then, it was immersed in its developer solution, in an ultrasonic bath, for another 5 minutes. After the developing process, the sample was immersed again in 100% isopropanol solution and washed with distilled water. At the end, it was placed at a hot plate at 120℃ for 45 minutes, in order to harden the ORDYL layer.

For the evaluation of the optimized biosensors in contrast to the biosensors without patterned wells, the type A and type B uncertainty was calculated in both cases, according to the formulas introduced at section 3.

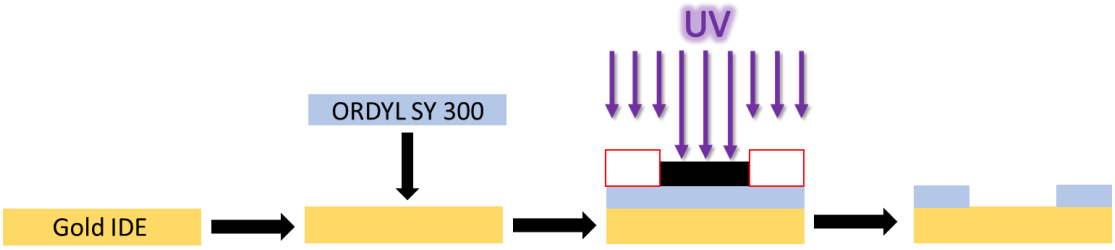

Figure 32. Coating and patterning ORDYL SY 300 at gold IDE surface.

5.2.2 Connector design

Due to the small size of the electrodes of the measuring capacitor, a connector had to be made in order to obtain readings with a non-destructive way, like soldering connectors on the surface. The design had to keep the capacitor in place at all times and also provide constant conductive connection with the readout circuit.

For the conductive connection we used stainless steel bands of circular shape, as shown in Figure 33. Part A (Red) is fixed on the base (Blue) with metallic rods and has holes for a screw and nut mechanism. Turning the screw will push Part B (Green) downwards and because the bands are hold on it, they will too, be pushed downwards ensuring conductive touch with the capacitor's electrodes.

Also, a case (yellow) was designed with ledges on top, so that the capacitor is fixed and can't be moved except when inserted or removed. On the back side the bands are connected with male headers which provide connectivity with the readout device.

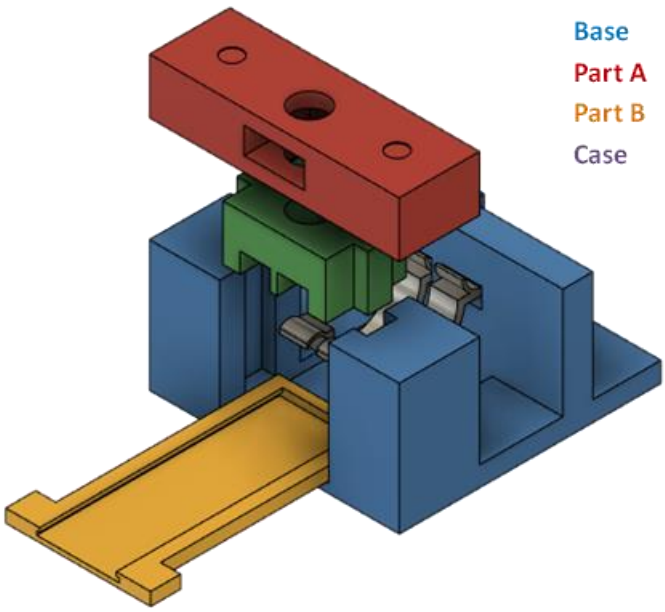

Figure 33. Connector design.

5.2.3 Packaging design of readout circuit

The design of the packaging for the readout circuit had to provide connectivity for the I/O components of the board. The most important of all was the ability for the circuit and the capacitor connector to form one unified package. With that in mind a case was designed so that it had proper holes and cutouts for the I/O components (Connector, LCD, Buttons etc.) and so that the board was held safely in place.

The packaging, which is illustrated in Figure 34, consisted of three parts:

- The base (blue) on which the board is mounted
- Bottom lid(red) for the lower part of the readout circuit
- Top lid (green) for the upper part of the readout circuit

All the parts were designed in Fusion360®, sliced in Simplify3D® and the 3D printed on an Anycubic i3 Mega-S FDM 3D printer with 1.75mm PLA of the same brand.

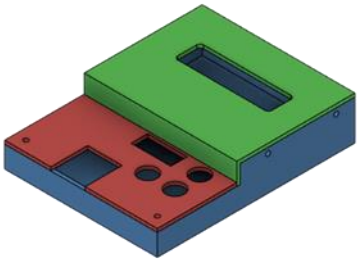

Figure 34. Readout circuit packaging design; Base (blue); Bottom lid (red); Top lid (green).

5.3 Results and discussion

5.3.1 Photosensitive layer on interdigitated surface

Following the procedure described in section 2.1, a ORDYL SY 300 layer was coated on the interdigitated capacitor surface. The aim of the coating was to achieve good control of the diffusion of the liquid sample on the sensory area of the capacitor, as well as to create a protective layer on the rest of the capacitor surface, in order to avoid any damage over time. As illustrated in Figure 35a, a 90 μm thick layer was coated at the capacitor surface, with the exception of a square area where the liquid sample is placed. A BRESSER JUNIOR DM400 Digital Microscope (Bresser, Rhede, Germany) was used for the optical characterization of the coating in 20X magnification. The magnified picture is shown in Figure 35b. Then, a liquid drop was placed at the non-covered square area, as illustrated in Figure 35c.

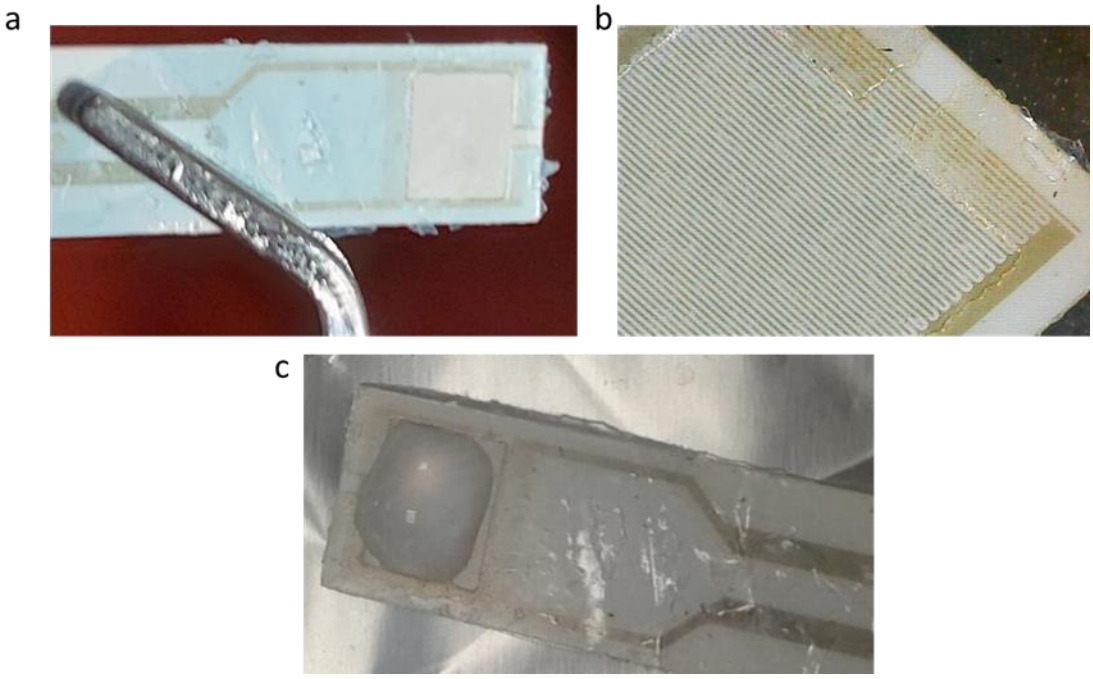

Figure 35. Patterning square-shaped wells on capacitor sensitive area; a) image of the patterned well; b) image of the well in 20X magnification; c) a droplet is placed at the well.

It was noticed that there was a problem with square geometry, as the liquid wasn't spreading well at the well corners. For that reason, a circular geometry was tested. An ORDYL layer was coated at a group of 4 capacitors. After UV exposure, a circular well was patterned at the sensitive area as shown in Figure 36a. ORDYL was removed as well from the capacitor pads, so that they could be connected with the readout device, as shown in Figure 36d (X20 magnification). After ORDYL treatment, the capacitors were separated and used one at a time. With this geometry the liquid was spreading perfectly in the well, as shown in Figure 36b and Figure 36c (X20 magnification).

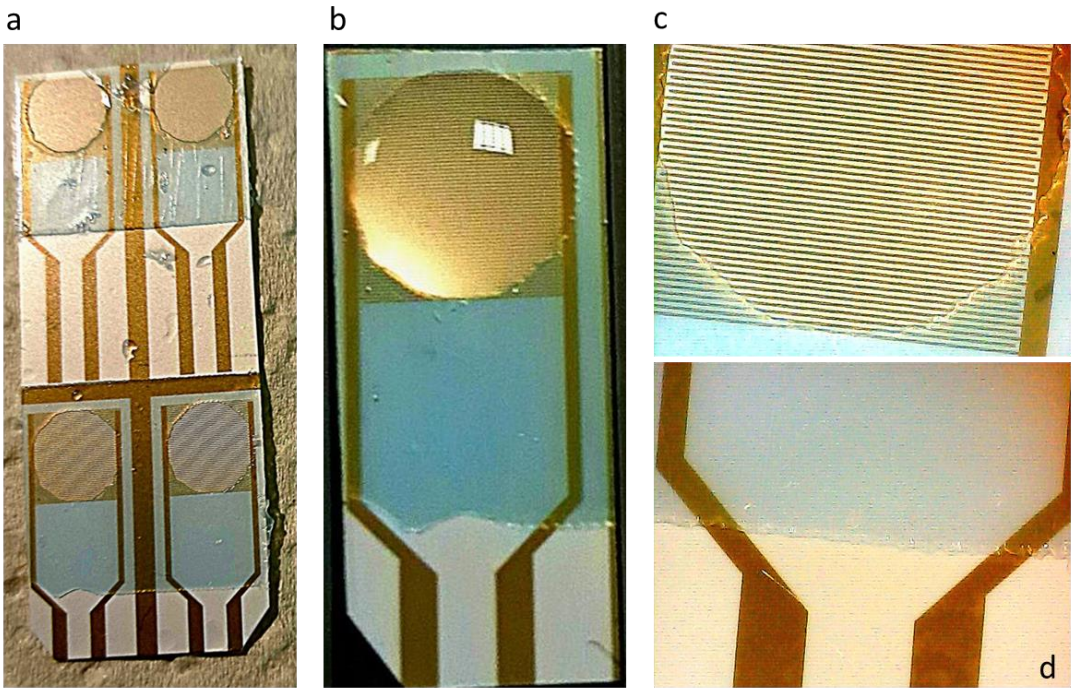

Figure 36. Patterning circular wells on capacitor sensitive area; a) wells patterned on a set of capacitors; b) a droplet is placed at the well; c) image of the well in 20X magnification; d) ORDYL layer doesn't cover the capacitor pads.

After the well-geometry configuration, the modified capacitors were utilized in SARS-CoV-2 biosensors. The biosensors were prepared following the procedure described in previous chapters and their response to different concentrations of S protein was monitored, as shown in Figure 37. For each S protein concentration, a total of 3 experiments were conducted. The lines shown in Figure 37 correspond to the average measurement for each concentration, whereas the error bars correspond to the standard error of the measurements. Main purpose of this measurements was to validate that the capacitors were not damaged and were still functional after the modification process. In addition, the uncertainty level of the measurements on the biosensors with patterned wells was lower than the uncertainty of the measurements on biosensors without wells.

Type A uncertainty:

$\sigma = 0.004951$
$\sigma^2 = 2.45078E-05$
$\sigma_{\bar{x}} = 0.001323085$
$v = 13$

Type B uncertainty (92,3%):

$\sigma = 0.004537$
$\sigma^2 = 2.05866E-05$
$\sigma_\chi = 0.001258406$
$v = 12$

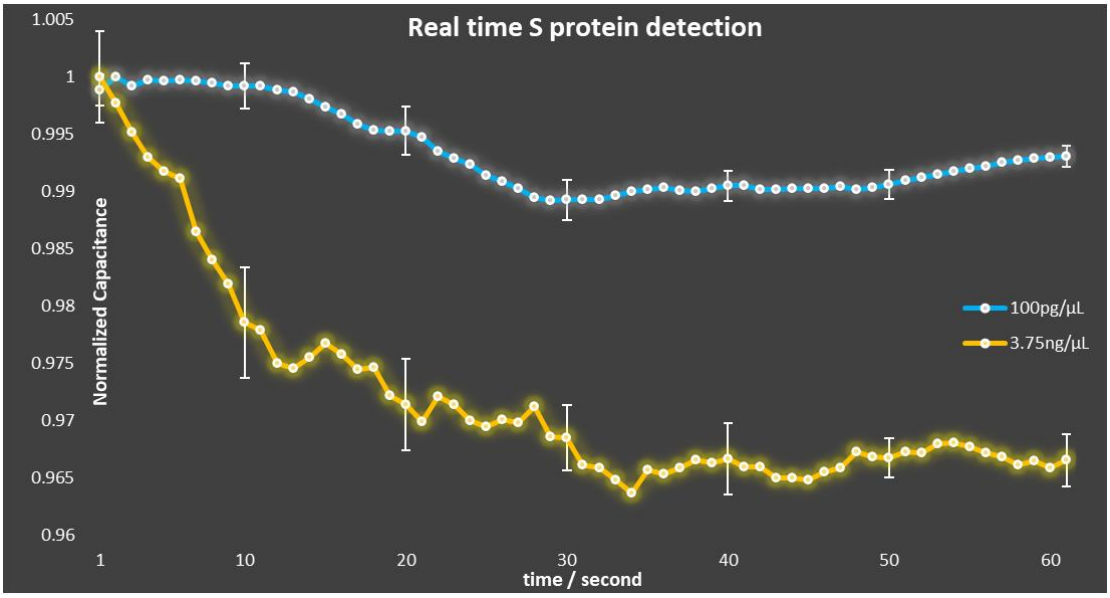

Figure 37. Normalized capacitance change over time due to the binding of S protein.

5.3.2 Connector development

The connector consisted of four total objects to be printed:

- Packaging base
- Driver
- Fixing cap
- Sensor case

Figure 38 shows the process of slicing the objects that make up the connector. Where necessary, support material was placed and optimal print settings, shown in Table 2, were selected.

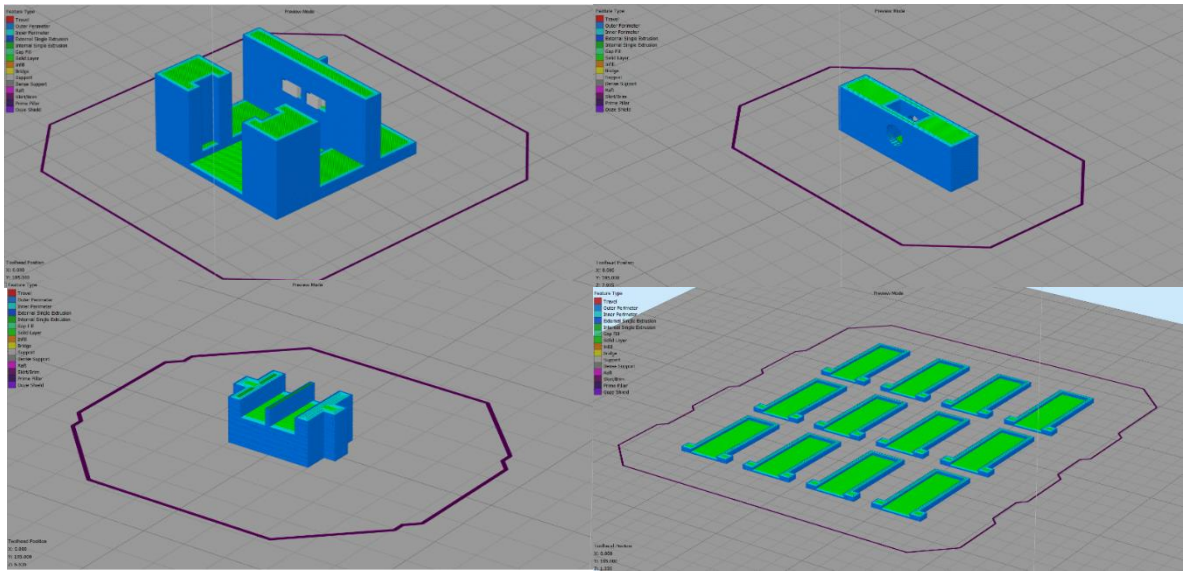

Figure 38. Connector slicing process.

Table 2. Connector printing settings.

	Base	Cap and driver	Case
Extrusion width	0.18 mm	0.2 mm	0.16 mm
Layer height	0.10 mm	0.12 mm	0.10 mm
Top/Bottom layers	2/3	3/3	2/2
Perimeter walls	4	3	2
Infill rate	30%	30%	30%
Print speed	55 mm/s	50 mm/s	40 mm/s

Next, the individual pieces of the connector were assembled, as shown in Figure 39a (front view) and Figure 39b (side view). Because the plates are made of stainless steel, welding them to the interface pins was not possible through conventional welding. For this reason, the back of the plates was wrapped with copper wire and then soldered. Also shown in Figure 39c is the position of the plates in relation to the electrodes, which was the best possible, since the plates touch the entire area of the electrodes. Finally, the conductive parts were insulated with silicone. Connector assembly was completed by placing the retaining screw and nut on the top of the package, which was braced with small diameter metal rods. The sensor case, shown with purple, was also manufactured.

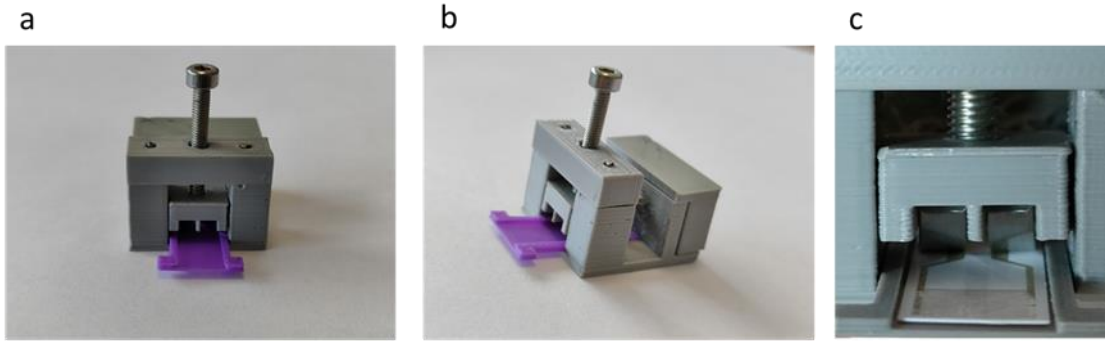

Figure 39. The 3D printed connector; a) front view; b) side view; c) the connection of the conductive plates to the sensor.

5.3.3 Electronic circuit packaging

The electronic circuit packaging consisted of three parts:

- The base of the package
- The lid of the upper part
- The bottom lid

Due to the size, but also the need for greater mechanical strength, in relation to the connector development, different printing settings were used during the slicing process, which are shown in Table 3.

Table 3. Printing settings for circuit packaging.

	Base	**Lids**
Extrusion width	0.40 mm	0.26 mm
Layer height	0.30 mm	0.20 mm
Top/Bottom layers	5/5	3/5
Perimeter walls	5	5
Infill rate	30%	30%
Print speed	65 mm/s	55 mm/s

Figure 40a illustrates the slicing process of the electronic circuit packaging base. No supporting material was needed at all, as there were no parts that were at large angles or without support from the construction itself. On the contrary, as shown by the printing settings in Table 3, emphasis was placed on the mechanical strength of the base, increasing the number of perimeter walls, but also changing from the advanced settings the thickness of the perimeter walls. To ensure that there will be no warping and that the surfaces created during printing will be as smooth as possible, great attention was paid to the process of levelling the printing surface. This was done through successive tests, with the aim of the nozzle being equidistant from every point on the print surface. Next, the top and bottom lids of the package were manufactured, where slightly different print settings were used, as shown in Table 3. During the slicing process (Figure 40b), the surfaces were placed in such a way that no support material was needed, but also to make the smoothest possible surface.

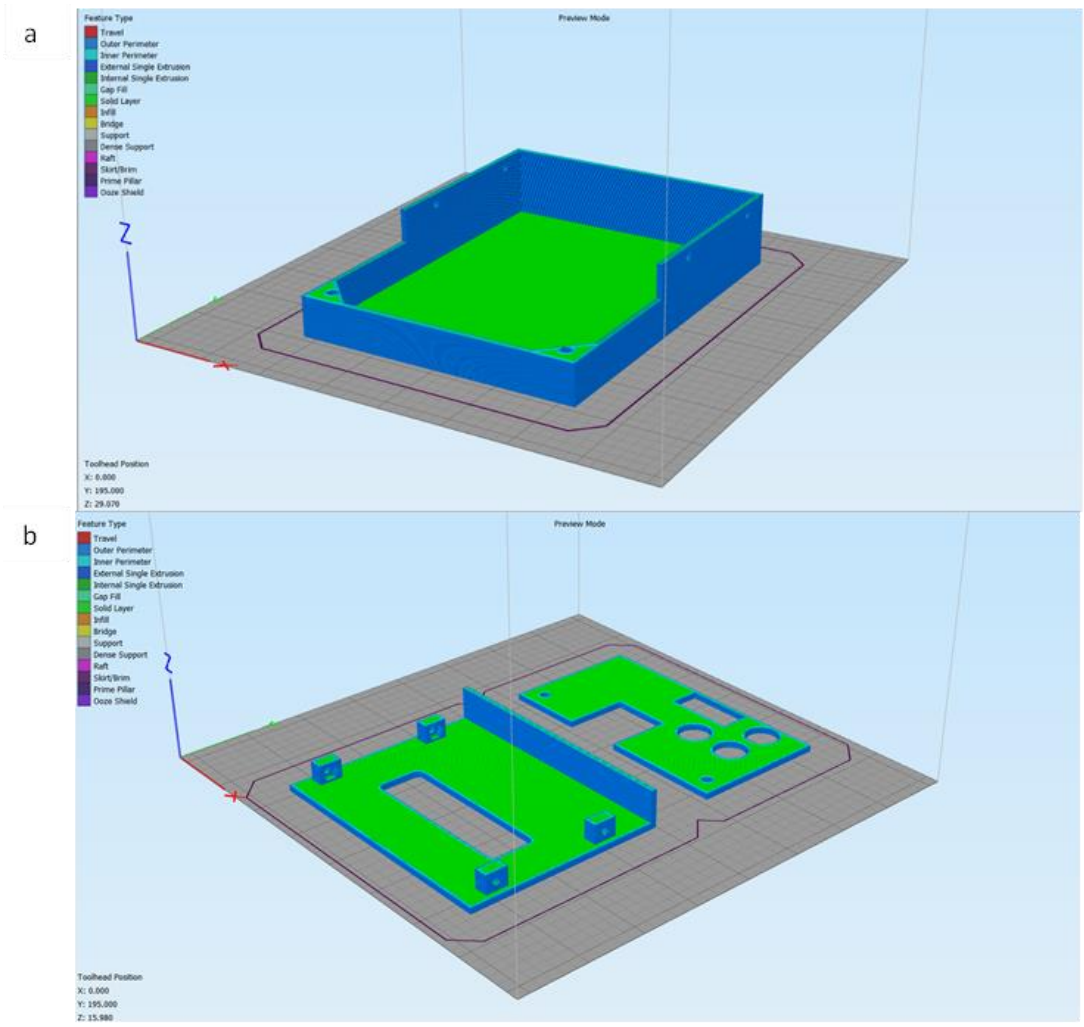

Figure 40. Slicing process of the electronic circuit packaging base.

All three pieces that make up the package of the measuring device are shown assembled in Figure 41a. Unlike the connector development, it was deemed necessary to further process the manufactured pieces. Specifically, a sanding and painting stage was added. Figure 41b shows the way the PCB is fixed inside the package and Figure 41c shows the final packaging of the electronic circuit, as well as where exactly the connector is placed. The LCD screen displays the reading of a biosensor.

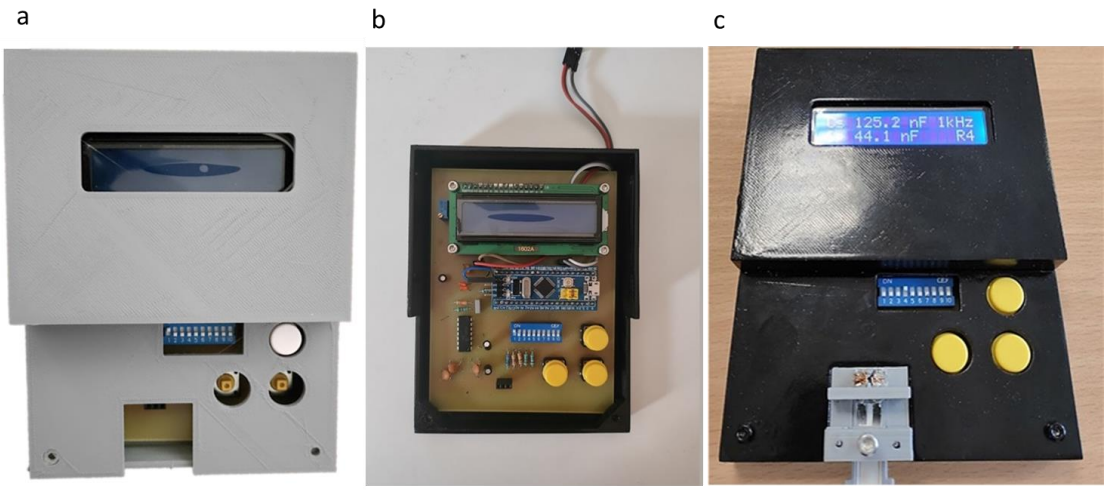

Figure 41. Packaging assembly; a) readout circuit packaging; b) the PCB placed inside the package; c) the package in its final form displaying the readings of a biosensor in its LCD screen.

5.4 Conclusion

This section described the optimization and packaging procedure of a SARS-CoV-2 biosensor and its readout circuit. The optimization procedure involved the coating of a photosensitive film, ORDYL SY 300, at the biosensor surface. The photosensitive film formed a layer that protects the biosensor against accidental damage. At the same time, after the exposure of the photosensitive film in UV, a well was patterned at the sensitive area of the biosensor. This well preserved the liquid analyte in a specific area, blocking in this way its random diffusion that introduces a significant error factor. Two different well geometries were tested, square and circular. The circular geometry was finally selected, as in the square geometry the liquid wasn't spreading well at the edges of the well. This method stabilized the measurement procedure and reduced measurement errors. Apart from the biosensor, its readout circuit was packaged as well. A protective case was 3D printed, utilizing fused deposition modeling. Additionally, a connector component was 3D printed as well, which allows the connection of the biosensor to the readout circuit. The optimization process improved the biosensor measurements and the packaging allowed the use of the total detecting system for PoC treatment.

6 Conclusion

- A capacitive biosensor was developed, utilizing the immobilization of ACE2 receptor on gold interdigitated electrode surface.
- The biosensor was able to detect SARS-CoV-2 S protein with good selectivity and a Limit of Detection of 750pg/μL/mm^2.
- The biosensor was able to detect SARS-CoV-2 in biological samples acquired from hospitalized patients. In swab samples, the biosensor was able to clearly detect the virus in samples with a viral load as low as 10^3 virus copy numbers/μL. In saliva samples, the detection limit was at a viral load as low as 10^4 virus copy numbers/μL.
- The biosensor measurements were in complete agreement with the real – time PCR measurements for the same samples.
- in less than 60 seconds, the biosensor performs quantitative measurements of S protein and semi – quantitative measurements of SARS-CoV-2 in swab or saliva samples.
- A portable electronic readout circuit was developed. The circuit replaced the laboratory LCR meter and allowed the use of the biosensor for Point of Care treatment.
- An android application was developed. The readout circuit wirelessly transmits the biosensor results to the android application via Bluetooth. In this way, the user can learn his/her results without having to interpret some visual observation.
- The packaging of the biosensor is performed with ORDYL SY 300. In this way a protective layer is formed. Additionally, a well is patterned in the biosensor sensitive area, resulting in the restriction of liquid diffusion.
- The packaging of the electronic circuit was performed with 3D printing. Additionally, a 3D printed connector was developed, which connects the biosensor to the circuit. Finally, a 3D printed socket was developed as well, where the biosensor is placed before entering the device.

7 Publications

In ISI Scientific Journals:

- A. Georgas et al., “ACE2-based capacitance sensor for rapid native SARS-CoV-2 detection in biological fluids and its correlation with real-time PCR,” Biosens. Bioelectron., vol. 202, p. 114021, 2022, doi: https://doi.org/10.1016/j.bios.2022.114021. [165]
- A. Georgas et al., “A Biosensor Platform for Point-of-Care SARS-CoV-2 Screening,” Biosensors, vol. 12, no. 7, p. 487, Jul. 2022, doi: 10.3390/bios12070487. [166]
- A. Georgas et al., “Packaging and optimization of a capacitive SARS-CoV-2 biosensor and its readout circuit.” **Submitted** in Sensors MDPI
- G. Banis, … , A. Georgas et al., “Design and Testing of a Disposable Flow Cuvette for Continuous Electroporation of a Bioreactor’s Initial Algae Cultivation,” Magnetochemistry, vol. 8, no. 11, p. 147, Nov. 2022, doi: 10.3390/magnetochemistry8110147. [167]
- Z. Wang, … , A. Georgas et al., “Ultra miniaturized InterDigitated electrodes platform for sensing applications,” Microelectron. Eng., vol. 225, p. 23955, 2020, doi: 10.1016/j.mee.2020.111253. [65]
- A. Vasilopoulou, A. Georgas, and E. Hristoforou, “Microcontroller Based Device for Capacitive Biosensor Readout,” MedPress Public Heal. Epidemiol., vol. 2, no. 1, 2022, doi: mpphe-202204002. [168]
- A. Vasilopoulou, A. Georgas, and E. Hristoforou, “A Review on Cardiac Biomarkers Detection for Heart Failure Prognosis,” J. Integr. Cardiol. Open Access, pp. 1–7, 2022, doi: 10.31487/j.jicoa.2022.02.02. [169]

In Scientific Conferences:

- Georgas, A., et al. "A Portable Screening Device for SARS-CoV-2 with Smartphone Readout. 2022, 4, x." Presented at the 2nd International Electronic Conference on Biosensors (IECB). Vol. 14, and published in Eng. Proc. 2022, 16, 7. https://doi.org/10.3390/IECB2022-12274
- Georgas, A., et al. "ΑΝΑΠΤΥΞΗ ΒΙΟΑΙΣΘΗΤΗΡΑ ΓΙΑ ΤΗΝ ΤΑΧΕΙΑ ΑΝΙΧΝΕΥΣΗ ΤΟΥ SARS-CoV-2, 2022" Presented at the 8th Metrology Conference, Thessaloniki, Greece. → **Best oral presentation award**

In National Journals:

- Georgas, A., et al. Commentary on paper ACE2-based capacitance sensor for rapid native SARS-CoV-2 detection in biological fuids and its correlation with real-time PCR. Accepted in Iatriko Vima, Journal of the Panhellenic Medical Association. https://iatrikionline.gr/IB_141/IATRIKO_VIMA_141_ALL.pdf

8 References

[1] M. Y. Wang, R. Zhao, L. J. Gao, X. F. Gao, D. P. Wang, and J. M. Cao, “SARS-CoV-2: Structure, Biology, and Structure-Based Therapeutics Development,” *Front. Cell. Infect. Microbiol.*, vol. 10, no. November, pp. 1–17, 2020, doi: 10.3389/fcimb.2020.587269.

[2] D. Cucinotta and M. Vanelli, “WHO declares COVID-19 a pandemic,” *Acta Bio Medica Atenei Parm.*, vol. 91, no. 1, p. 157, 2020.

[3] B. Zhang, H. Zhou, and F. Zhou, “Study on SARS-CoV-2 transmission and the effects of control measures in China,” *PLoS One*, vol. 15, no. 11, p. e0242649, Nov. 2020.

[4] B. Pfefferbaum and C. S. North, “Mental health and the Covid-19 pandemic,” *N. Engl. J. Med.*, vol. 383, no. 6, pp. 510–512, 2020.

[5] Centers for Disease Control and Prevention, “Interim clinical guidance for management of patients with confirmed coronavirus disease (COVID-19),” Feb-2020.

[6] Z. Gao *et al.*, “A systematic review of asymptomatic infections with COVID-19,” *J. Microbiol. Immunol. Infect.*, vol. 54, no. 1, pp. 12–16, 2021, doi: https://doi.org/10.1016/j.jmii.2020.05.001.

[7] Q. Long, “X, Tang X-J, Shi Q-L, et al,” *Clin. Immunol. Assess. asymptomatic SARS-CoV-2 Infect. Nat Med*, vol. 26, no. 8, pp. 1200–1204, 2020.

[8] B. Blomberg *et al.*, “Long COVID in a prospective cohort of home-isolated patients,” *Nat. Med.*, vol. 27, no. 9, pp. 1607–1613, 2021, doi: 10.1038/s41591-021-01433-3.

[9] Nanographics, “Real SARS-CoV-2 virion in 3D,” 2021.

[10] H. Harapan *et al.*, “Coronavirus disease 2019 (COVID-19): A literature review,” *J. Infect. Public Health*, vol. 13, no. 5, pp. 667–673, 2020.

[11] A. C. Walls, Y.-J. Park, M. A. Tortorici, A. Wall, A. T. McGuire, and D. Veesler, “Structure, function, and antigenicity of the SARS-CoV-2 spike glycoprotein,”

Cell, vol. 181, no. 2, pp. 281–292, 2020.

[12] J. Lan *et al.*, "Structure of the SARS-CoV-2 spike receptor-binding domain bound to the ACE2 receptor," *Nature*, vol. 581, no. 7807, pp. 215–220, 2020, doi: 10.1038/s41586-020-2180-5.

[13] E. Janik, M. Bartos, M. Niemcewicz, L. Gorniak, and M. Bijak, "SARS-CoV-2: Outline, Prevention, and Decontamination," *Pathogens* , vol. 10, no. 2. 2021, doi: 10.3390/pathogens10020114.

[14] R. S. Glass, *Fundamentals of organic chemistry*, vol. 60, no. 10. 1983.

[15] J. Shang *et al.*, "Structural basis of receptor recognition by SARS-CoV-2," *Nature*, vol. 581, no. 7807, pp. 221–224, 2020, doi: 10.1038/s41586-020-2179-y.

[16] M. Dong *et al.*, "ACE2, TMPRSS2 distribution and extrapulmonary organ injury in patients with COVID-19," *Biomed. Pharmacother.*, vol. 131, p. 110678, 2020.

[17] C. Gros and B. Labouesse, "Study of the dansylation reaction of amino acids, peptides and proteins," *Eur. J. Biochem.*, vol. 7, no. 4, pp. 463–470, 1969.

[18] M. K. Reddy, "Amino acid reactions," *Britannica*. .

[19] A. Heurich, H. Hofmann-Winkler, S. Gierer, T. Liepold, O. Jahn, and S. Pöhlmann, "TMPRSS2 and ADAM17 cleave ACE2 differentially and only proteolysis by TMPRSS2 augments entry driven by the severe acute respiratory syndrome coronavirus spike protein," *J. Virol.*, vol. 88, no. 2, pp. 1293–1307, 2014.

[20] "Latest Insights & Products for SARS-CoV-2/COVID-19 Research." [Online]. Available: http://www.cogershop.com/sars-cov-2-covid-19.htm?page=1. [Accessed: 06-Dec-2022].

[21] Y. Xie *et al.*, "Spike Proteins of SARS-CoV and SARS-CoV-2 Utilize Different Mechanisms to Bind With Human ACE2," *Front. Mol. Biosci.*, vol. 7, no. December, pp. 1–14, 2020, doi: 10.3389/fmolb.2020.591873.

[22] I. Torjesen, "Covid-19: Omicron may be more transmissible than other

variants and partly resistant to existing vaccines, scientists fear," *BMJ*, vol. 375, no. November, p. n2943, 2021, doi: 10.1136/bmj.n2943.

[23] R. Wu *et al.*, "An update on current therapeutic drugs treating COVID-19," *Curr. Pharmacol. reports*, vol. 6, no. 3, pp. 56–70, 2020.

[24] G. Schochetman, C.-Y. Ou, and W. K. Jones, "Polymerase chain reaction," *J. Infect. Dis.*, vol. 158, no. 6, pp. 1154–1157, 1988.

[25] L. COVID, "Rt-pcr test eua summary," *Accelerated Emergency Use Authorization (EUA) Summary COVID-19 RT-PCR Test (Laboratory Corporation of America). Available online: www. fda. gov (accessed on 20 March 2020)*, vol. 19, 19AD.

[26] M. T. Dorak, *Real-time PCR*. Taylor & Francis, 2007.

[27] W. F. Sule and D. O. Oluwayelu, "Real-time RT-PCR for COVID-19 diagnosis: challenges and prospects," *Pan Afr. Med. J.*, vol. 35, no. Suppl 2, 2020.

[28] National Cancer Institute, "Antigen." [Online]. Available: https://www.cancer.gov/publications/dictionaries/cancer-terms/def/antigen.

[29] A. MacDonald, "COVID-19 Antibody Testing: S vs. N Protein," *Technology Networks Diagnostics*, Sep-2020.

[30] E. S. Goudouris, "Laboratory diagnosis of COVID-19," *J. Pediatr. (Rio. J).*, vol. 97, no. 1, pp. 7–12, 2021, doi: https://doi.org/10.1016/j.jped.2020.08.001.

[31] J. Fraden, "Handbook of modern sensors." Springer, 1994.

[32] G. Seippel, *Transducers, Sensors and Detectors*. Reston Publishing Company, 1983.

[33] J. W. Gardner, "Microsensors: Principles and Applications (John Wiley and Sons)," 1994.

[34] N. Bhalla, P. Jolly, N. Formisano, and P. Estrela, "Introduction to biosensors," *Essays Biochem.*, vol. 60, no. 1, pp. 1–8, Jun. 2016, doi: 10.1042/EBC20150001.

[35] P. Bollella, "Biosensors – Recent Advances and Future Challenges," *Biosens.* –

Recent Adv. Futur. Challenges, 2021, doi: 10.3390/books978-3-03943-888-4.

[36] J. J. Ramsden, "Optical biosensors," *J. Mol. Recognit.*, vol. 10, no. 3, pp. 109–120, 1997.

[37] R. J. Leatherbarrow and P. R. Edwards, "Analysis of molecular recognition using optical biosensors," *Curr. Opin. Chem. Biol.*, vol. 3, no. 5, pp. 544–547, 1999.

[38] J. Svitel and J. Katrl, "Optical biosensors," *Essays. Biochem.*, vol. 60, pp. 91–100, 2016.

[39] Y. Sandoval, S. W. Smith, S. A. Love, A. Sexter, K. Schulz, and F. S. Apple, "Single high-sensitivity cardiac troponin I to rule out acute myocardial infarction," *Am. J. Med.*, vol. 130, no. 9, pp. 1076–1083, 2017.

[40] V. Nabaei, R. Chandrawati, and H. Heidari, "Magnetic biosensors: Modelling and simulation," *Biosensors and Bioelectronics*, vol. 103. Elsevier Ltd, pp. 69–86, Apr-2018, doi: 10.1016/j.bios.2017.12.023.

[41] L. Wang and J. Lin, "Recent advances on magnetic nanobead based biosensors: From separation to detection," *TrAC - Trends in Analytical Chemistry*, vol. 128. Elsevier B.V., Jul-2020, doi: 10.1016/j.trac.2020.115915.

[42] M. de la Guardia, "Biochemical sensors: The state of the art," *Microchim. Acta*, vol. 120, no. 1, pp. 243–255, 1995.

[43] M. E. Tess and J. A. Cox, "Chemical and biochemical sensors based on advances in materials chemistry," *J. Pharm. Biomed. Anal.*, vol. 19, no. 1–2, pp. 55–68, 1999.

[44] S. J. Sadeghi, "Amperometric Biosensors," *Encycl. Biophys.*, pp. 61–67, 2013, doi: 10.1007/978-3-642-16712-6_713.

[45] C. Berggren, B. Bjarnason, and G. Johansson, "Capacitive biosensors," *Electroanalysis*, vol. 13, no. 3, pp. 173–180, 2001, doi: 10.1002/1521-4109(200103)13:3<173::AID-ELAN173>3.0.CO;2-B.

[46] G. Ertürk and B. Mattiasson, "Capacitive biosensors and molecularly imprinted electrodes," *Sensors (Switzerland)*, vol. 17, no. 2. MDPI AG, Feb-2017, doi:

10.3390/s17020390.

[47] S. S. Bekić *et al.*, “Use of fluorescent yeast-based biosensors for evaluation of the binding affinities of new steroid hormone and bile acid derivatives for select steroid receptors,” *Eng. Proc.*, vol. 16, no. 1, p. 4, 2022.

[48] D. Leech, “Affinity biosensors,” *Chem. Soc. Rev.*, vol. 23, no. 3, pp. 205–213, 1994.

[49] K. R. Rogers, “Principles of affinity-based biosensors,” *Mol. Biotechnol.*, vol. 14, no. 2, pp. 109–129, 2000.

[50] D. R. Thevenot, K. Toth, R. A. Durst, and G. S. Wilson, “Electrochemical biosensors: recommended definitions and classification,” *Pure Appl. Chem.*, vol. 71, no. 12, pp. 2333–2348, 1999.

[51] G. A. Evtugyn, H. C. Budnikov, and E. B. Nikolskaya, “Sensitivity and selectivity of electrochemical enzyme sensors for inhibitor determination,” *Talanta*, vol. 46, no. 4, pp. 465–484, 1998.

[52] H. C. Budnikov and G. A. Evtugyn, “Electrochemical biosensors for inhibitor determination: selectivity and sensitivity control,” *Electroanalysis*, vol. 8, no. 8-9, pp. 817–820, 1996.

[53] M. Varshney and Y. Li, “Interdigitated array microelectrodes based impedance biosensors for detection of bacterial cells,” *Biosens. Bioelectron.*, vol. 24, no. 10, pp. 2951–2960, 2009, doi: 10.1016/j.bios.2008.10.001.

[54] N. S. Mazlan *et al.*, “Interdigitated electrodes as impedance and capacitance biosensors: A review,” *AIP Conf. Proc.*, vol. 1885, 2017, doi: 10.1063/1.5002470.

[55] H. W. Jung, Y. W. Chang, G. yeon Lee, S. Cho, M. J. Kang, and J. C. Pyun, “A capacitive biosensor based on an interdigitated electrode with nanoislands,” *Anal. Chim. Acta*, vol. 844, pp. 27–34, 2014, doi: 10.1016/j.aca.2014.07.006.

[56] A. Alhoshany, S. Sivashankar, Y. Mashraei, H. Omran, and K. N. Salama, “A biosensor-CMOS platform and integrated readout circuit in 0.18-µm CMOS technology for cancer biomarker detection,”

Sensofile:///C:/Users/anton/Downloads/scholar(8).risrs (Switzerland), vol. 17, no. 9, 2017, doi: 10.3390/s17091942.

[57] G. D. Alley, “Interdigital Capacitors and Their Application to Lumped-Element Microwave Integrated Circuits,” *IEEE Trans. Microw. Theory Tech.*, vol. 18, no. 12, pp. 1028–1033, 1970, doi: 10.1109/TMTT.1970.1127407.

[58] K. Reinmut, “Hoffman.,‘Handbook of Microwave Integrated Circuits,’” *Artech House, Inc*, 1987.

[59] J. S. Wei, “Distributed Capacitance of Planar Electrodes in Optic and Acoustic Surface Wave Devices,” *IEEE J. Quantum Electron.*, vol. 13, no. 4, pp. 152–158, 1977, doi: 10.1109/JQE.1977.1069319.

[60] K. Kotani, I. Kawayama, and M. Tonouchi, “Dielectric response of c-oriented SrBi2Ta2O9 thin films observed with interdigital electrodes,” *Jpn. J. Appl. Phys.*, vol. 41, no. 11S, p. 6790, 2002.

[61] I. Bilican, M. T. Guler, N. Gulener, M. Yuksel, and S. Agan, “Capacitive solvent sensing with interdigitated microelectrodes,” *Microsyst. Technol.*, vol. 22, no. 3, pp. 659–668, 2016, doi: 10.1007/s00542-015-2617-1.

[62] V. Tsouti, C. Boutopoulos, I. Zergioti, and S. Chatzandroulis, “Capacitive microsystems for biological sensing,” *Biosens. Bioelectron.*, vol. 27, no. 1, pp. 1–11, 2011, doi: 10.1016/j.bios.2011.05.047.

[63] C. Sapsanis *et al.*, “Insights on Capacitive Interdigitated Electrodes Coated with MOF Thin Films: Humidity and VOCs Sensing as a Case Study,” *Sensors 2015, Vol. 15, Pages 18153-18166*, vol. 15, no. 8, pp. 18153–18166, 2015, doi: 10.3390/S150818153.

[64] K. Nakama, M. Sedki, and A. Mulchandani, “Label-free chemiresistor biosensor based on reduced graphene oxide and M13 bacteriophage for detection of coliforms,” *Anal. Chim. Acta*, vol. 1150, p. 338232, 2021, doi: 10.1016/j.aca.2021.338232.

[65] Z. Wang *et al.*, “Ultra miniaturized InterDigitated electrodes platform for sensing applications,” *Microelectron. Eng.*, vol. 225, p. 23955, 2020, doi:

10.1016/j.mee.2020.111253.

[66] S.-W. Chiu and K.-T. Tang, “Towards a chemiresistive sensor-integrated electronic nose: a review,” *Sensors*, vol. 13, no. 10, pp. 14214–14247, 2013.

[67] M. G. Campbell, S. F. Liu, T. M. Swager, and M. Dinca, “Chemiresistive sensor arrays from conductive 2D metal–organic frameworks,” *J. Am. Chem. Soc.*, vol. 137, no. 43, pp. 13780–13783, 2015.

[68] W.-T. Koo, J.-S. Jang, and I.-D. Kim, “Metal-organic frameworks for chemiresistive sensors,” *Chem*, vol. 5, no. 8, pp. 1938–1963, 2019.

[69] H. Nazemi, A. Joseph, J. Park, and A. Emadi, “Advanced micro-and nano-gas sensor technology: A review,” *Sensors*, vol. 19, no. 6, p. 1285, 2019.

[70] K. Alzoubi *et al.*, “Stability of interdigitated microelectrodes of flexible chemiresistor sensors,” *J. Disp. Technol.*, vol. 8, no. 7, pp. 377–384, 2012.

[71] J. Zhang *et al.*, “Pencil-trace on printed silver interdigitated electrodes for paper-based NO2 gas sensors,” *Appl. Phys. Lett.*, vol. 106, no. 14, p. 143101, 2015.

[72] L. Wang *et al.*, “Sensing arrays constructed from nanoparticle thin films and interdigitated microelectrodes,” *Sensors*, vol. 6, no. 6, pp. 667–679, 2006.

[73] A. G. Phadke and J. S. Thorp, “History and applications of phasor measurements,” in *2006 IEEE PES Power Systems Conference and Exposition*, 2006, pp. 331–335.

[74] J. De La Ree, V. Centeno, J. S. Thorp, and A. G. Phadke, “Synchronized phasor measurement applications in power systems,” *IEEE Trans. Smart Grid*, vol. 1, no. 1, pp. 20–27, 2010.

[75] H. Wu and A. C. Cangellaris, “Model-order reduction of finite-element approximations of passive electromagnetic devices including lumped electrical-circuit models,” *IEEE Trans. Microw. Theory Tech.*, vol. 52, no. 9, pp. 2305–2313, 2004.

[76] D. C. Hamill, “Lumped equivalent circuits of magnetic components: the gyrator-capacitor approach,” *IEEE Trans. power Electron.*, vol. 8, no. 2, pp. 97–

103, 1993.

[77] S. Bilbao and J. O. Smith, “Energy-conserving finite difference schemes for nonlinear strings,” *Acta Acust. united with Acust.*, vol. 91, no. 2, pp. 299–311, 2005.

[78] A. Agarwal and J. Lang, *Foundations of analog and digital electronic circuits*. Elsevier, 2005.

[79] A. Baldi, W. Choi, and B. Ziaie, “A self-resonant frequency-modulated micromachined passive pressure transensor,” *IEEE Sens. J.*, vol. 3, no. 6, pp. 728–733, 2003.

[80] P. Ahmadi, B. Maundy, A. S. Elwakil, and L. Belostotski, “High-quality factor asymmetric-slope band-pass filters: a fractional-order capacitor approach,” *IET circuits, devices Syst.*, vol. 6, no. 3, pp. 187–197, 2012.

[81] K. D. Satapathy *et al.*, “High-quality factor poly (vinylidenefluoride) based novel nanocomposites filled with graphene nanoplatelets and vanadium pentoxide for high-Q capacitor applications,” *Adv. Mater. Lett*, vol. 8, no. 3, pp. 288–294, 2017.

[82] L. J. A. Marcilin, “Analysis of Nano Capacitor using Scattering Parameters Equivalent Series Resistance and Quality Factor,” *Biosci. Biotechnol. Res. ASIA*, vol. 12, no. 2, 2015, doi: 10.13005/bbra/1853.

[83] V. G. Gokhare, D. N. Raut, and D. K. Shinde, “A review paper on 3D-printing aspects and various processes used in the 3D-printing,” *Int. J. Eng. Res. Technol*, vol. 6, no. 06, pp. 953–958, 2017.

[84] M. Leinster, “Things Pass By.” Ace Books: New York, NY, 1957.

[85] R. F. Jones, *Tools of the Trade*. Thrilling Publishing, 1950.

[86] C. W. Hull, “US4575330 A: apparatus for production of three-dimensional objects by stereolithography (1984).” 2019.

[87] S. S. Crump, “US5121329 A-Apparatus and method for creating three-dimensional objects.” 1992.

[88] R. Jones *et al.*, “RepRap–the replicating rapid prototyper,” *Robotica*, vol. 29, no. 1, pp. 177–191, 2011.

[89] E. Malone and H. Lipson, “Fab@ Home: the personal desktop fabricator kit,” *Rapid Prototyp. J.*, 2007.

[90] A. Su and S. J. Al’Aref, “History of 3D printing,” in *3D Printing Applications in Cardiovascular Medicine*, Elsevier, 2018, pp. 1–10.

[91] F. M. Mwema and E. T. Akinlabi, *Fused Deposition Modeling: Strategies for Quality Enhancement*. Springer Nature, 2020.

[92] G. Keeper, T. Graule, and F. Clemens, “Fused Deposition Modeling.”

[93] D. Kazmer, “Three-dimensional printing of plastics,” in *Applied plastics engineering handbook*, Elsevier, 2017, pp. 617–634.

[94] F. Fina, “Fused deposition modeling (FDM) 3D printing of oral modified release dosage forms.” UCL (Univerity College London), 2020.

[95] A. Davoudinejad, “Vat photopolymerization methods in additive manufacturing,” in *Additive Manufacturing*, Elsevier, 2021, pp. 159–181.

[96] A. Mostafaei *et al.*, “Binder jet 3D printing—Process parameters, materials, properties, modeling, and challenges,” *Prog. Mater. Sci.*, vol. 119, p. 100707, 2021.

[97] Y. L. Yap, C. Wang, S. L. Sing, V. Dikshit, W. Y. Yeong, and J. Wei, “Material jetting additive manufacturing: An experimental study using designed metrological benchmarks,” *Precis. Eng.*, vol. 50, pp. 275–285, 2017.

[98] C. Iancu, D. Iancu, and A. Stăncioiu, “FROM CAD MODEL TO 3D PRINT VIA" STL" FILE FORMAT.,” *Fiability Durability/Fiabilitate si Durabilitate*, no. 1, 2010.

[99] K. Latif, A. Adam, Y. Yusof, and A. Z. A. Kadir, “A review of G code, STEP, STEP-NC, and open architecture control technologies based embedded CNC systems,” *Int. J. Adv. Manuf. Technol.*, vol. 114, no. 9, pp. 2549–2566, 2021.

[100] M. Šljivic, A. Pavlovic, M. Kraišnik, and J. Ilić, “Comparing the accuracy of 3D slicer software in printed enduse parts,” in *IOP Conference Series: Materials*

Science and Engineering, 2019, vol. 659, no. 1, p. 12082.

[101] C. Bailey, S. Stoyanov, T. Tilford, and G. Tourloukis, "3D-printing and electronic packaging," in *2016 Pan Pacific Microelectronics Symposium (Pan Pacific)*, 2016, pp. 1–7.

[102] E. Morales-Narváez and C. Dincer, "The impact of biosensing in a pandemic outbreak: COVID-19," *Biosens. Bioelectron.*, vol. 163, no. April, 2020, doi: 10.1016/j.bios.2020.112274.

[103] S. Imran, S. Ahmadi, and K. Kerman, "Electrochemical biosensors for the detection of sars-cov-2 and other viruses," *Micromachines*, vol. 12, no. 2, pp. 1–23, 2021, doi: 10.3390/mi12020174.

[104] P. Fathi-Hafshejani *et al.*, "Two-Dimensional-Material-Based Field-Effect Transistor Biosensor for Detecting COVID-19 Virus (SARS-CoV-2)," *ACS Nano*, vol. 15, no. 7, pp. 11461–11469, 2021, doi: 10.1021/acsnano.1c01188.

[105] S. Mavrikou *et al.*, "Clinical Application of the Novel Cell-Based Biosensor for the Ultra-Rapid Detection of the SARS-CoV-2 S1 Spike Protein Antigen: A Practical Approach," *Biosensors*, vol. 11, no. 7. p. 224, 2021, doi: 10.3390/bios11070224.

[106] G. C. Mak *et al.*, "Evaluation of rapid antigen test for detection of SARS-CoV-2 virus," *J. Clin. Virol.*, vol. 129, no. June, p. 104500, 2020, doi: 10.1016/j.jcv.2020.104500.

[107] G. Seo *et al.*, "Rapid Detection of COVID-19 Causative Virus (SARS-CoV-2) in Human Nasopharyngeal Swab Specimens Using Field-Effect Transistor-Based Biosensor," *ACS Nano*, vol. 14, no. 4, pp. 5135–5142, 2020, doi: 10.1021/acsnano.0c02823.

[108] M. Z. Rashed *et al.*, "Rapid detection of SARS-CoV-2 antibodies using electrochemical impedance-based detector," *Biosens. Bioelectron.*, vol. 171, no. October 2020, p. 112709, 2021, doi: 10.1016/j.bios.2020.112709.

[109] M. Garg, A. L. Sharma, and S. Singh, "Advancement in biosensors for inflammatory biomarkers of SARS-CoV-2 during 2019–2020," *Biosens.*

Bioelectron., vol. 171, no. July 2020, p. 112703, 2021, doi: 10.1016/j.bios.2020.112703.

[110] C. A. Devaux, J. M. Rolain, and D. Raoult, "ACE2 receptor polymorphism: Susceptibility to SARS-CoV-2, hypertension, multi-organ failure, and COVID-19 disease outcome," *J. Microbiol. Immunol. Infect.*, vol. 53, no. 3, pp. 425–435, 2020, doi: 10.1016/j.jmii.2020.04.015.

[111] Y. Xie *et al.*, "Spike proteins of SARS-CoV and SARS-CoV-2 utilize different mechanisms to bind with human ACE2," *Front. Mol. Biosci.*, p. 392, 2020.

[112] N. S. Mazlan *et al.*, "Interdigitated electrodes as impedance and capacitance biosensors: A review," *AIP Conf. Proc.*, vol. 1885, no. 1, p. 20276, Sep. 2017, doi: 10.1063/1.5002470.

[113] C. Sontimuang, R. Suedee, and F. Dickert, "Interdigitated capacitive biosensor based on molecularly imprinted polymer for rapid detection of Hev b1 latex allergen," *Anal. Biochem.*, vol. 410, no. 2, pp. 224–233, 2011, doi: 10.1016/j.ab.2010.11.043.

[114] A. Quershi, Y. Gurbuz, W. P. Kang, and J. L. Davidson, "A novel interdigitated capacitor based biosensor for detection of cardiovascular risk marker," *Biosens. Bioelectron.*, vol. 25, no. 4, pp. 877–882, 2009, doi: 10.1016/j.bios.2009.08.043.

[115] M. R. R. Khan, A. Khalilian, and S. W. Kang, "Fast, highly-sensitive, and wide-dynamic-range interdigitated capacitor glucose biosensor using solvatochromic dye-containing sensing membrane," *Sensors (Switzerland)*, vol. 16, no. 2, p. 265, 2016, doi: 10.3390/s16020265.

[116] T. Q. Huy, N. T. H. Hanh, N. T. Thuy, P. Van Chung, P. T. Nga, and M. A. Tuan, "A novel biosensor based on serum antibody immobilization for rapid detection of viral antigens," *Talanta*, vol. 86, no. 1, pp. 271–277, 2011, doi: 10.1016/j.talanta.2011.09.012.

[117] R. Wang *et al.*, "Interdigitated array microelectrode based impedance immunosensor for detection of avian influenza virus H5N1," *Talanta*, vol. 79,

no. 2, pp. 159–164, 2009, doi: 10.1016/j.talanta.2009.03.017.

[118] G. M. Birnbaumer *et al.*, “Detection of viruses with molecularly imprinted polymers integrated on a microfluidic biochip using contact-less dielectric microsensors,” *Lab Chip*, vol. 9, no. 24, pp. 3549–3556, 2009, doi: 10.1039/b914738a.

[119] C. Y. Yao and W. L. Fu, “Biosensors for hepatitis B virus detection,” *World J. Gastroenterol.*, vol. 20, no. 35, pp. 12485–12492, 2014, doi: 10.3748/wjg.v20.i35.12485.

[120] C. Cheng, H. Cui, J. Wu, and S. Eda, “A PCR-free point-of-care capacitive immunoassay for influenza A virus,” *Microchim. Acta*, vol. 184, no. 6, pp. 1649–1657, 2017, doi: 10.1007/s00604-017-2140-4.

[121] S. Ramanathan, S. C. B. Gopinath, Z. H. Ismail, M. K. Md Arshad, and P. Poopalan, “Aptasensing nucleocapsid protein on nanodiamond assembled gold interdigitated electrodes for impedimetric SARS-CoV-2 infectious disease assessment,” *Biosens. Bioelectron.*, vol. 197, no. October 2021, p. 113735, 2022, doi: 10.1016/j.bios.2021.113735.

[122] P. K. Sharma *et al.*, “Ultrasensitive and Reusable Graphene Oxide-Modified Double-Interdigitated Capacitive (DIDC) Sensing Chip for Detecting SARS-CoV-2,” *ACS Sensors*, vol. 6, no. 9, pp. 3468–3476, Sep. 2021, doi: 10.1021/acssensors.1c01437.

[123] B. Mattiasson and M. Hedström, “Capacitive biosensors for ultra-sensitive assays,” *TrAC - Trends Anal. Chem.*, vol. 79, pp. 233–238, 2016, doi: 10.1016/j.trac.2015.10.016.

[124] A. Qureshi, J. H. Niazi, S. Kallempudi, and Y. Gurbuz, “Label-free capacitive biosensor for sensitive detection of multiple biomarkers using gold interdigitated capacitor arrays,” *Biosens. Bioelectron.*, vol. 25, no. 10, pp. 2318–2323, 2010, doi: 10.1016/j.bios.2010.03.018.

[125] L. Wang, M. Veselinovic, L. Yang, B. J. Geiss, D. S. Dandy, and T. Chen, “A sensitive DNA capacitive biosensor using interdigitated electrodes,” *Biosens.*

Bioelectron., vol. 87, pp. 646–653, 2017, doi: 10.1016/j.bios.2016.09.006.

[126] R. Li, J. Liu, and H. Zhang, "The challenge of emerging SARS-CoV-2 mutants to vaccine development," *J. Genet. Genomics*, 2021, doi: https://doi.org/10.1016/j.jgg.2021.03.001.

[127] J. T. Ortega, M. L. Serrano, F. H. Pujol, and H. R. Rangel, "Role of changes in SARS-CoV-2 spike protein in the interaction with the human ACE2 receptor: An in silico analysis," *EXCLI J.*, vol. 19, pp. 410–417, Mar. 2020, doi: 10.17179/excli2020-1167.

[128] S. P. Anand *et al.*, "Interaction of Human ACE2 to Membrane-Bound SARS-CoV-1 and SARS-CoV-2 S Glycoproteins," *Viruses* , vol. 12, no. 10. 2020, doi: 10.3390/v12101104.

[129] Z. Bai, Y. Cao, W. Liu, and J. Li, "The sars-cov-2 nucleocapsid protein and its role in viral structure, biological functions, and a potential target for drug or vaccine mitigation," *Viruses*, vol. 13, no. 6, 2021, doi: 10.3390/v13061115.

[130] F. Mahmoudinobar, D. Britton, and J. K. Montclare, "Protein-based lateral flow assays for COVID-19 detection," *Protein Eng. Des. Sel.*, vol. 34, pp. 1–10, 2021, doi: 10.1093/protein/gzab010.

[131] L. T. Allan-Blitz and J. D. Klausner, "A Real-World Comparison of SARS-CoV-2 Rapid Antigen Testing versus PCR Testing in Florida," *J. Clin. Microbiol.*, vol. 59, no. 10, 2021, doi: 10.1128/JCM.01107-21.

[132] N. Kohmer *et al.*, "Article the comparative clinical performance of four SARS-CoV-2 rapid antigen tests and their correlation to infectivity in vitro," *J. Clin. Med.*, vol. 10, no. 2, pp. 1–11, 2021, doi: 10.3390/jcm10020328.

[133] A. Scohy, A. Anantharajah, M. Bodéus, B. Kabamba-Mukadi, A. Verroken, and H. Rodriguez-Villalobos, "Low performance of rapid antigen detection test as frontline testing for COVID-19 diagnosis," *J. Clin. Virol.*, vol. 129, no. May, p. 104455, 2020, doi: 10.1016/j.jcv.2020.104455.

[134] N. Eshghifar, A. Busheri, R. Shrestha, and S. Beqaj, "Evaluation of Analytical Performance of Seven Rapid Antigen Detection Kits for Detection of SARS-

CoV-2 Virus," *Int. J. Gen. Med.*, vol. 14, pp. 435–440, Feb. 2021, doi: 10.2147/IJGM.S297762.

[135] S. A. Abid *et al.*, "Biosensors as a future diagnostic approach for COVID-19," *Life Sci.*, vol. 273, no. October 2020, p. 119117, 2021, doi: 10.1016/j.lfs.2021.119117.

[136] A. Tahamtan and A. Ardebili, "Real-time RT-PCR in COVID-19 detection: issues affecting the results," *Expert Rev. Mol. Diagn.*, vol. 20, no. 5, pp. 453–454, 2020.

[137] Y. Rasmi, X. Li, J. Khan, T. Ozer, and J. R. Choi, "Emerging point-of-care biosensors for rapid diagnosis of COVID-19: current progress, challenges, and future prospects," *Anal. Bioanal. Chem.*, vol. 413, no. 16, pp. 4137–4159, 2021, doi: 10.1007/s00216-021-03377-6.

[138] Y. Shen, T. Bin Anwar, and A. Mulchandani, "Current status, advances, challenges and perspectives on biosensors for COVID-19 diagnosis in resource-limited settings," *Sensors and Actuators Reports*, vol. 3, no. January, p. 100025, 2021, doi: 10.1016/j.snr.2021.100025.

[139] F. S. Iliescu *et al.*, "Point-of-care testing-the key in the battle against SARS-CoV-2 pandemic," *Micromachines*, vol. 12, no. 12, pp. 1–33, 2021, doi: 10.3390/mi12121464.

[140] S. Mehrdad, Y. Wang, and S. F. Atashzar, "Perspective: Wearable Internet of Medical Things for Remote Tracking of Symptoms, Prediction of Health Anomalies, Implementation of Preventative Measures, and Control of Virus Spread During the Era of COVID-19," *Front. Robot. AI*, vol. 8, 2021, doi: 10.3389/frobt.2021.610653.

[141] M. Chandra, K. Kumar, P. Thakur, S. Chattopadhyaya, F. Alam, and S. Kumar, "Digital technologies, healthcare and Covid-19: insights from developing and emerging nations," *Health Technol. (Berl).*, vol. 12, no. 2, pp. 547–568, 2022, doi: 10.1007/s12553-022-00650-1.

[142] S. Malliga, S. V Kogilavani, and P. S. Nandhini, "A Comprehensive Review of

Applications of Internet of Things for Covid-19 Pandemic," *IOP Conf. Ser. Mater. Sci. Eng.*, vol. 1055, no. 1, p. 012083, 2021, doi: 10.1088/1757-899x/1055/1/012083.

[143] M. W. McCarthy, "At-home coronavirus testing: the next game-changer?," *Expert Rev. Mol. Diagn.*, vol. 21, no. 1, pp. 1–2, Jan. 2021, doi: 10.1080/14737159.2021.1873133.

[144] N. B. Toppings *et al.*, "A rapid near-patient detection system for SARS-CoV-2 using saliva," *Sci. Rep.*, vol. 11, no. 1, p. 13378, 2021, doi: 10.1038/s41598-021-92677-z.

[145] L. J. Donato *et al.*, "Evaluation of the Cue Health point-of-care COVID-19 (SARS-CoV-2 nucleic acid amplification) test at a community drive through collection center," *Diagn. Microbiol. Infect. Dis.*, vol. 100, no. 1, p. 115307, 2021.

[146] N. Ravi, D. L. Cortade, E. Ng, and S. X. Wang, "Diagnostics for SARS-CoV-2 detection: A comprehensive review of the FDA-EUA COVID-19 testing landscape," *Biosens. Bioelectron.*, vol. 165, p. 112454, 2020.

[147] A. Singh *et al.*, "Recent advances in electrochemical biosensors: Applications, challenges, and future scope," *Biosensors*, vol. 11, no. 9, pp. 1–31, 2021, doi: 10.3390/bios11090336.

[148] V. Vásquez, M.-C. Navas, J. A. Jaimes, and J. Orozco, "SARS-CoV-2 electrochemical immunosensor based on the spike-ACE2 complex," *Anal. Chim. Acta*, vol. 1205, p. 339718, 2022, doi: https://doi.org/10.1016/j.aca.2022.339718.

[149] J.-S. Suh, H.-S. Kim, and T.-J. Kim, "Development of a SARS-CoV-2-derived receptor-binding domain-based ACE2 biosensor," *Sensors Actuators B Chem.*, vol. 334, p. 129663, 2021, doi: https://doi.org/10.1016/j.snb.2021.129663.

[150] J.-H. Lee *et al.*, "Versatile role of ACE2-based biosensors for detection of SARS-CoV-2 variants and neutralizing antibodies," *Biosens. Bioelectron.*, vol. 203, p. 114034, 2022, doi: https://doi.org/10.1016/j.bios.2022.114034.

[151] J. Karki, “Active low-pass filter design,” 2000.

[152] Y. Cheon, “Multiplatform Application Development for Android and Java,” in *2019 IEEE 17th International Conference on Software Engineering Research, Management and Applications (SERA)*, 2019, pp. 1–5, doi: 10.1109/SERA.2019.8886800.

[153] C. L. Ng, M. B. I. Reaz, and M. E. H. Chowdhury, “A Low Noise Capacitive Electromyography Monitoring System for Remote Healthcare Applications,” *IEEE Sens. J.*, vol. 20, no. 6, pp. 3333–3342, 2020, doi: 10.1109/JSEN.2019.2957068.

[154] C. L. Ng and M. B. I. Reaz, “Characterization of textile-insulated capacitive biosensors,” *Sensors (Switzerland)*, vol. 17, no. 3, 2017, doi: 10.3390/s17030574.

[155] K. H. Lee, S. Choi, J. O. Lee, J. B. Yoon, and G. H. Cho, “CMOS capacitive biosensor with enhanced sensitivity for label-free DNA detection,” *Dig. Tech. Pap. - IEEE Int. Solid-State Circuits Conf.*, vol. 55, pp. 120–121, 2012, doi: 10.1109/ISSCC.2012.6176945.

[156] M. Ruf, O. Morgan, and K. Mackenzie, “Differences between screening and diagnostic tests and case finding,” *Public Heal. Action Support Team*, 2008.

[157] D. J. Pike, N. Kapur, P. A. Millner, and D. I. Stewart, “Flow cell design for effective biosensing,” *Sensors (Switzerland)*, vol. 13, no. 1, pp. 58–70, 2013, doi: 10.3390/s130100058.

[158] F. Giacomozzi, V. Mulloni, G. Resta, and B. Margesin, “MEMS packaging by using dry film resist,” *Proc. 2015 18th AISEM Annu. Conf. AISEM 2015*, pp. 12–15, 2015, doi: 10.1109/AISEM.2015.7066828.

[159] A. Lancaster and M. Keswani, “Integrated circuit packaging review with an emphasis on 3D packaging,” *Integration*, vol. 60, pp. 204–212, 2018, doi: https://doi.org/10.1016/j.vlsi.2017.09.008.

[160] B. K. Tehrani, B. S. Cook, and M. M. Tentzeris, “Inkjet-printed 3D interconnects for millimeter-wave system-on-package solutions,” in *2016 IEEE MTT-S*

International Microwave Symposium (IMS), 2016, pp. 1–4, doi: 10.1109/MWSYM.2016.7540084.

[161] R. Bahr, A. Nauroze, W. Su, and M. M. Tentzeris, "Self-Actuating 3D Printed Packaging for Deployable Antennas," in *2017 IEEE 67th Electronic Components and Technology Conference (ECTC)*, 2017, pp. 1425–1430, doi: 10.1109/ECTC.2017.186.

[162] E. S. Park, J. Jeon, V. Subramanian, and T.-. K. Liu, "Inkjet-printed microshell encapsulation: A new zero-level packaging technology," in *2012 IEEE 25th International Conference on Micro Electro Mechanical Systems (MEMS)*, 2012, pp. 357–360, doi: 10.1109/MEMSYS.2012.6170208.

[163] E. Kukharenka, M. M. Farooqui, L. Grigore, and M. Kraft, "Electroplating moulds using dry film thick negative photoresist," *J. Micromech. Microeng.*, vol. 67, 2003, doi: S0960-1317(03)59956-9.

[164] P. Vulto, T. Huesgen, and G. A. Urban, "NOTE A full-wafer fabrication process for glass microfluidic chips with integrated electroplated electrodes by direct bonding of dry film resist," *J. Micromech. Microeng*, vol. 077001, 2009, doi: 10.1088/0960-1317/19/7/077001.

[165] A. Georgas *et al.*, "ACE2-based capacitance sensor for rapid native SARS-CoV-2 detection in biological fluids and its correlation with real-time PCR," *Biosens. Bioelectron.*, vol. 202, p. 114021, 2022, doi: https://doi.org/10.1016/j.bios.2022.114021.

[166] A. Georgas *et al.*, "A Biosensor Platform for Point-of-Care SARS-CoV-2 Screening," *Biosensors*, vol. 12, no. 7. 2022, doi: 10.3390/bios12070487.

[167] G. Banis *et al.*, "Design and Testing of a Disposable Flow Cuvette for Continuous Electroporation of a Bioreactor's Initial Algae Cultivation," *Magnetochemistry*, vol. 8, no. 11, p. 147, 2022, doi: 10.3390/magnetochemistry8110147.

[168] A. Vasilopoulou, A. Georgas, and E. Hristoforou, "Microcontroller Based Device for Capacitive Biosensor Readout," *MedPress Public Heal. Epidemiol.*,

vol. 2, no. 1, 2022, doi: mpphe-202204002.

[169] A. Vasilopoulou, A. Georgas, and E. Hristoforou, “A Review on Cardiac Biomarkers Detection for Heart Failure Prognosis,” *J. Integr. Cardiol. Open Access*, pp. 1–7, 2022, doi: 10.31487/j.jicoa.2022.02.02.